Intercomparison of Soil Hydrology Modules in the MIT Integrated Global System Model for Analysis of Climate Issues

by

Radhika N. de Silva

S.B., Engineering Sciences
Harvard University, 1995

Submitted to the Department of Civil and Environmental Engineering
in partial fulfillment of the requirements for the degrees of

Master of Science in Civil and Environmental Engineering
and
Master of Science in Technology and Policy

at the

MASSACHUSETTS INSTITUTE OF TECHNOLOGY

May 1998

Author .....
Department of Civil and Environmental Engineering
May 08, 1998

Certified by .....
Dara Entekhabi
Associate Professor
Thesis Supervisor

Certified by .....
Richard de Neufville
Chairman, Technology and Policy Program

Accepted by .....
Joseph M. Sussman
Chairman, Department Committee on Graduate Students

Eng.

Intercomparison of Soil Hydrology Modules in the MIT Integrated Global System Model for Analysis of Climate Issues

by

Radhika N. de Silva

Submitted to the Department of Civil and Environmental Engineering
on May 08, 1998, in partial fulfillment of the requirements for the degrees of
Master of Science in Civil and Environmental Engineering
and
Master of Science in Technology and Policy

Abstract

The availability of water at or near the surface determines the way incident radiative energy is partitioned at the ground surface. The goal of this thesis is to determine if better hydrological representation in the MIT Integrated Global System Model will improve its climate prediction capability. This thesis compares the performances of the hydrological modules in the MIT Climate Model and the Natural Emissions Model (NEM) with the off-line National Center for Atmospheric Research (NCAR) *Land Surface Model (LSM version 1.0) for Ecological, Hydrological, and Atmospheric Studies.* The models are forced with the First International Satellite Land Surface Climatology Project (ISLSCP) Field Experiment (FIFE) data, and outputs are validated using FIFE Intensive Field Campaigns measurements. Validation and analyses include comparisons between daily and diurnal model outputs and FIFE measurements, and evaluations of diurnal root mean square errors (RMSE).

All three models simulate FIFE conditions well. The NEM is particularly good at tracing the diurnal trend of most diagnostic parameters; but the large and numerous fluctuations in this model's outputs result in large diurnal RMSEs as well. Many of the errors in this model are due to deficient representation of soil moisture movement in its shallow soil column. The deep lower soil layer in the hydrological module in the Climate Model over-drains the thin upper soil layer; the dryness of the upper layer adversely affects energy partition at the land-atmosphere boundary. The NCAR LSM avoids many of the problems encountered with the other two modules and simulates FIFE conditions best; the doubled computational requirement is its main drawback. Hence, comprehensive hydrological representation in climate models will improve climate prediction capacity by providing consistent and more accurate hydrological inputs to all submodels.

Thesis Supervisor: Dara Entekhabi
Title: Associate Professor

Acknowledgments

Many individuals and institutions contributed towards this work in different ways.

The Department of Energy grant DE-FG02-94ER61937 supported me at MIT for the project duration. I wish to acknowledge the Climate and Global Dynamics Division of the National Center for Atmospheric Research in Boulder, Colorado, for allowing the use of the *Land Surface Model (LSM version 1.0)* whose outputs and derivatives constitute much of this thesis. And I am grateful to the different FIFE teams for the unrestricted use of their data.

For his confidence in me to work on this project, his guidance in my research, and his exemplary ethics as a researcher and when resolving problems and concerns, I am grateful to my advisor, Professor Dara Entekhabi.

I am truly grateful to MIT's *Athena* On-line Consultants for helping me resolve numerous software problems; and particularly thankful to Ms. Laura Balwin for her patient helpfulness.

A special thank you to Ms. Mala Ranawake for the efficient editing service, and for the frequent morale-boosts she provided.

I am thankful to my sister for her constant encouragement, and for her confidence in me. Her love and spiritual support certainly helped me face many challenges in the past two years.

And to my parents I am most grateful for their guidance over the years.

I owe much of my sanity and peace of mind to *Deutoronomy 31:6.*

Contents

List of Figures

List of Tables

Chapter 1

Introduction

1.1 Synopsis of Global Warming

The hypothesis of global warming can be understood by considering the radiation energy from the sun which warms the Earth's surface, and the thermal radiation from the Earth and the atmosphere which is radiated out to space. On average, the net incoming solar radiation and outgoing thermal radiation must balance. The amount of thermal radiation emitted depends on the temperature of the emitting body—the higher the body temperature, the greater the amount of thermal radiation emitted. So if the radiation balance is disturbed it can be restored by changing the Earth's surface temperature [15]. If the Earth had no atmosphere, the surface temperature of the Earth would be considerably colder than it is now. But greenhouse gases—such as water vapor, carbon dioxide (CO_2), methane (CH_4), nitrous oxide (N_2O), and chlorofluorocarbons (CFCs)—absorb and re-emit some of the outgoing radiation, and thus change the energy balance at the surface. The Earth restores its radiation balance by increasing its emitting temperature.

Radiation imbalances occur due to both natural and human influences. In fact, variability due to natural causes is very much larger than the variability due to anthropogenic influences, and therefore, it is often difficult to differentiate between the two influences. The "natural greenhouse effect," caused by greenhouse gases that have been in the atmosphere for a very long time, is essential to Earth's habitability.

But any increase in these greenhouse gases, whether due to natural or human influences, can increase global temperature. Time-series globally averaged temperature indicates a clear and rapidly increasing trend in temperature in the last century; this rate is thought to be too large to be naturally occurring. Furthermore, this rapid increase in temperature and the emissions of greenhouse gases from the beginning of the industrial revolution correlate well. Therefore, the increase in greenhouse gases—in particular, increase in carbon dioxide—is suspected to be the cause of the temperature rise. And it is this "enhanced greenhouse effect" due to anthropogenic emissions that is causing concern.

1.2 Agents of Global Warming

The relative importance of a greenhouse gas depends on its abundance and radiating capacity. Therefore, the most important of the greenhouse gases is water vapor; the greenhouse effect of water vapor accounts for 96% of the total greenhouse effect of all greenhouse gases [24]; but its abundance in the atmosphere has not changed significantly. However, increased atmospheric temperature will increase the vapor-holding capacity of the atmosphere and enhance the greenhouse effect of water vapor in the atmosphere [2]. The amounts of CO_2, CH_4, N_2O, CFCs and ozone in the atmosphere have been increasing rapidly since the beginning of this century. Figure 1-1 shows CO_2 measurements taken at Mauna Loa Observatory since 1958. The rapid fluctuations correspond to the seasonal changes in the rate of vegetative CO_2 uptake; the general upward trend corresponds to the net increase of CO_2 in the atmosphere. If, in fact, the increasing trend in temperature were due to increase in greenhouse gases, and if the adverse effects of global warming were to be curbed, the amounts of greenhouse gases in the atmosphere must be reduced, or at least stabilized at present levels.

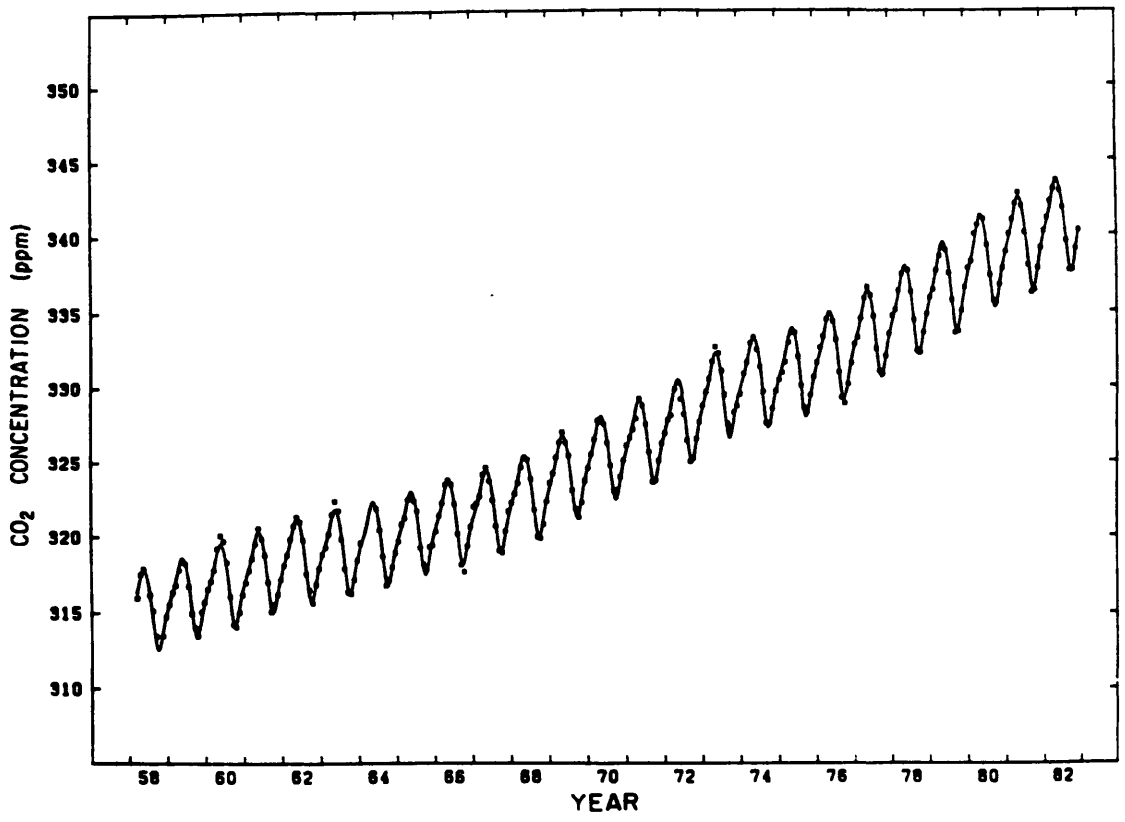

Figure 1-1: The mixing ratio of carbon dioxide in the Earth's atmosphere, from 1958 to 1982, as measured at Mauna Loa Observatory.
Source [1]

Carbon dioxide (CO_2): The radiating capacities of CH_4, N_2O and CFCs are greater than that of CO_2. Yet CO_2 has received more attention of researchers and policy-makers because of the large quantities of CO_2 released every year, the long atmospheric life-time of CO_2, and because CO_2 emissions are somewhat easier to quantify than other greenhouse gas emissions. The main anthropogenic emissions of CO_2 are due to fossil fuel use and deforestation. What is remarkable is that the minute amount of about 7.5 Gt of anthropogenic emissions, compared to about 190 Gt of natural emissions from biospheric respiration, decomposition, and physical and chemical processes, may have the potential to de-stabilize the climate system. The main sinks for CO_2 are the forests through photosynthesis, and the ocean through ocean biotic uptake. If the release of greenhouse gases were not reduced and global warming not mitigated, the increased global temperature will increase the ocean temperature and reduce its CO_2 sequestration capacity. In addition, freshening of the oceans due to the addition of fresh-water from melted polar ice will further reduce the ocean's CO_2 uptake. Thus, additional CO_2 may have a positive feedback effect. The increased temperature is expected to decrease soil moisture content in different regions of the world. Loss of soil moisture may lead to desertification of many of the forests in those regions. Then the rate and amount of CO_2 uptake by forests will also reduce. This reduced sequestration capacity of the forests and oceans will increase the atmospheric CO_2 content, and this increase will aggravate global warming.

Methane (CH_4): Unlike with CO_2, anthropogenic emissions of CH_4 are comparable to natural emissions. Wetlands, termites, oceans, and fresh-water are among the main natural sources of CH_4; coal mining, natural gas and petroleum industries, rice paddies, enteric fermentation, biomass burning, landfills, animal wastes, and domestic sewage treatment are among the main human-induced sources. Chemical destruction in the atmosphere and sorbtion into soils are the main sinks for CH_4. As the surface temperature increases, the amount of CH_4 sorbed to soil will decline. Furthermore, the large amounts of CH_4 presently trapped in ice cores will be released to the atmosphere as ice melts; this will be another positive feedback to global warming.

1.3 Effects of Climate Change

The effects of climate change are diverse, and their impacts may be felt not only by humans, but also by most ecosystems, forests, aquatic systems, and oceans. Climate change can also affect countries' economic and health sectors, and exacerbate tensions between groups of people in water scarce regions of the world. Some of these effects of climate change are discussed below.

Increase in the probability of extreme climates An increased atmospheric temperature will intensify the amount of evapotranspiration from both vegetated and non-vegetated surfaces. Although the evaporated water must precipitate back, it does not precipitate uniformly—some regions may have less rain in the Summer and others may have more precipitation in the winter. Thus the frequency and extent of extreme climates will worsen [8].

Sea-level rise As the global average temperature increases, the temperatures in higher latitudes are expected to increase more than the temperatures in the tropics [15]. And the temperature increase in the northern hemisphere will be greater than in the southern hemisphere [8]. The increase in temperature will both melt some of the polar ice and expand ocean water. The increase in the quantity of ocean waters will submerge lands at lower elevations. In most countries, population densities along the coasts are usually higher than in inlands. Therefore, sea-level rise will require nations to relocate people living in low-lands or take measures to avoid land submergence. Both these strategies are feasible—at a high cost.

Change in ocean circulation patterns Ocean sequestration is the most important sink for many of the greenhouse gases. Present ocean circulation models indicate that increased ocean temperatures could alter ocean circulation patterns. While there is considerable uncertainty associated with these predictions, the possibility of such alterations is unthinkable [21].

Changes to agriculture The extended Summers in the mid-latitudes where most developed countries are located will allow longer growing seasons in those regions; but extended warmer periods in the already warm tropics will increase evapotranspiration from plants, bare soils and free water surfaces. Although increased transpiration will increase the yield of a given plant, increased evaporation from a region will reduce the amount of water available for the entire season's crop [22]. Thus nations that heavily depend on their agricultural sectors must either change the type of crops grown, or use more efficient irrigation schemes if the regional temperatures were allowed to increase.

Agro-pests are also more common among water-stressed crops [3]. In addition, the expected accentuated flood and drought conditions will further reduce the cultivable land extent and period in some of the regions.

First and third worlds may drift further apart Water scarcity can increase the disparity between the developed and developing nations in semi-arid climates by altering their food production capacities. Due to reduced agricultural productivity in developing nations, these nations will have to import most of their food. But since agriculture is the main line of employment in most developing countries, reduced agricultural production will shrink employment opportunities and the nation's buying power, and leave even less money to import food. Therefore, global warming can aggravate the already scarce food situation in developing countries. On the other hand, longer growing seasons in the mid-latitudes will enable most developed nations to further increase their food production.

Health issues aggravate Water scarcities in highly populated regions, and reduced soil moisture impinging on agricultural productivity and food availability will affect human health and well-being. Furthermore, stresses from elevated temperatures and increased spreading of diseases under warmer climates will degrade living standards of people who already lack adequate health care. Pest attacks and epidemics are not uncommon under dry conditions. In fact, many of the current diseases in the

third world are water-related. This situation will only aggravate as the dry regions are further water-stressed.

Changes to water availability Increased temperatures and increased evaporation will allow less in-stream water availability and less groundwater replenishment. Many of the drier regions are already tapping into large quantities of their groundwater reserves. With lower replenishing rates, there will be still less groundwater to tap into. High rates of groundwater pumping causes land submergence. Land submergence, together with sea-level rise, may cause rapid loss of low-lying regions. Countries like Bangladesh are particularly vulnerable to such land losses [3].

Many riparian nations and regions already experience water-related tensions. Egypt-Sudan and India-Bangladesh are two of the many examples. Further water scarcity will intensify these riparian tensions.

Destruction of forests Lower runoff under warmer drier conditions will, in turn, reduce soil moisture and water available to plants. Under extreme conditions large forested areas can turn into grasslands. Loss of forests will reduce CO_2 uptake.

Loss of biodiversity Most species move to regions with favorable climates rather than themselves adapting to a changed climate. As the global temperature increases, species will need to move to higher latitudes. It is calculated that for each 1°C rise in temperature, land plants would have to shift their ranges towards the pole by 100-150 km [26]. The warming predicted by 2100 would mean shifts of a few hundred kilometers. Those species that propogate by spores or dust seeds might be able to achieve these rates [16]; most others would not [23]. Therefore, if the globe were to warm as fast as projected, many species will become extinct due to loss of their habitats.

Changes to aquatic ecosystems Aquatic ecosystems are determined by water quality, hydrological regimes and variability through the year. Change in the regimes and quality will therefore affect aquatic systems. Fish spawning is very sensitive to

temperature variations. Increased or decreased temperatures can destroy many types of fish. Ironically, the "higher" species are the least adaptable to new conditions; and changes to habitat can wipe off these species. In addition, higher water temperatures can increase incidence of fungal infections and fish diseases, and further destroy fish populations.

Destruction of wetlands Sea-level rise and sea-water intrusion into land destroys wetlands in coastal zones. Wetlands are diverse ecosystems that harbor many different types of species. Loss of wetlands will, thus, result in the loss of those species as well. Wetlands play a key role in filtering and purifying runoff. A powerful and efficient natural filter system will be lost if the wetlands were to be destroyed. Then the direct contaminated runoff to rivers and streams may lead to a myriad of new diseases.

1.4 Why Bother About Global Warming?

Past records indicate that in the Little Ice Age, which occurred during the seventeenth and eighteenth centuries [15], the global average temperature decreased by about 1°C. But the consequences of even that small change in the globally averaged temperature were catastrophic. Now, the predicted global average increase in temperature for the next century is only a few degrees—between 2-5°C. The possibilities of another catastrophic event is motivating the "climate-community" to research and advise policy-makers to mitigate possible changes in the climate.

The most important aspect of climate change is its global nature. The entire globe may be affected by the excessive emissions of greenhouse gases by a single nation. But the adverse effects are not equally distributed. A few regions might even benefit while others suffer severe losses. These global effects and the disparate consequences of the effects call for global action to mitigate this problem.

A better understanding of future consequences is essential for human societies to prepare for a changed or uncertain climatic future, and for policy development and implementation. But obtaining that understanding in itself is a problem. The

planet's processes are too complex to physically reproduce in a laboratory. Fortunately, computer models can be used to circumvent this problem to a large extent. Each of these models employ many of the relevant laws of physics—represented in the form of equations. The model then solves the equations for a series of "boxes" into which the "system," the planet's processes in this instance, are divided. The complexity and magnitude of the system varies with each model, and depends on the number of different processes and regions the modeler wishes to incorporate in the model. The boxes are all mathematically and logically linked to one another; and the integrity of the model depends on the accurate representation of the linkages between these boxes.

The variables commonly used to describe the climate are mainly concerned with the atmosphere. But the climate cannot be described in terms of the atmosphere alone; atmospheric processes are strongly coupled to the ocean, the land-surface, the cryosphere, and the biosphere. This coupling and feedback effects call for the full treatment of natural and man-made surface processes in climate models [15]. On the other hand, many climate change assessments focus on one or a few sectors—such as agriculture, forests, water resources—assuming that other sectors remain unchanged. But realistic climate change predictions cannot be made with climate-related sectors assumed to be constant. Therefore, climate change predictions have to be made in an integrated fashion. Integrated assessments include methodologies that explicitly account for simultaneous changes in climate-sensitive sectors, so that the net effects of climatic change can be determined. There are many different integrated global climate change models that have been compiled by different organizations and institutions. And MIT's Integrated Framework for Analysis of Climate Issues is one of them.

1.5 Overview of the MIT Integrated Global System Model for Analysis of Climate Issues

The MIT model consists of four submodels.

- Anthropogenic Emissions Prediction and Policy Analysis Model;
- Natural Emissions Model;
- Atmospheric Chemistry and Climate Model; and,
- Terrestrial Ecosystems Model.

Figure 1-2 is a schematic of this Framework.

In the MIT model, the Anthropogenic (Section 1.5.1) and Natural Emissions Models' (Section 1.5.2) outputs drive the coupled Atmospheric Chemistry and Climate Model (Section 1.5.3); the outputs of this model, in turn, drive the Terrestrial Ecosystems Model (Section 1.5.4); and the Terrestrial Ecosystems Model feeds back into the Natural Emissions, and Atmospheric Chemistry and Climate Models [13].

1.5.1 The Anthropogenic Emissions Prediction and Policy Analysis (EPPA) Model

The EPPA Model is a multi-region, multi-sector, recursive-dynamic computable general equilibrium model [30]. This model divides the world into 12 regions; each region consists of a number of production and consumption sectors, a government sector, and an investment sector. Energy use in production and consumption sectors generate varying amounts of CO_2, CH_4, N_2O, SO_2, CO and NO_x, by latitude, depending on energy use, fossil fuel source, and policies assumed to be in place in the different regions. The model also accounts for the role of trade between the regions; the costs of control of emissions; the impacts of population growth and development the less developed countries will have on global emissions; technological transformations; and the use of alternate energy sources in the future.

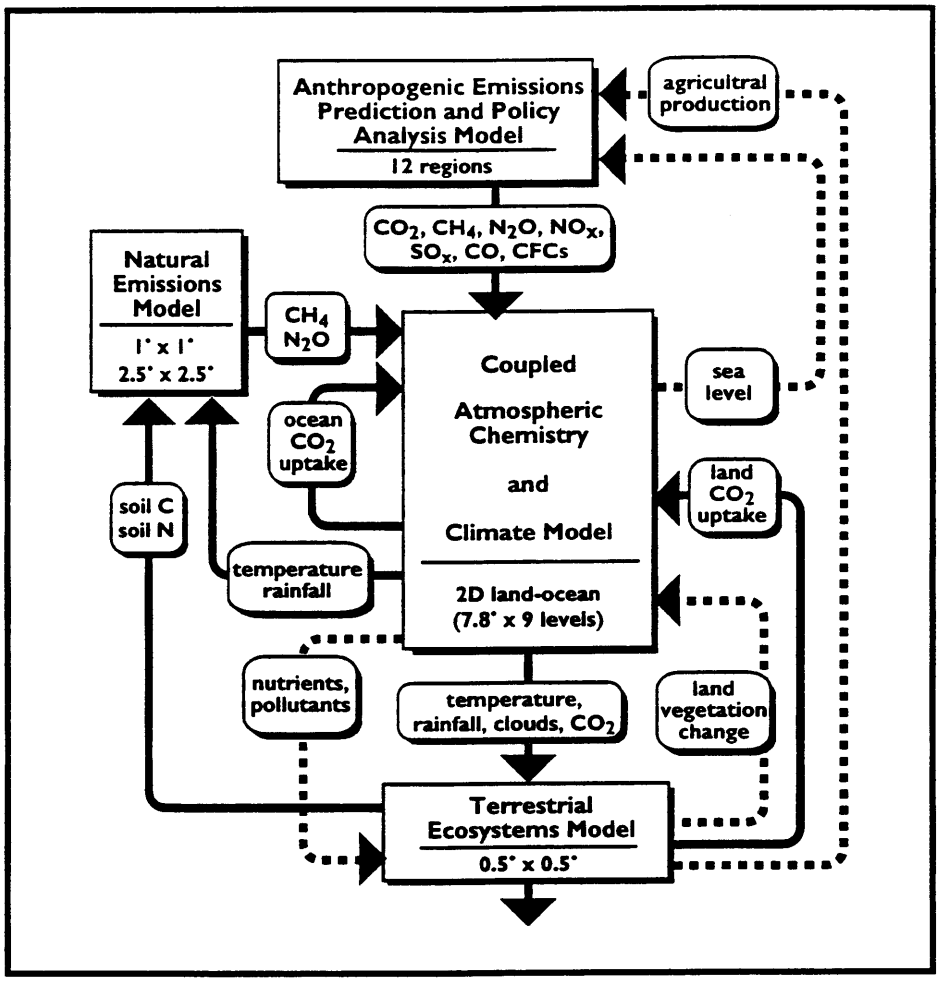

Figure 1-2: The schematic illustrates the framework and components of the MIT global system Model. Feedbacks between the submodels which are currently included are shown by solid lines; those that are under development for future inclusion are shown by dashed lines.
Source [25].

1.5.2 Natural Emissions Model (NEM)

There are two main classes of natural emissions: terrestrial and oceanic fluxes. The terrestrial emissions calculations account for the spatial and temporal variations such as soil texture, vegetation type, total soil organic carbon, and climate parameters; and processes such as decomposition, nitrification, and denitrification [25]. The model can predict daily emissions of N_2O, N_2, NH_3, and CO_2, and daily soil uptake of CH_4.

The monthly oceanic CO_2 fluxes are calculated by the oceanic carbon model and is driven by inputs from the coupled Chemistry Model detailed in section 1.5.3. These oceanic fluxes are calculated at latitudinal resolution using Henry's law. This oceanic carbon model will be interactively coupled with the Atmospheric Chemistry Model in the future [25].

1.5.3 The Atmospheric Chemistry and Climate Model

The Climate Model is a two-dimensional model, derived from another two-dimensional statistical-dynamical model, originally developed from a general circulation model by scientists at MIT and the National Aeronautics and Space Administration's (NASA) Goddard Institute for Space Studies (GISS). The revised MIT version of the model gives special consideration for clouds, and incorporates a real land and ocean distribution. The Chemistry Model is a finite-difference model. It computes zonal mean concentrations of twenty-five chemical species including CO_2, CH_4, N_2O, O_3, CO, NO_x, SO_2, sulfate aerosols, and CFCs [25].

The Atmospheric Chemistry and Climate Models are coupled to run interactively and simultaneously to predict atmospheric concentrations of radiatively and chemically important trace species. The Climate Model provides predictions of water vapor, wind speeds, temperature, solar radiation flux and precipitation to the Chemistry Model; the Chemistry Model, in turn, provides concentrations of the greenhouse gases and aerosols to the Climate Model. Together they predict climate and air composition over land and ocean as a function of latitude [25].

1.5.4 The Terrestrial Ecosystems Model (TEM)

This model allows for the study of the impacts of climate on the natural ecosystems and agriculture, and analyzes the feedback from the ecosystem [13]. This is a process-based ecosystem model, run on transient mode, and uses spatially referenced information on climate, elevation, soils, vegetation, and water availability to make monthly estimates of key carbon and nitrogen fluxes. Its soil moisture and temperature are controlled by the climate model. Major biogeochemical processes such as decomposition, ammonium and nitrate absorption and leaching, ammonia emissions, and denitrification are included in this model as well [25].

1.6 Climate Models and Policy Decisions

Policy makers and the scientific community have worked together on many important issues. But there still seems to be mis-communication between the two groups. Policy-makers often expect the scientists to provide them with one-number solutions to global problems. Scientists, on the other hand, fail to convey the many uncertainties associated with scientific findings and model predictions.

In the climate change debate, for instance, policy-makers like to know how the temperature in different regions will change in the future; or the exact reasons for the temperature change; and what steps need to be taken to avoid that change. The most truthful answer to all these questions is "don't know." Between the political and scientific communities, there is a constant disparity between expectations and interests in the scale of both temporal and spatial issues. While most scientific predictions are long-term and long-range that extend beyond political agendas and national boundaries, political expectations focus on smaller regions and shorter durations. But this does not imply that the scientific community cannot provide realistic "guestimates" that will aid the policy process. John Houghton's [15] comparison of climate change predictions with weather forecasting exemplifies the benefits of modeling and predicting future scenarios. In comparing the tasks of the weather forecasters and climate predictors, he states that "even though [weather forecasters] may feel uncertain about

tomorrow's weather, they cannot refuse to make a forecast. If they do refuse, they withhold from the public most of the useful information they possess. Despite the uncertainty in a weather forecast it provides useful guidance to a wide range of people. In a similar way the climate models, although subject to uncertainty, provide useful guidance for policy." Thus, despite the many criticisms lashed out at climate models and model predictions, the modeling process goes on. And, in fact, model predictions often set the pace for policy decisions and negotiations.

1.7 Uncertainties of Integrated Assessment Models Under a Policy Setting

Climate models are based on many assumptions like that the surface temperature of the Earth is increasing beyond the usual variability; that the unusual warming is mostly due to anthropogenic influences; and that the main reason for warming is the increase in greenhouse gases. Then to predict the effects of further increases in greenhouse gases, computer models are formulated to simulate the atmosphere, biosphere, and hydrosphere.

Although many of the behavioral patterns of these spheres are quite well known, not all patterns are known completely. Even the patterns that are known could be a subset of the many possible explanations and not the exact process. Therefore, uncertainties factor-in at every modeling stage—in the fundamental understanding of the climate system; in the understanding of the interactions between submodels; in the knowledge of the natural climate and temperature variability; in the reasons for the observed increase in temperature; in the relationship between greenhouse gases and temperature; in the understanding of the impact of clouds; and many more instances. Predictions of the economic sector and future emissions have the greatest uncertainties. Population growth in different countries are not known for certain; changes in trade patterns, and rise and fall in economies cannot be predicted well in advance; there may be changes in consumption patterns in different countries;

exact effects and impacts of policies are unclear; breakthroughs in technologies are not known until the innovations take place.

When all these uncertainties are accounted for, it is impossible to predict future climatic scenarios in any great detail, or with great accuracy. The best possible quantification is but a range of possibilities. Nevertheless, as more powerful computers become available, and different processes are better understood, this range of possible future temperatures and scenarios will become narrower.

Yet, it will be difficult to make predictions at the regional scale. Most climate change scenarios are modeled at the global scale; but the effects of climate change are felt at the regional scale. Since the effects are not equally distributed, the global trend will convey little direct information about the impacts that can be expected at national, state, or town level. Once the global trend is deciphered, the scientific community has to analyze past records to understand regional effects.

While there is much uncertainty in model predictions, those predictions still convey a wealth of information. These models can be successfully used to get a better understanding of the possible climatic scenarios, and the effects and impacts of different policies. It was this potential contribution to climate change prediction that motivated this project.

1.8 The Role of Water and the Hydrological Cycle in Global Change

The driving mechanisms of the climate system and of climate change is the Earth's capacity to capture solar energy, and then distribute this energy within the atmosphere. On average, about half of the solar energy that enters the Earth's atmosphere reaches the Earth's surface. The energy that reaches the surface returns to the atmosphere in many forms—as reflected or emitted radiation, or as latent or sensible heat flux. The way this solar energy is partitioned is mostly determined, by the extent and availability of water at or near the surface; evaporation of surface water and

its subsequent condensation and precipitation in the atmosphere redistribute heat between the Earth's surface and the atmosphere, and between different parts of the atmosphere [28]. Thus, the hydrological cycle and the Earth's energy budget are intrinsically coupled. Specifically, soil water influences the climate by affecting the partitioning of net radiation into latent and sensible heats. Furthermore, water mediates the global cycles of C, N, P, and S by providing the processes and transportation between the biosphere, atmosphere, hydrosphere, and geosphere. The atmospheric C and S budgets, in turn, affect atmospheric temperature and downward thermal radiation. Water also controls the type of vegetation that can survive at any location by influencing the soil moisture and temperature at that location [2]. The Earth's surface characteristics control the upward thermal radiation which, in turn affects the atmospheric temperature. In addition, moist soils sequester many types of pollutants and nutrient residues, but release them to the atmosphere, rivers and aquifers if the hydrological conditions change. The abundance of atmospheric pollutants, which can act as greenhouse agents, can affect the Earth's radiation budget. At any rate, water and the hydrological cycle play a critical role in the climate and in climate change processes. Therefore, the hydrological cycle is or should be a key component in climate change models. This thesis attempts to determine if more accurate analysis of the role of water will, in fact, improve prediction capabilities of climate models.

1.9 The Technical Thesis

This thesis work analyzed the competence of the hydrological modules of the MIT Climate Model and the Natural Emissions Model (NEM), and a Land Surface Model (LSM) developed by Gordon B. Bonan of the National Center for Atmospheric Research (NCAR) [6]. Each model's capacity to simulate current hydrological conditions and temperatures when forced with current atmospheric data was considered to be the measure of its capacity to predict future conditions. Thus, all three modules or submodels were forced with data from a field experiment site in Kansas and the outputs of the models were analyzed against validation data from the same site for the

same period. Forcing data included solar radiation, downward long-wave radiation, atmospheric pressure and temperature, precipitation, zonal and meridional wind, and specific humidity. Validation data included soil moisture profile, soil temperature profile, surface temperature, and latent and sensible heat fluxes. Results indicate that the NCAR LSM out-performs the other two models in every respect except compilation and computational time.

NEM models soil temperature and moisture profiles in the process of modeling C, N, and trace gas generation from the soil. Originally, this hydrological section was forced with monthly averaged data. But for consistency, and after observing the short-period validity of mathematical representations of some of the hydrological processes, the hydrology module was changed to accept data at half-hourly time-steps. The hydrological module used in NEM, and other changes made to it are further discussed in Section 2.2.

The hydrological module of the Climate Model is a simplified part of the GISS model [14]. This model was coded as given in Hansen *et al.* (1983), and was also forced with data at half-hourly time-steps. This model is further discussed in Section 2.1.

The NCAR *Land Surface Model for Ecological, Hydrological, and Atmospheric Studies* is an off-line model that represents essential land atmospheric interactions important for climate simulations. This model has the capacity to calculate evaporative, sensible and ground heat fluxes, soil moisture and temperature at different levels, for a small enough region that can be represented by a single point, or for the entire globe. This model can be coupled with an atmospheric model, or can run on stand-alone mode. This model is discussed in greater detail in Section 2.3.

The data sets used to force and validate the models were obtained from the First International Satellite Land Surface Climatology Project (ISLSCP) Field Experiment (FIFE) Project. These remotely-sensed and field data were collected on a 15 X 15 square kilometer prairie site in Kansas between 1987 and 1989. The data set is discussed in greater detail in Section 2.4.

1.10 Uncertainties in Hydrological Processes

Hydrological processes can be modeled and solved in two ways—by parameterizing surface characteristics or by solving the physical equations that describe these characteristics [12]. Both forms pose problems. Heterogeneities due to overlying vegetation, underlying soil, topography, and atmospheric processes make detailed calculations solely based on physical equations tedious, if not impossible. Alternatively, parameterizations of surface characteristics are often arbitrary. On the other hand, parameterizing, in itself, is extremely difficult. While characteristics such as soil albedo can be linearly aggregated, roughness length cannot be linearly aggregated [27]. The high variability of these hydrological parameters, even on small regions, adds to the uncertainties in models [28]. While free water surfaces can be relatively easily expressed as a function of vapor pressure differences and the capacity of the receiving medium to accept newly gassified molecules, vegetated surfaces are much more difficult to understand and represent mathematically. Plant rate and amount of transpiration depend on their water requirements and the atmospheric demand of water [28]. Therefore, accurately modeling a tropical forest—a myriad of different soil and vegetation types—is extremely challenging.

Furthermore, most mathematical representations of hydrological processes hold only for small spatial and temporal scales—typically hour-meter-scales. But most climate models require mathematical representations valid for monthly-100-kilometer scales. Methods to extrapolate and expand these representations to longer time-scales are not well understood [27]. Regardless of these difficulties and deficiencies of hydrological representations, a combination of both parameters and physical equations are used in climate models.

Most models resolve the problems associated with soil and plant heterogeneities by allowing each model grid many different soils and plants types. While this solves some of the hydrological problems, this makes the model extremely data intensive. Such a data intense model may be impossible to use at the global scale. Invariably modelers sacrifice accuracy of physical representation for practical use of climate models.

Chapter 2

The Hydrological Modules and Data Sets

This thesis compares the competence of two hydrological modules used in the MIT Integrated Global System Model for Analysis of Climate Issues, with an off-line land surface model. The hydrological module used in the Climate Model is a simplified derivative of that in the Goddard Institute for Space Studies (GISS) model that focuses on the land surface hydrology components. The hydrological module in the Natural Emissions Model (NEM) was developed by Yuexin Liu [19]. The National Center for Atmospheric Research (NCAR) *Land Surface Model (LSM version 1.0) for Ecological, Hydrological, and Atmospheric Studies*, developed by Gordon B. Bonan, is the benchmark model against which the above two hydrological modules are compared.

All three models treat incoming radiation as two distinct streams of shortwave and longwave radiation. The models partition the incoming energy into sensible, latent, and ground heat fluxes, depending on the atmospheric and ground temperatures, and soil moisture content. The order in which energy is partitioned differs in different models. The latent heat of vaporization links the energy and mass balance equations; the sensible heat flux influences turbulence at the surface, and therefore, the movement of water vapor. Once energy and mass movement have been described for one time step in the model, the state variables—the stores of water and energy in vegeta-

tion and soil—are updated, and the new values are then used to compute energy and mass flows at the next time step. Darcy and Richards' equations are used to model water movement within the soil [6],[28]. The treatment of vegetation structures and characteristics vary widely between the different models. Many of the intermediate processes are parameterized to make the models computationally feasible. The detail of the parameterizations of soil processes and properties also vary widely among different models. As mentioned in Section 1.10 hydrological parameters vary even over small regions and thus add to the uncertainties in models. These uncertainties and difficulties compound as one moves from the micro-scale to the macro regional or global scales.

Brief descriptions of hydrological modules in the Climate Model and NEM, and the special features of the NCAR LSM are given below. The reader is referred to the original papers—Hansen *et al.* (1983), Liu (1996), and the Technical Description and User's Guide by G. B. Bonan(1996)—for detailed descriptions.

The notation used in all the equations is consistent with the NCAR LSM. Appendix B lists the original notation used in the other two documents.

2.1 The Hydrological Module in the MIT Climate Model

This section describes the essential ground temperature and soil moisture calculations incorporated in the MIT Climate Model. As stated above, this hydrological module is a simplified derivative of the hydrological section of the GISS model developed by Hansen *et al.* (1983). The module simulates diurnal and seasonal ground temperature variations, and seasonal soil moisture fluctuations.

2.1.1 Soil temperatures

The ground heat flux at the upper boundary is given by

$$G(0) = \overline{S_g} - \overline{L} - H - \lambda E, \tag{2.1}$$

where, $\overline{S_g}$ is the net solar radiation, $\overline{L}$ the net longwave radiation, H the sensible heat flux, and λE the latent heat flux [14]. Latent and sensible heat fluxes, and upward longwave radiation demonstrate a nonlinear dependence on ground temperature. Therefore, merely averaged values do not accurately represent the ground temperature relationship to these variables. This model accounts for the nonlinear dependence by simulating the diurnal cycles of latent and sensible heat fluxes. At each time step, these are calculated as

$$H = c_p \rho C_h V_s (T_g - T_s), \text{ and,} \tag{2.2}$$

$$\lambda E = \lambda W \rho C_h V_s (q_g - q_s). \tag{2.3}$$

c_p is the specific heat of air, λ is latent heat of evaporation, ρ is air density, W is relative saturation, C_h is a temperature dependent parameter explained in Section 2.1.2, and V_s wind speed. The temperature difference between the ground (T_g) and the surface (T_s) drives the sensible heat flux; the humidity deficit between the ground (q_g) and surface (q_s) drives the latent heat flux.

This model has two soil layers. The thin (10 cm thick) upper soil layer which interacts with the atmosphere is used to simulate the diurnal temperature cycle. The deep (190 cm thick) lower layer is used as a seasonal heat storage and reservoir. The basic equation used to calculate the ground temperatures is the one-dimensional heat conduction equation

$$\frac{\partial T}{\partial t} = \frac{k}{\rho c} \frac{\partial^2 T}{\partial z^2} = K_g \frac{\partial^2 T}{\partial z^2}, \tag{2.4}$$

where, T is the temperature at depth z, t is time, k is thermal conductivity, ρc is heat capacity per unit volume, and K_g is thermal diffusivity.

The temperatures in the two layers are calculated, using $G(-z_1)$—the heat flux

between the two layers—as the link between the two layers.

$$z_1 \rho c_1 \frac{dT_1}{dt} = G(0) - G(-z_1), \tag{2.5}$$

$$z_2 \rho c_2 \frac{dT_2}{dt} = G(-z_1), \text{ where,} \tag{2.6}$$

$$G(-z_1) = \frac{3T_1 - 3T_2 - (1/2)G(0)z_1/\lambda_1}{z_1/\lambda_1 + z_2/\lambda_2}. \tag{2.7}$$

This model assumes that the heat capacity (ρc) and thermal conductivity (k) are uniform in each layer, and that no heat crosses the lower boundary of the bottom layer [14].

2.1.2 Soil moisture

The soil moisture is calculated in a similar manner using the same two soil layers—the upper layer responds to evaporation (E), precipitation (P_r), and surface runoff (R); the lower layer acts as the reservoir. The rates of change of moisture in the two layers are calculated as

$$\frac{\partial W_1}{\partial t} = \frac{P_r - E - R}{f_1} + \frac{W_2 - W_1}{\tau}, \text{ and,} \tag{2.8}$$

$$\frac{\partial W_2}{\partial t} = \frac{f_1}{f_2}\frac{W_1 - W_2}{\tau}. \tag{2.9}$$

W_i is relative saturation in the i^{th} layer; τ, the time constant for diffusion of moisture between the layers, is two days; and f water content at saturation [14].

All ground hydrology calculations conserve water and energy because (a) the ground heat flux at the upper boundary, $G(0)$, is calculated as the residual of net solar and longwave radiative fluxes, and the latent and sensible heat fluxes, (b) excess of precipitation and evaporation infiltrates into the soil, and (c) the soil column is deep enough to not allow any water to cross the lower boundary.

Fluxes of momentum, heat, and water vapor from the ground to the atmosphere are computed using drag law parameters like C_h. The parameters depend on wind speed, ground surface temperature, air temperature, specific humidities at the ground

Climate Model	NEM model
air temperature	air temperature
surface pressure	surface pressure
incident longwave radiation	net radiation
precipitation	precipitation
incident solar radiation	specific humidity
wind speed	wind speed
specific humidity	

Table 2.1: Input variables to hydrological modules in Climate and Natural Emissions Models.

level and of air 2 m above ground, and surface roughness length. The user must specify the surface albedo and soil porosity for the modeled region. This hydrological module accommodates only one surface type. Therefore, heterogeneous surface and vegetation types need to be integrated in some fashion to accurately represent the entire modeled region. The albedo and roughness length used for the Konza Prairie that was modeled in this project were 17.7% and 10 cm. All surface processes and unsaturated flows are assumed to be vertical; all soil properties such as hydraulic conductivity are assumed to be uniform throughout the modeled region. The time-series inputs and outputs of this model are given in Tables 2.1 and 2.2.

2.2 The Hydrological Module in the MIT Natural Emissions Model

The hydrological module in NEM uses a one-dimensional heat and moisture diffusion model—assuming there to be no horizontal heat or moisture transport in soils [25]. This module was developed by Yuexin Liu to aid the calculations of nitrous oxide and methane emissions from the terrestrial biosphere to the atmosphere, and is an integral part of the Natural Emissions component of the MIT Global System Model.

Climate Model	NEM	NCAR LSM
latent heat flux	latent heat flux	latent heat flux
sensible heat flux	sensible heat flux	sensible heat flux
soil temperatures at 10 and 100 cm	soil temperatures at 10, 20, 30, 40 and 50 cm	soil temperatures at 5, 20 50, 110, 230, 470 cm
soil moisture at 10 and 100 cm	soil moisture at 10, 20, 30, 40 and 50 cm	soil moisture at 5, 20 50, 110, 230, 470 cm
ground heat flux		ground heat flux
net radiation		net radiation
		vegetation temperature
		ground temperature
		absorbed solar radiation
		reflected solar radiation
		canopy transpiration
		canopy evaporation
		ground evaporation
		snow melt heat flux
		microbial respiration
		photosynthesis
		net CO_2 flux
		net primary production
		infiltration
		subsurface runoff
		subsurface drainage
		interception
		throughfall
		$\vdots$
		about another 10 fields

Table 2.2: Output variables of hydrological modules in the Climate Model, NEM and NCAR LSM.

2.2.1 Soil temperatures

NEM also uses the one-dimensional heat diffusion relationship given in Equation 2.4. The heat flux at the soil surface, G, is calculated as $G = R_n - \lambda E - H$. Net radiation, R_n, is an input to the module; λE and H are calculated from within the module. Heat flux at the lower boundary is driven by the temperature gradient between the model's bottom soil layer and the annual mean air temperature assigned at a depth of 500 cm. This model has five 10 cm soil layers in which temperature is updated at the end of each time step.

2.2.2 Soil moisture

Water movement and water balance in the soil column are represented by a one-dimensional moisture diffusion process as

$$q_i = -K\frac{dh}{dz}, \text{ and,} \tag{2.10}$$

$$\frac{\partial W}{\partial t} = \frac{1}{n}\frac{\partial q_i}{\partial z}, \tag{2.11}$$

where, K is hydraulic conductivity, h is hydraulic head, W is relative saturation, q_i is the water flow between soil layers, and n is soil porosity.

Rainfall and evaporation affect the top soil layer; but interception effects of overlying vegetation are disregarded. Just as with temperature, the soil moisture in each layer is updated at the end of each time step. Water addition during a rain event progresses from top to bottom—water is added to a deeper layer only when each layer is completely saturated.

Soils are categorized into twelve different types, and their parameterizations are from DeVries [10], and Clapp and Hornberger [9]. The user selects one of the twelve soil types appropriate for the region, and then the model assigns the corresponding soil clay content, soil porosity, saturated hydraulic conductivity, water content at field capacity, water content at plant wilting point, soil heat capacity, water tension parameter, and soil water parameter. Thereafter however, the model assumes that

the soils are vertically homogeneous. The hydraulic head and conductivity calculations for unsaturated conditions incorporate soil water parameters and soil water content, but assume that unsaturated flow and surface processes are vertical. Thermal conductivity and heat capacity calculations incorporate soil porosity and soil water content.

Originally, this module updated its state variables at monthly intervals and calculated monthly potential evapotranspiration using Thornthwaite's formula [29]. But in order to allow for intercomparisons with the other two models that were forced at half-hourly time steps, this hydrological module was modified to accept data at half-hourly time steps as well. Then Thornthwaite's formula was replaced by the GISS sensible heat and potential evaporation algorithm (Section 2.1).

The time-series inputs and outputs of this model are also given in Tables 2.1 and 2.2.

2.3 The NCAR LSM for Ecological, Hydrological, and Atmospheric Studies

This land surface model, developed by Gordon B. Bonan of the Climate and Global Dynamics Division of NCAR, mimics the essential biophysical and biogeochemical land-atmosphere interactions, and is especially useful to examine the effects of land surfaces on climate and atmospheric chemistry.

This LSM is a one-dimensional model of energy, momentum, water, and CO_2 exchange between the atmosphere and land, which accounts for ecological differences among vegetation types, hydraulic and thermal differences among soil types, and also allows up to three vegetation types, in addition to possible lakes and wetlands, within a single grid cell [7]. Calculations for each subgrid point are carried-out independently. The resulting fluxes from the subgrid cells are later averaged, using appropriate weights, to calculate the total flux from a given grid cell. This procedure avoids the complications and errors associated with averaging roughness lengths over

different vegetation types. The model's spatial grid can range from one point to the entire globe.

Vegetation effects are included by allowing for twelve plant types that differ in leaf and stem areas, root profile, height, leaf dimension, optical properties, stomatal physiology, roughness length, displacement height, or biomass. Different combinations of plant types and bare ground form 29 different surface types. Soil effects are included by allowing thermal properties and hydraulic properties to vary depending on the relative amounts of sand and clay present; soil color affects soil albedo [7].

In this model [7]:

- leaf and stem areas vary in time;
- absorption, reflection, and transmittance of solar radiation, accounts for the different optical properties of vegetation, soil, water, snow, and ice;
- absorption and emission of longwave radiation allows for emissivities less than one;
- latent heat fluxes incorporate intercepted canopy evaporation, soil evaporation, and transpiration;
- turbulent transfer processes are allowed above and within plant canopies;
- vegetation and ground temperatures balance the surface energy budget;
- the model accounts for stomatal physiology and CO_2 fluxes;
- water flow through the canopy considers interception, throughfall, and stemflow;
- the model incorporates snow hydrology;
- water flow at the ground surface is partitioned between infiltration and runoff;
- the model calculates temperatures of six soil layers using a heat diffusion equation that accounts for phase change;
- the LSM also calculates soil water for the same six layers using a one-dimensional conservation equation that accounts for infiltration input, gravitational drainage at the bottom of the column, evapotranspiration losses, and vertical water flow based on head gradients;
- the model can calculate temperatures for six layers of deep and shallow lakes accounting for eddy diffusion and convective mixing.

Time-series Atmospheric Inputs to NCAR Land Surface Model	Time-invariant input data
reference height, z_{atm}	latitude at center of the grid cell
temperature at z_{atm}	longitude at center of the grid cell
zonal wind at z_{atm}	surface type
meridional wind at z_{atm}	soil color type
convective precipitation	percent sand
large-scale precipitation	percent silt
pressure at z_{atm}	percent clay
surface pressure	percent of grid covered with lake
specific humidity at z_{atm}	percent of grid covered with wetland
incident longwave radiation	
incident direct beam solar radiation, *vis*	
incident direct beam solar radiation, *nir*	
incident diffuse solar radiation, *vis*	
incident diffuse solar radiation, *nir*	

Table 2.3: Time-series and time-invariant input variables to the NCAR LSM.

Table 2.3 gives the required input data to the NCAR LSM. When coupled to an atmospheric model, that model must provide these data. Table 2.2 gives the output fields. And if coupled to an atmospheric model, the LSM outputs feed back into the atmospheric model.

2.3.1 Ground temperature

For non-vegetated surfaces, the net longwave radiative flux, latent and sensible heat fluxes, and ground heat flux depend on ground surface temperature. And this model calculates the ground temperature by iteratively solving for the ground temperature, T_g, that balances the energy budget at the surface. The energy budget is described by

$$-\overline{S}_g + \overline{L}(T_g) + H(T_g) + \lambda E(T_g) + G(T_g) + M = 0. \tag{2.12}$$

$\overline{S}_g$ is the net solar radiation at ground level; and $\overline{L}(T_g)$ is the net longwave radiation at ground level. H and λE are sensible and latent heat fluxes, the calculations of which are detailed in Section 2.3.2. M is snow-melt heat flux; and G is ground heat

flux.

Net solar radiation incorporates ground albedos and the structure of the surface cover. Albedo, in turn, is a function of zenith angle, soil color, fraction of snow cover, and soil water content. Over vegetated surfaces, albedo calculations incorporate plant type, and stem and leaf areas in addition to the above characteristics, and thus feed in vegetation effects to net solar radiation calculations.

The ground heat flux is given by

$$G = \frac{2k_1}{\Delta z_1}(T_g - T_1), \tag{2.13}$$

where k_1 is thermal conductivity, Δz_1 is the thickness of the uppermost soil layer, and T_1 is the temperature of that same soil layer. If the calculated T_g is greater than freezing temperature and there is snow on the ground, snow is allowed to melt until the excess energy or snow runs out. Then, $\overline{L}$, G, H and λE are re-evaluated.

Net longwave radiation is defined as $\overline{L} = -L_{atm}\downarrow + L\uparrow$. And

$$L\uparrow = (1 - \alpha_g)L_{atm}\downarrow + \varepsilon_g \sigma T_g^4. \tag{2.14}$$

α_g is ground absorptivity, ε_g is ground emissivity, σ is the Stefan-Boltzmann constant, and $L_{atm}\downarrow$ is the downward atmospheric longwave radiation. Over vegetated surfaces, the net longwave radiative fluxes for vegetation $\overline{L}_v$ and the ground surface $\overline{L}_g$ are calculated separately, and later aggregated, as $\overline{L} = \overline{L}_v + \overline{L}_g$, to calculate the total net longwave radiation for the grid.

2.3.2 Latent and sensible heat fluxes

The sensible heat flux is driven by the temperature gradient between the reference height and ground level. Evaporation is driven by the humidity deficit of the atmosphere. For non-vegetated surfaces, these relationships are given by

$$H = -\rho_{atm} c_p \frac{(\theta_{atm} - \theta_s)}{r_{ah}}, \text{ and} \tag{2.15}$$

$$E = -\rho_{atm}\frac{(q_{atm} - q_s)}{r_{aw}}, \tag{2.16}$$

where θ_{atm} and q_{atm} are potential temperature and specific humidity at the reference height, and θ_s and q_s are those at the surface. ρ_{atm} and c_p are density and heat capacity of air. r_{ah} and r_{aw} are aerodynamic resistances to sensible heat and water vapor. In an attempt to accurately represent latent and sensible heat fluxes, this model incorporates descriptions of ecological and biogeochemical controls, in addition to the physical environment. Therefore, on vegetated surfaces, the latent and sensible heat fluxes are composed of vegetated and ground flux components, so that sensible heat, for instance, is represented as

$$H = H_v + H_g = -\rho_{atm}c_p\frac{(\theta_{atm} - \theta_s)}{r_{ah}}, \text{ where} \tag{2.17}$$

$$H_v = -\rho_{atm}c_p(T_s - T_v)\frac{2(L+S)}{\overline{r}_b} \tag{2.18}$$

$$H_g = -\rho_{atm}c_p\frac{(T_s - T_g)}{r'_{ah}}. \tag{2.19}$$

Here, $\overline{r}_b$ is the average leaf boundary layer resistance to sensible heat flux, and r'_{ah} is the aerodynamic resistance to sensible heat flux between the ground and the reference height. L and S are leaf and stem area indices, and T_s is the temperature at the surface.

Similarly, λE is also composed of vegetated and ground fluxes, and incorporates sun-lit and shaded leaf and stem area indices, shaded and sun-lit stomatal resistances, evaporation from the wetted fraction of the canopy, and transpiration from leaves in its calculations [6]. For a more complete description of the processes and parameterizations used in the model, the reader is referred to the model technical guide.

2.3.3 Soil temperatures

This model uses six soil layers with thicknesses 10, 20, 40, 80, 160, and 320 cm. The thermal properties are defined at the center of each layer. The temperature at the center of each layer is numerically calculated using heat flux and one-dimensional

energy conservation equations (Equation 2.4) presented in Section 2.1.1. The ground heat flux at the top of the soil column and zero heat flux at the bottom of the soil column de-mark the boundary conditions for these calculations.

The model has the capacity to calculate temperatures of six layers in lakes as well, but this capability is not utilized in this project.

2.3.4 Soil moisture

This model parameterizes processes such as interception, throughfall, snow accumulation and melt, infiltration, surface runoff, subsurface drainage, and redistribution within the soil column and the canopy, in its soil water calculations. It allows spatial heterogeneity of precipitation, throughfall and soil water.

Soil water is calculated using the conservation equation given by

$$\frac{\Delta\theta\Delta z}{\Delta t} = -q_i + q_o - e, \tag{2.20}$$

where, θ is volumetric soil water content, Δz is the soil layer thickness, Δt is the time step. q_i and q_o are fluxes of water into and out of the soil layer. e, the evaporation loss, integrates both soil evaporation and transpiration: evaporation removes water from the first soil layer, transpiration removes water from each soil layer in proportion to the relative root abundance in that layer. Partial time steps smaller than 10 minutes were advised for soil water calculations.

The flux of water into the soil at the top of the soil column and gravitational drainage at the bottom of the column are the boundary conditions for moisture calculations. The six soil layers, briefed in Section 2.3.3 are used for soil water calculations as well. This model also uses the Clapp and Hornberger (1978) relationships and soil properties to calculate the hydraulic properties of the soil matrix.

2.4 The FIFE Data Sets

The First International Satellite Land Surface Climatology Project (ISLSCP) Field Experiment (FIFE) was conducted on the Konza Prairie Natural Research Area near Manhattan in Kansas. This is a 15 X 15 square kilometer grassland. Data acquisition procedure fell into two categories that the FIFE team called the continuous monitoring effort, and the Intensive Field Campaigns (IFCs) [17]. The former process gathered meteorological data, gravimetric soil moisture data, streamflow data and biometric measurements from 16 automated stations within the site. These data are available from Summer 1987 to 1989. The IFCs acquired surface and airborne data. The ground measurements were made at 19 sites in Konza [11]. These sites were believed to represent the major spatial variations in soil depth, the seasonally integrated incident solar radiation and the region's management practices related to grazing and burning. Due to large human resource requirements in IFCs, the duration of these data is limited to four 2-week periods in 1987 [17]; but only three of these IFC data blocks are used in this project because subsurface temperatures in the models drop to those below freezing during the fourth data block. In this thesis work general analyses were conducted for five months in 1987, but the detailed comparisons between calculations and observed flux values were limited to the first three IFC data periods.

Three FIFE data sets were used for this project—atmospheric, flux, and soil moisture [20]. The atmospheric data consisted of surface pressure, wet and dry-bulb air temperatures, rain-rate, zonal and meridional wind components, surface temperature, soil temperatures at 10 and 50 cm depths, incident and reflected solar radiation, net radiation, incident longwave radiation, and water vapor mixing ratio calculated using wet and dry-bulb temperatures and surface pressure. The flux data set used to validate the models consisted of net radiation, sensible and latent heat fluxes, ground heat flux, and incident and reflected solar radiative fluxes. Volumetric soil moisture measurements were available at 20, 30, 40, 50, 60, 80, 100, 120, 140, 160, 180, and 200 cm depths; these had been gathered for 17 days; the FIFE teams then extrapolated the data over many months [11]. But unlike the atmospheric and

flux data sets, the soil moisture data set does not differentiate between measurements and extrapolated values. Therefore, the soil moisture values are not used in decisive analyses. The atmospheric and flux data sets contain 30-minute averaged time series fields; soil moisture data set comprise of daily averaged values.

The atmospheric data set provides total precipitation. But the NCAR LSM requires the user to differentiate between large-scale and convective precipitation. Due to the lack of better information, convective and large-scale precipitations were allocated 75% and 25% of the total precipitation.

The next three Chapters discuss each model's capacity to simulate atmospheric and soil conditions observed at the Konza Prairie.

Chapter 3

Model Performances at Daily Time Scales

The uncertainties associated with model results call for model performance evaluations. A model's true capacity to simulate future climates will be known only many years after the model formulation. But in the meantime a model's capacity to simulate land and atmospheric processes can be evaluated by checking its ability to simulate historical climates; or by comparing its outputs with observations of current atmospheric conditions. And the latter approach was used in this project.

Three main types of tests were performed on each hydrological module: comparisons of calculated and observed daily mean values of prognostic and diagnostic variables; comparisons of calculated and observed diurnal cycles of the same variables; and comparisons of diurnal root mean square errors of those variables between models. These three categories of tests convey different information about the robustness of each model's soil hydrology simulations.

Chapter 3 outlines the significance of accurate daily mean simulations, and then discusses each module's capacity to calculate daily trends of diagnostic variables. Chapter 4 presents soil temperature and moisture profiles, and discusses long-term trend prediction capabilities of models. The diurnal cycles of the models are simultaneously compared with the observed diurnal cycles in Chapter 5. Root mean square error comparisons immediately follow each diurnal cycle comparison.

3.1 Significance of Daily Mean Values

Each model was forced with data at half-hourly time steps. Then the daily mean of each prognostic or diagnostic variable was calculated by averaging the 48 output values for that day; the models were not forced to explicitly calculate daily mean values. Therefore, the daily mean values test a model's capacity to retain long-term information and simulate the general characteristics of the soil column and surface layer, while using and generating diurnal high-frequency fluctuations. Soil water content and soil temperature are models' state variables. So a model's long-term "memory" capacity is determined by its moisture and heat storages. A deep soil column with multiple layers is better able to provide the required moisture and heat reservoir and storage. The atmospheric forcings are continuously dampened as they progress to deeper layers; and therefore, the deeper soil layers are less sensitive to individual atmospheric excitations, yet they capture long-term trends in atmospheric conditions. Further, the resistance provided by deeper layers prevent large fluctuations in shallower upper layers.

3.2 Limitations of the Analysis

The analysis period for these models was limited due to the dearth of validation data. Latent heat, sensible heat, and ground heat fluxes applicable to this project, were available for only four 2-week intensive observing periods in 1987 (Section 2.4) and the fourth of these data blocks could not be used in the analyses because the ground surface was too cold during this period; but micrometeorological atmospheric forcing data were available from May 1987 to December 1989. Earlier model runs indicated that they needed a few months to initialize the prognostic variables. Therefore, a two-year spin-up period, from May 1987 through April 1989, was used for this project. The spin-up run was followed by a five-month analysis run, from May through September, 1987. Since the first flux data block starts on May 27, 1987, the outputs from the 1987 re-visit run were used in the analysis. If longer data series were available, seasonal-

and annual-scale comparisons would have further attested to the robustness of each model's long-term prediction capability.

Simulations from May 27 through September 30 are used in daily mean figures and calculations. Diurnal means and root mean square errors of simulated values were calculated only if the corresponding FIFE IFC measurement were available. FIFE data have been compiled by averaging over several stations in the Konza prairie. The stations used to calculate the average value for different time steps were not always the same. In addition, atmospheric and flux data are from two sets of stations. While there are slight differences in observed values from these two sets of stations, the data are sufficiently accurate for the purposes of this project [11].

3.3 Comparisons of Simulated and Observed Daily Mean Values

The NCAR Land Surface Model (LSM) solves for latent heat, sensible heat and ground heat fluxes simultaneously. But the hydrological modules in the Climate Model and Natural Emissions Model (NEM) calculate these fluxes in sequence—considering ground heat flux to be the residual of incident radiation not partitioned to latent or sensible heat flux. This discussion will follow the same sequence used in the sequential calculations.

3.3.1 The hydrological module in the Climate Model

Latent heat flux The latent heat fluxes (λE) calculated by the hydrological module in the Climate Model are compared with FIFE observations in Figure 3-1. Evaporation from the ground surface is shown as positive. The bar-graph shows 24-hour precipitation; its scale is given on the right axis. In late May and early June (Julian days 147 to 157), the calculated values are consistently smaller than the FIFE measurements; but the simulations improve as the Summer progresses. Usually, the early and late Summer differences are due to the effect of vegetation. But here the

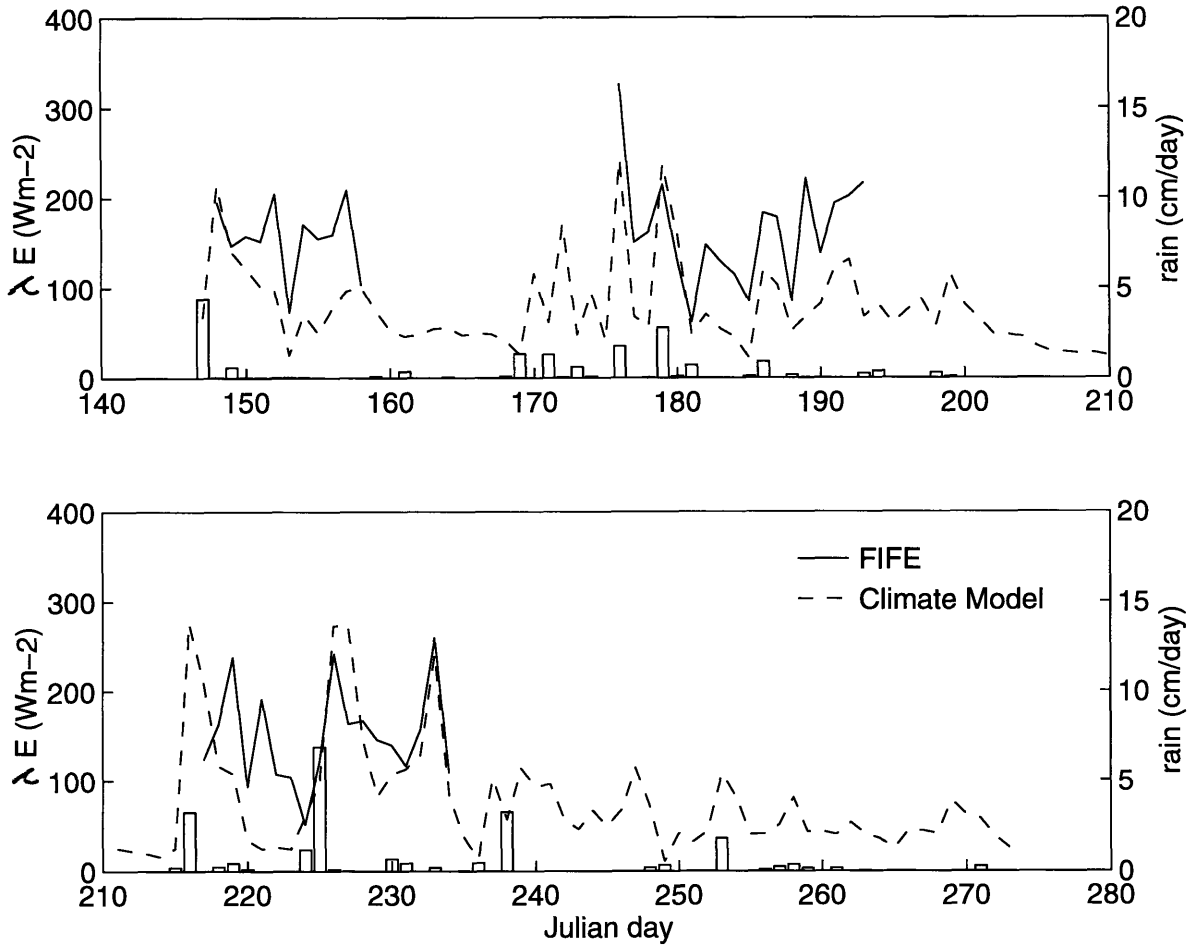

Figure 3-1: The daily mean latent heat fluxes (λE) of the hydrological module in the Climate Model and FIFE observations. The bar-graph shows 24-hour precipitation with the scale on the right axis.

difference is due to soil moisture levels.

This model's latent heat flux is calculated using the atmospheric humidity deficit and moisture content in the upper soil layer, together with several parameterizations as:

$$\lambda E = soil\ water\ content\ *\ drag\ coefficients\ *\ humidity\ deficit. \quad (3.1)$$

Much of the error is introduced through the underestimated soil water content. As discussed later with Figure 3-26 the soil moisture calculations of this model are much lower than those calculated by other models or FIFE observations. The third set of FIFE measurements (Julian days 217-234) corresponds to a wet period. During this period, soil water content is comparable with other models and observations, and is sufficiently large to render accurate λE calculations.

The model's immediate response to rain events is good. λE increases sharply on rainy days, but the upper soil layer dries so fast that λE decreases soon after precipitation stops. In general, the module lacks the necessary persistent nature to simulate the lasting effect of the rain event. But the amplitude and range of the daily λE are comparable to those of observations.

Sensible heat flux Comparisons of the sensible heat fluxes (H) from the hydrological module in the Climate Model and FIFE observations are shown in Figure 3-2. Upward H is positive. This module utilizes too little of the available energy to evaporate water from the surface, but uses too much energy to heat the surface. The fluxes due to sensible heat are consistently larger than the observed values; but the disparity decreases as the Summer progresses. H is calculated using Equation 2.2. The same set of drag coefficients are used to calculate both λE and H. Therefore, errors in calculated H can be expected whenever there are errors in calculated λE. During the first two months of the analysis period, λE was underestimated; then H was correspondingly overestimated. In August both λE and H calculations compare well with FIFE values. Just as with λE flux calculations, the model responds to rain events well—rain cools the surface and reduces H loss from the surface—but this response is rather exaggerated when compared with observations.

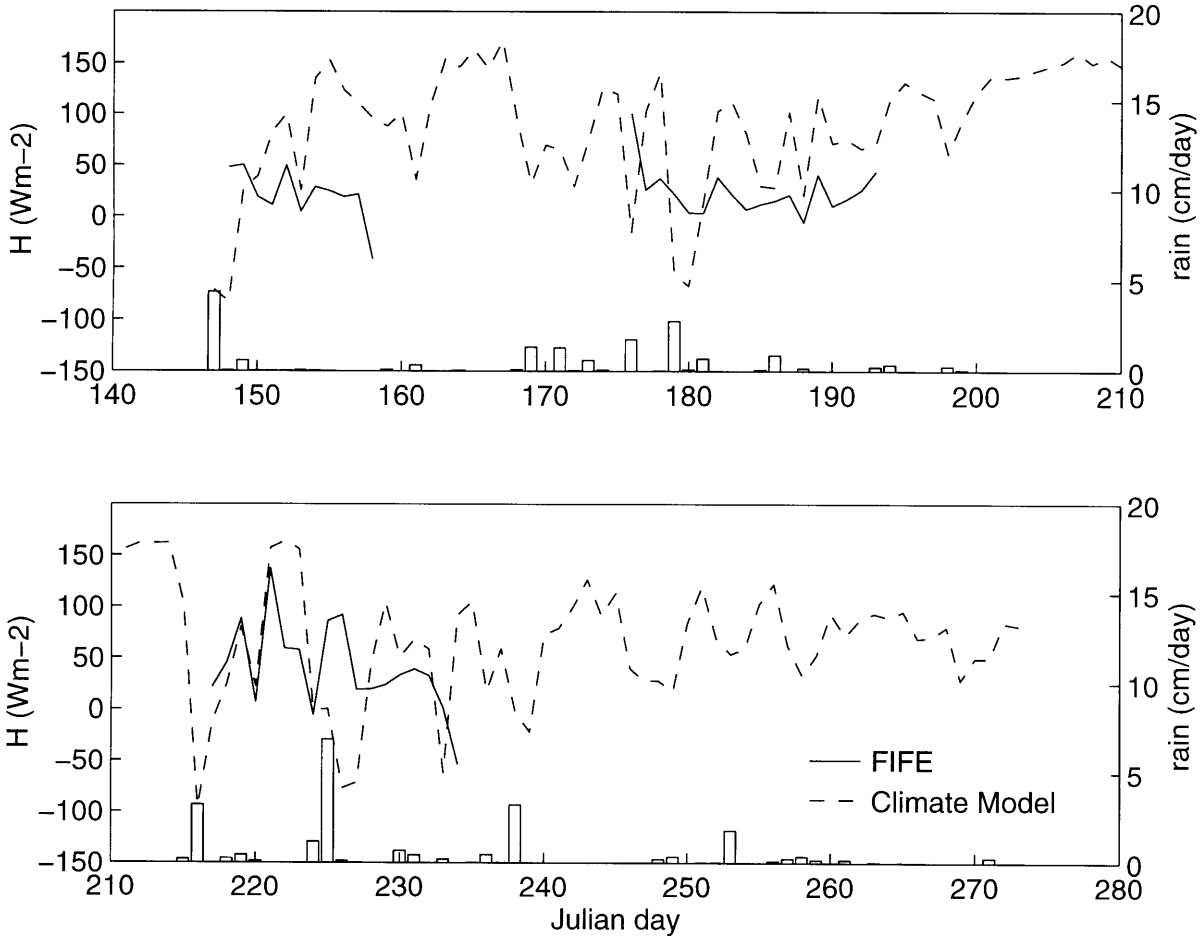

Figure 3-2: The daily mean sensible heat fluxes (H) of the hydrological module in the Climate Model are compared with FIFE observations. The 24-hour precipitation is shown by the bar-graph.

The H flux simulations for the second and third weeks of August (Julian days 217-234) follow observations best. Two reasons influence the better agreement between calculated and measured H during this period—reduction in calculated H when T_g is lowered during this wet period, and more importantly, increase in observed H. During mid to late Summer taller grass and additional grass cover help convect H more efficiently. Therefore, H flux in the Konza prairie increases during this period. But this better agreement between observations and calculations in August is only by coincidence since this module does not explicitly incorporate vegetation effects; hence it does not capture the variations in land cover and vegetation influences on surface fluxes. Therefore, this module evaluates large H fluxes even when there is little vegetation, and no enhanced H convection in early summer.

Evaporative fraction The evaporative fraction (EF) was calculated using daily mean λE and H as

$$EF = \frac{\overline{\lambda E}}{\overline{\lambda E} + \overline{H}}, \tag{3.2}$$

and the EF values for the hydrological module in the Climate Model and FIFE measurements are shown in Figure 3-3. In early and mid Summer periods the calculated evaporative fractions are smaller than the FIFE observations. Calculated EF are mostly dominated by H; too little of the available heat is channelled into λE. But as previously noted agreement between calculated and observed λE and H improve during mid-late Summer when the upper soil layer is wetter, and the effect of vegetation is more pronounced in the FIFE measurements. Then calculated and observed EF too agree better. A more robust representation of soil water content in this module will improve energy partition into λE and H throughout the analysis period.

In the FIFE observations, on the other hand, evaporative fraction calculations are dominated by λE fluxes: the observed λE fluxes are often about three or four times as large as the observed H fluxes. When the daily mean ground temperature is less than the daily mean atmospheric temperature, indicating a net groundward H flux, the observed evaporative fraction is further enhanced.

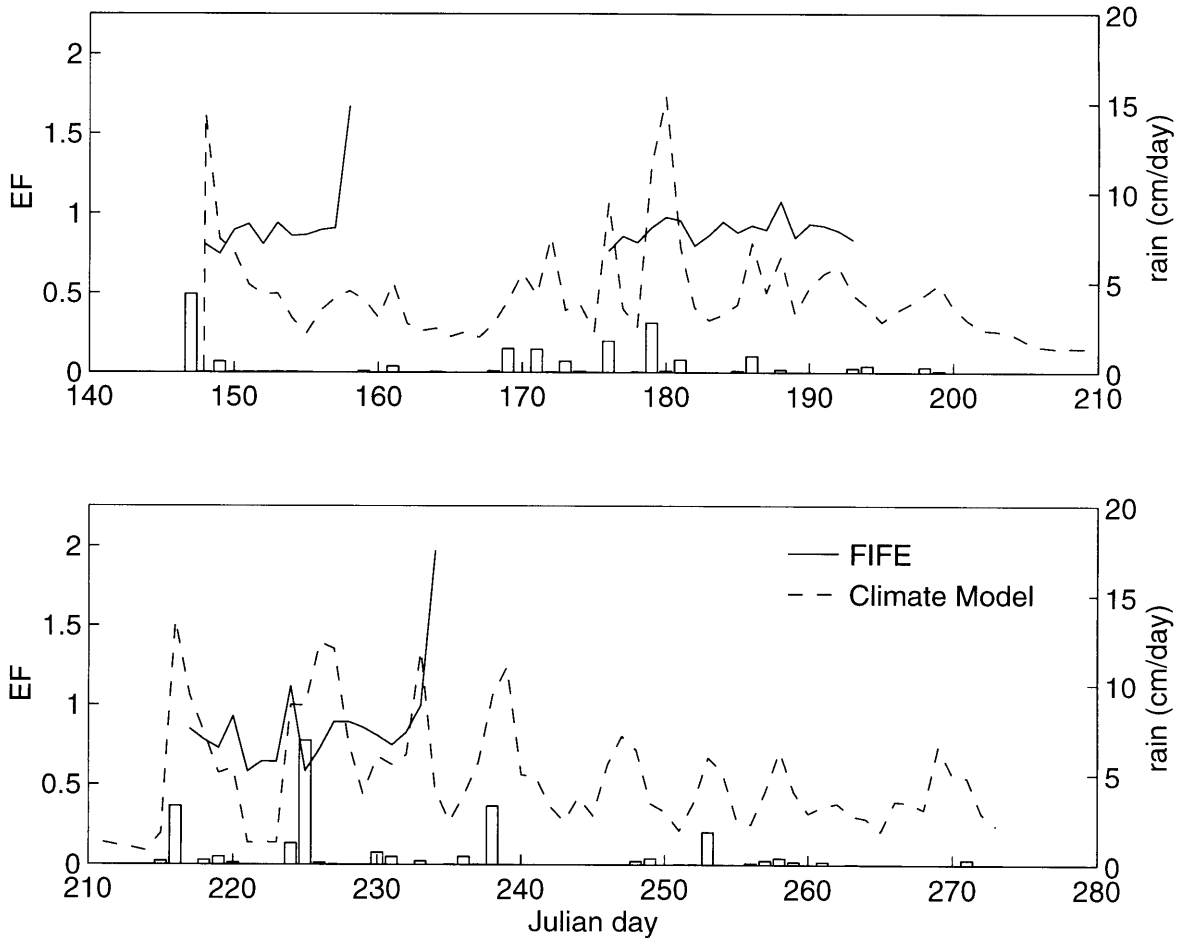

Figure 3-3: The daily mean evaporative fractions (EF) calculated using latent and sensible heat fluxes from the hydrological module in the Climate Model. The bar-graph shows 24-hour precipitation with the scale on the right axis.

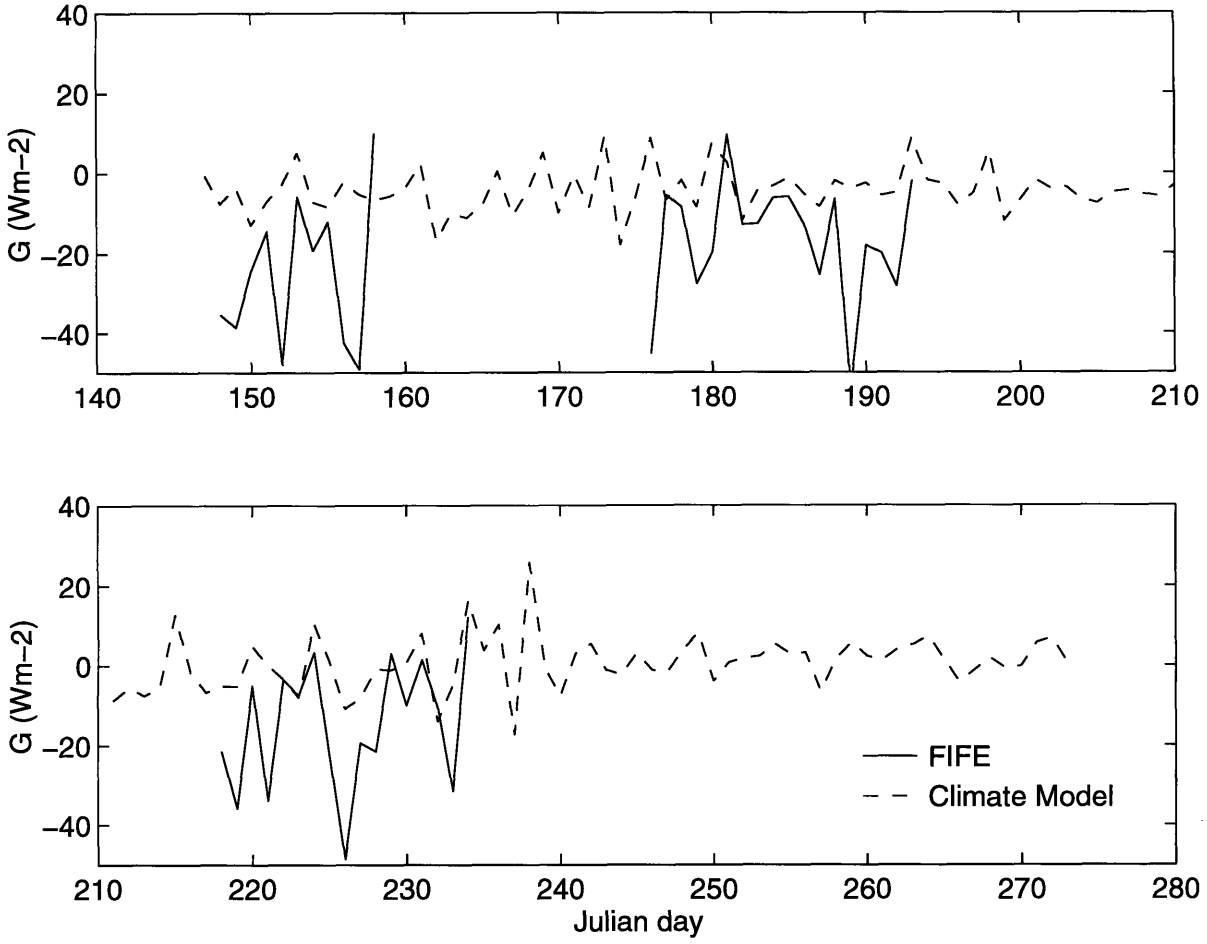

Figure 3-4: The daily mean ground heat fluxes (G) calculated by the hydrological module in the Climate Model are compared with three 2-week FIFE observational periods.

Ground heat flux The calculated ground heat fluxes (G) are compared with FIFE observations in Figure 3-4; fluxes are positive towards the surface. The magnitude of the calculated fluxes are always smaller than FIFE measurements, but the disparities are not large. Furthermore, the simulated G values do not reflect the large fluctuations or large amplitude observed in the Konza region. According to Betts [4], measurements of G are site specific and are less representative of large scale measurements. The aggregation of measurements over the 19 stations may have disturbed possible small-scale trends. This may be one instance when the exact locations of the atmospheric and flux data collection stations could play a role. Therefore, the disparity may be due to either deficiencies in the model's representation of the Konza site, or the differences in the atmospheric and flux data collection stations.

Net radiative flux Net radiative fluxes (R_n) calculated by the hydrological module in the Climate Model show a very good fit to FIFE observations in Figure 3-5. Net radiation is one of the fields measured along with atmospheric data, and therefore is available for the entire analysis period. This module calculates net radiation as

$$net\ radiation = net\ solar\ radiation - net\ longwave\ radiation, \quad (3.3)$$

$$net\ solar\ radiation = solar\ radiation * (1 - albedo), \quad \text{and,} \quad (3.4)$$

$$net\ longwave\ radiation = upward\ longwave - downward\ longwave. \quad (3.5)$$

All the above values except upward longwave radiation are inputs to the module; and upward longwave radiation is calculated using the Stefan-Boltzmann relationship. Therefore, the model calculates R_n with ease.

Upper soil layer temperature The upper soil layer temperature (T_g) of the hydrological module in the Climate Model are compared with FIFE observations in Figure 3-6. Here too, observations are available for the entire analysis period. In general, the calculated ground temperatures compare well with observations. The amplitude of calculations is larger, and the fluctuations in the calculations are more

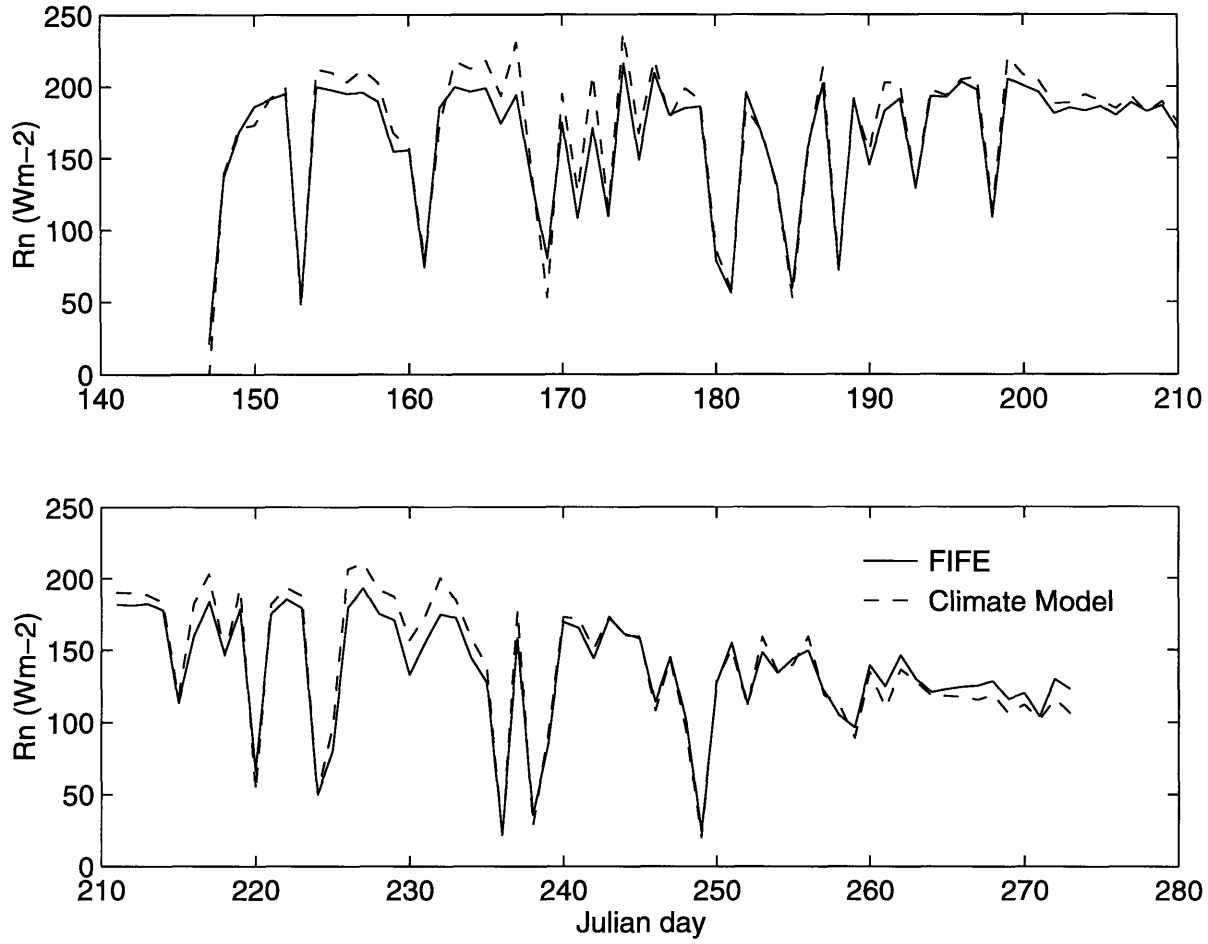

Figure 3-5: The daily mean net radiative fluxes (R_n) calculated by the hydrological module in the Climate Model are compared with FIFE observations.

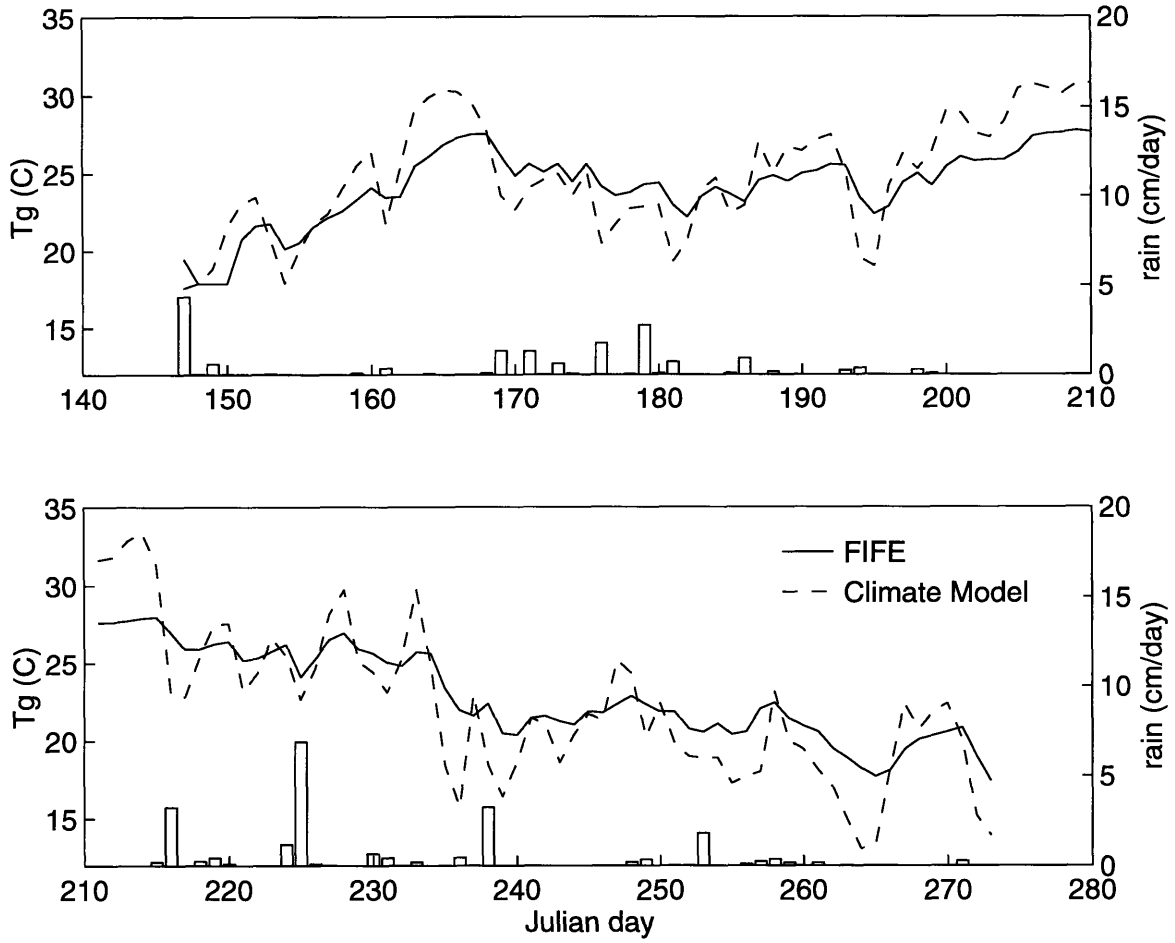

Figure 3-6: The daily mean upper soil layer temperatures (T_g) calculated by the hydrological module in the Climate Model are compared with FIFE observations at 10 cm depth. The two soil layers in this module are 10 and 190 cm thick.

pronounced than in observed values.

The larger fluctuations are also related to soil moisture availability. At each time step ground temperature is updated as

$$new\ T_g = old\ T_g + \frac{(heat\ flux\ in\ at\ upper\ bdy - heat\ flux\ out\ of\ lower\ bdy)}{soil\ moisture\ availability\ *\ heat\ capacity}. \quad (3.6)$$

Since the model's soil moisture values are often smaller than those observed in the Prairie, fluctuations in calculated T_g are exaggerated than observed T_g. In addition, the model overestimates T_g when the soil is dry and underestimates T_g when the soil is wet. Errors in T_g calculations feed into H calculations since the difference in T_g calculated in the previous time step and atmospheric temperature in the current time step drives H flux calculations. A more accurate soil moisture estimate will improve T_g calculations as well.

3.3.2 The hydrological module in the Natural Emissions Model

Latent heat flux The latent heat fluxes (λE) calculated by the hydrological module in NEM are compared with FIFE observations in Figure 3-7. Upward fluxes are shown as positive. Unlike in the previous module, the calculated fluxes are larger than FIFE observations. Mid-Summer λE correspond to observations best. This model is extremely sensitive to heavy rain events: evaporation far exceeds observed values immediately after a rain event, but decreases to values far below observed levels if the initial rain event were not followed by successive smaller rain events.

As mentioned in Section 2.2.2, the Thornthwaite [29] monthly potential evaporation equation that was initially used in this module was replaced with Hansen *et al.* [14] potential evaporation relationships. The evaporation algorithm in this module is formulated such that if the water content in either of the first two soil layers were greater than its assigned field capacity, water from that layer evaporates at half the potential rate. While this method successfully estimates evaporation from the uppermost layer, which is 10 cm thick, this overestimates evaporation from the second

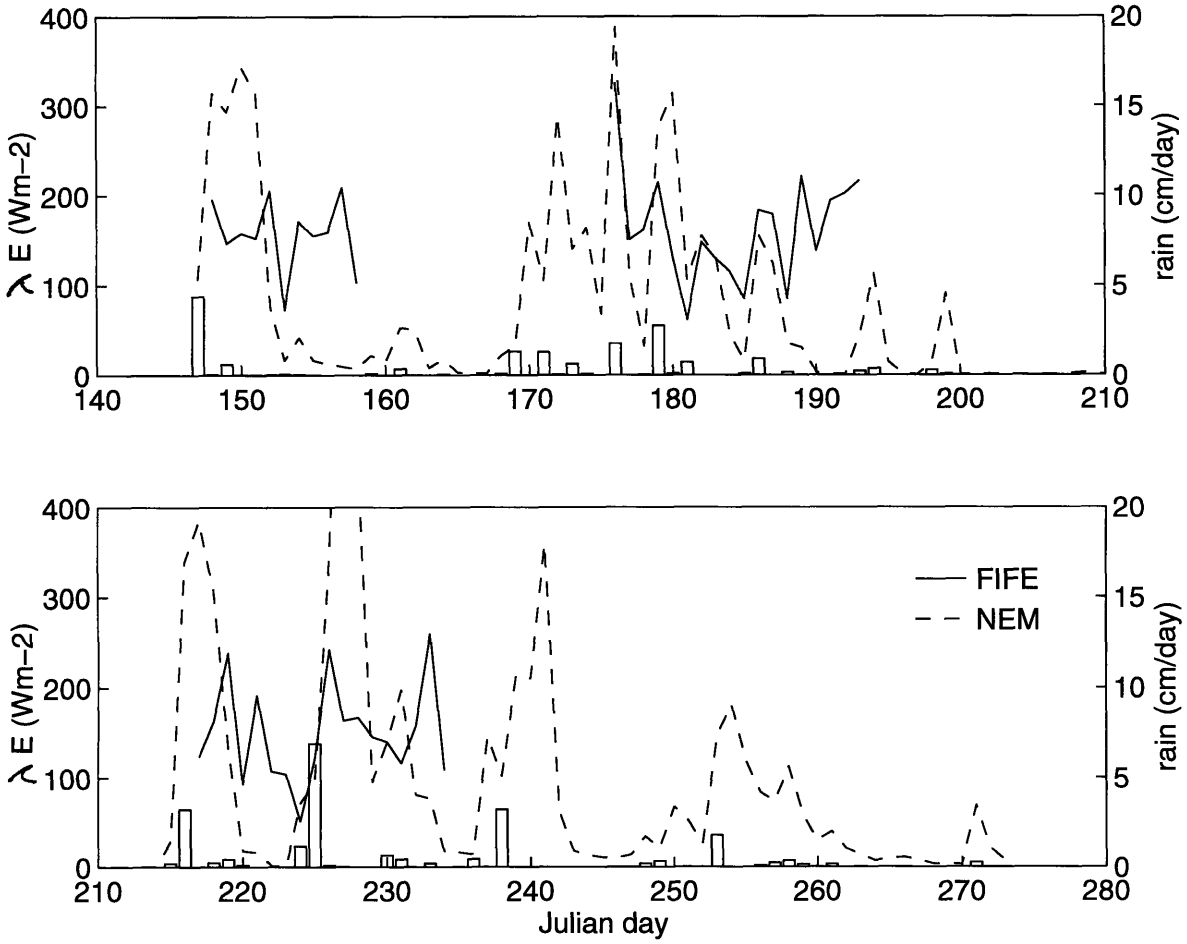

Figure 3-7: The daily mean latent heat fluxes (λE) calculated by the NEM hydrological module are compared with FIFE observations. The bar-graph shows 24-hour precipitation with the scale on the right axis.

layer, which has boundaries at 10 and 20 cm depths. Furthermore, in this module each layer is totally saturated before rain water is added to the next layer. Recall Section 2.2.2. Therefore, soon after a heavy rain event the water contents in the two top layers of the module are often larger than they actually are in the Konza site; this excessive moisture content then triggers larger than observed λE fluxes. But the model successfully captures the observed λE trend during less intense but prolonged rainy periods. During such periods the model has enough time to infiltrate water to deeper layers and avoid large moisture levels in the upper layers.

In addition, the amplitude of the calculations are larger than the amplitude of the observations, and the disparity between the observed and calculated values does not decrease as the Summer progresses. This model does not explicitly represent the vegetative cover of this site. But the three periods of observations do not allow generalizations about seasonal flux variations or about the lack of vegetation cover representation.

Sensible heat flux Comparisons of the sensible heat fluxes from the hydrological module in NEM and FIFE observations are shown in Figure 3-8. Here too, errors in both λE and H tend to occur together since the same drag coefficient parameterization from Hansen*et al.* [14] was substituted for both latent and sensible heat calculations. H fluxes fluctuate a lot. Sensible heat flux calculations of this module appear to be overly sensitive to rain events, and causes the module to lose large amounts of H on wet days. This does not mimic FIFE observations well.

Evaporative fraction The evaporative fractions (EF) for the hydrological module in NEM are compared with FIFE values in Figure 3-9. The already large λE calculations together with the negative H fluxes result in large evaporative fractions for this module. The calculated EF after rain events are often about three times as large as the observed value. Unlike in the Climate Model, too much of available heat is channeled as λE flux in this model.

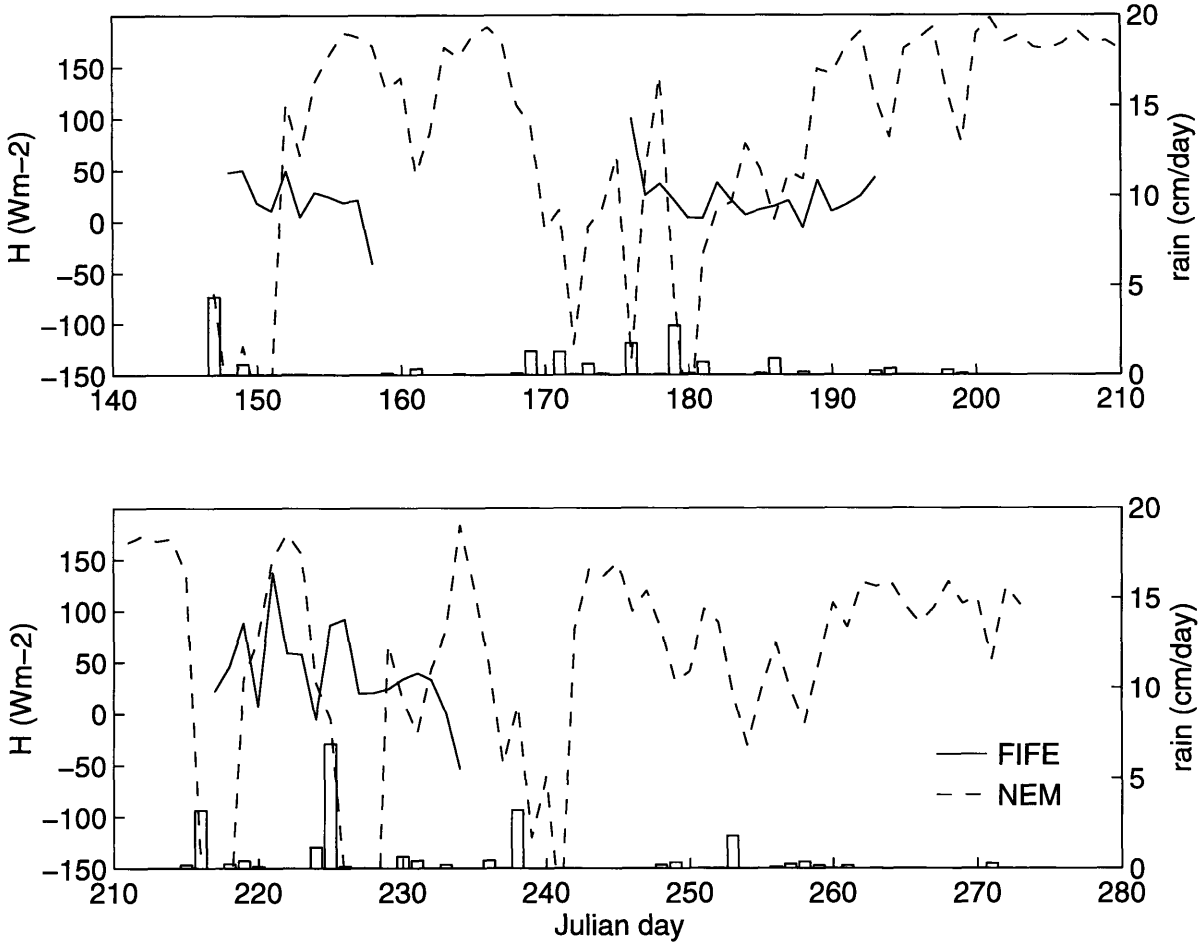

Figure 3-8: The daily mean sensible heat fluxes (H) calculated by the NEM hydrological module are compared with FIFE observations. The 24-hour precipitation is shown by the bar-graph.

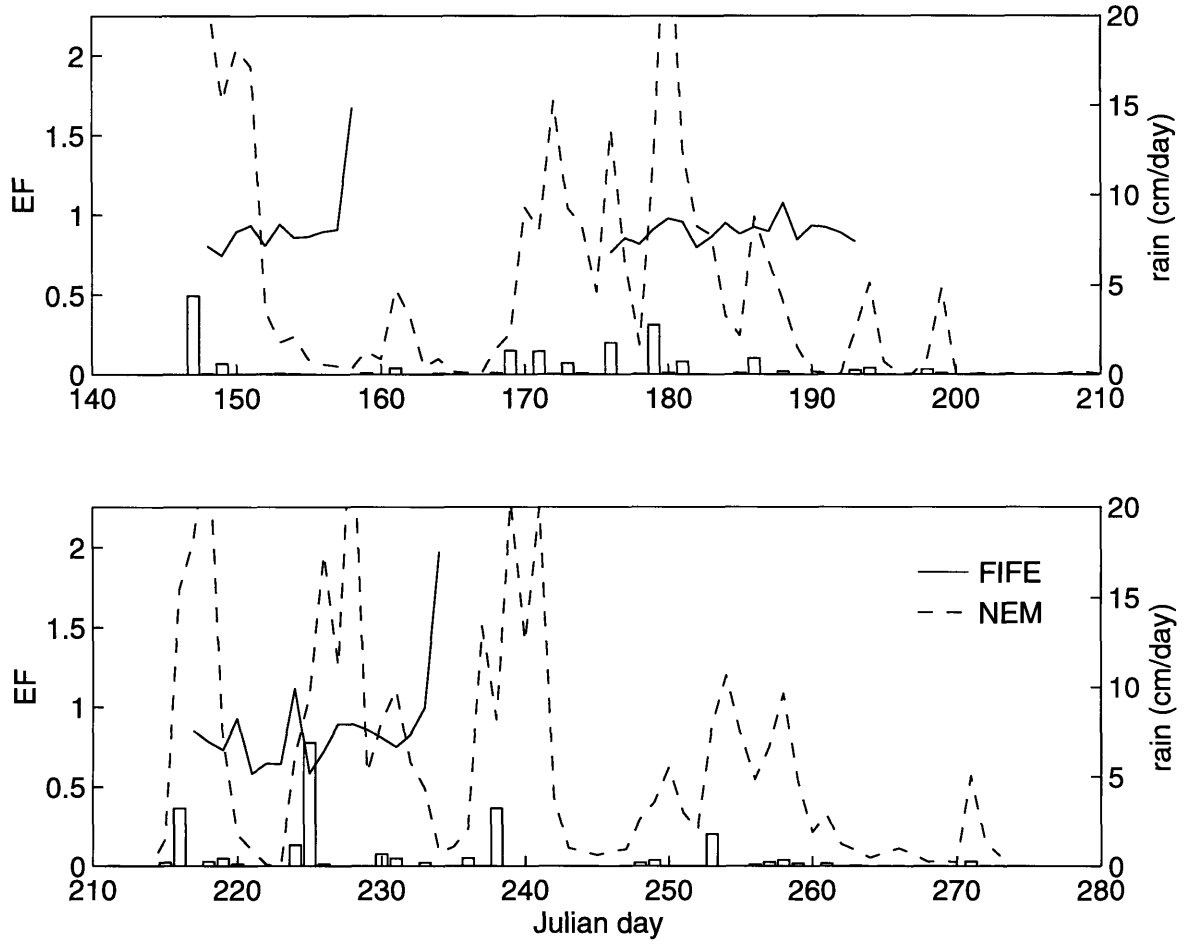

Figure 3-9: The daily mean evaporative fractions (EF) calculated using latent and sensible heat fluxes from the hydrological module in NEM are compared with observed evaporative fractions for three 2-week periods. The bar-graph shows 24-hour precipitation with the scale on the right axis.

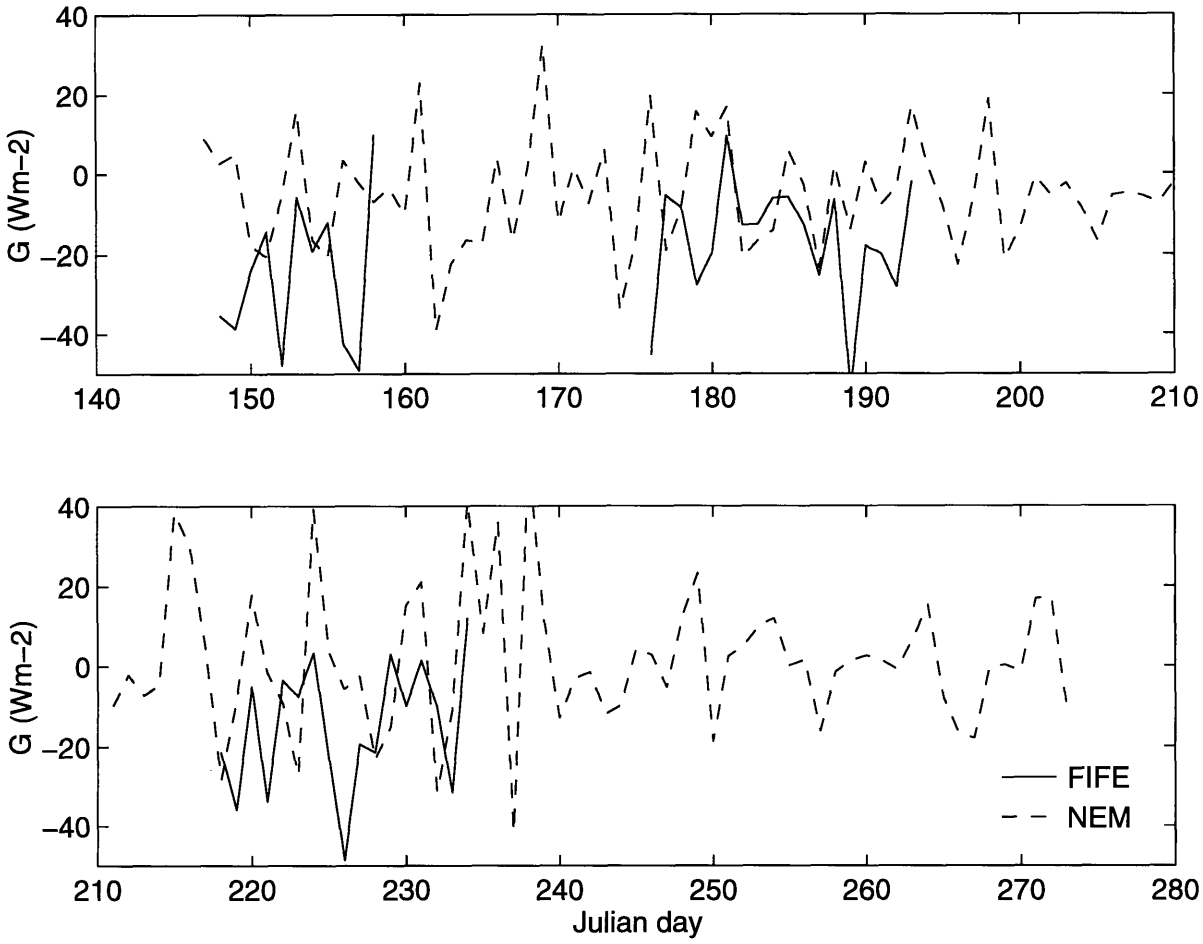

Figure 3-10: The daily mean ground heat fluxes (G) calculated by the NEM hyrological module compared with FIFE observations.

Ground heat flux The ground heat flux calculations (G) of NEM are compared with FIFE observations in Figure 3-10. G is positive towards the surface. G is calculated as

$$G = R_n - \lambda E - H, \tag{3.7}$$

where λE and H are calculated from within the module; and R_n is an input to the module. The magnitudes of simulated G are often larger than FIFE measurements, but the disparities are not large. The amplitude of the calculated values are comparable to those observed.

Uppermost soil layer temperature The uppermost soil layer temperature of the hydrological module in the NEM and FIFE observations are compared in Figure 3-11. Calculated T_g compare reasonably well with observations. And just as with the Climate Model, when the top soil layer is wet the model predicts the soil layer to be slightly cooler than FIFE measurements, and when the top soil layer is dry the model predicts a warmer surface layer than observed. This discrepancy feeds into the H calculations as seen earlier. This error is consistent throughout the analysis period.

Just as in the previous module, the amplitude of the calculated values are larger than the observed values. This model uses a ground temperature updating mechanism similar to the one in the Climate Model.

$$new\ T_g = old\ T_g + \frac{(heat\ flux\ in\ at\ upper\ bdy - heat\ flux\ out\ of\ lower\ bdy)}{heat\ capacity\ of\ the\ soil\ and\ water\ mixture}. \tag{3.8}$$

This calculation is influenced by two main entities—the heat flux at the upper boundary and the heat capacity of the soil-water mixture. As previously mentioned, the ground heat flux at the upper boundary is calculated with Equation 3.7; therefore, errors in λE, H, and R_n fluxes influence G calculations. Next, the heat capacity depends on soil water content—when the soil layer is drier the heat capacity is smaller, therefore, the relative change in temperature is larger. So T_g is allowed to increase above the observed value when the soil is dry. Conversely, (a) the saturated conditions allowed in the uppermost layer during heavy rain events, (b) the large net loss of heat

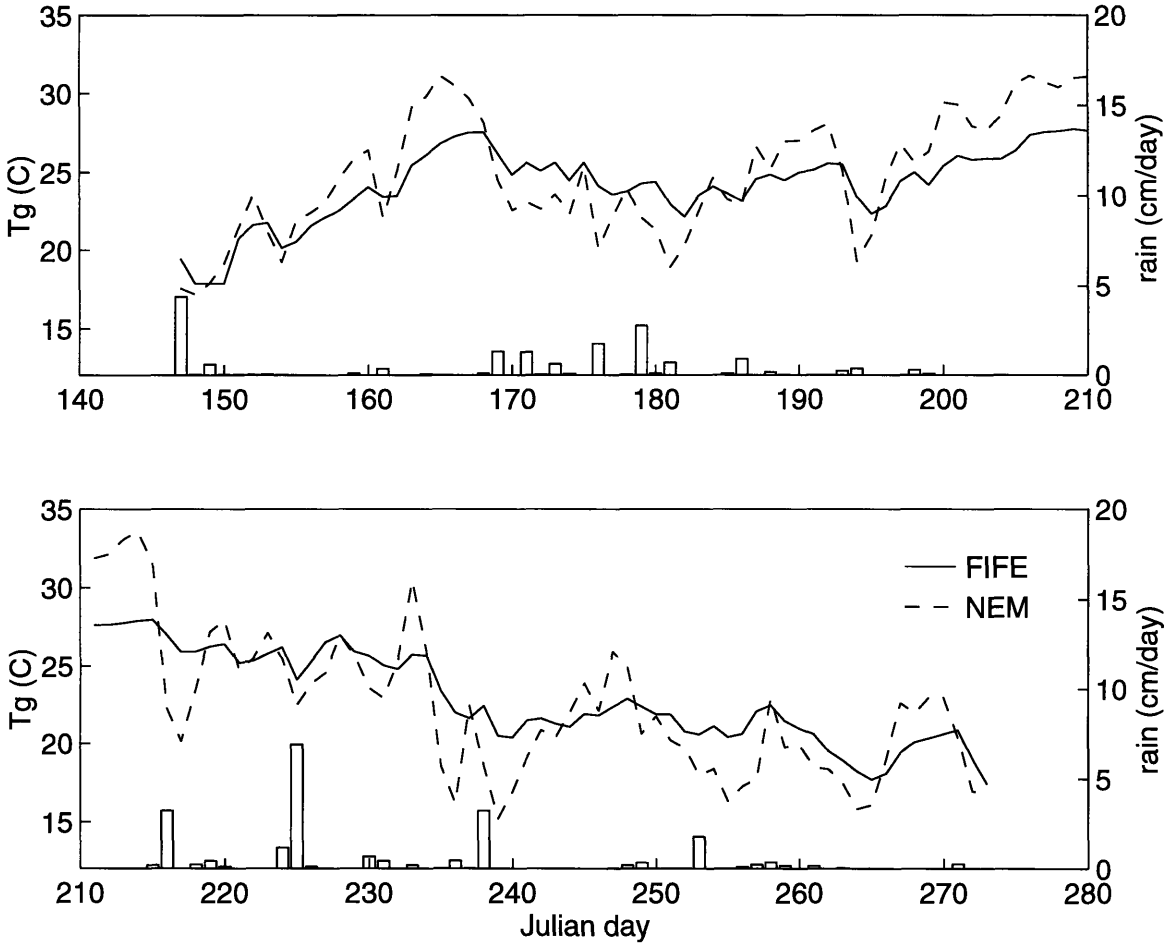

Figure 3-11: The daily mean uppermost soil layer temperatures (T_g) calculated by the NEM hydrological module are compared with FIFE observations. Each of the five soil layers used in this model is 10 cm thick; calculations are done at the center of each layer. The first set of FIFE ground temperature measurements is at a 10 cm depth.

in the form of λE from the top layer, and (c) the large calculated heat capacities in the uppermost layer yield smaller ground temperatures on wet days.

3.3.3 The NCAR LSM

Latent heat flux Latent heat fluxes of the NCAR LSM and FIFE observations are compared in Figure 3-12. Simulated values compare well with observations—especially those for the late June-early July period (176-193 Julian days). But the model is overly sensitive to heavy rain events: the model simulates sharp λE peaks after the rainy 216^{th} and 225^{th} Julian days, but λE drops once the very wet period is over. The model follows the observed trend well during the first two months of the analysis period and less well during the third month; the amplitude of the calculated values is larger than that of the observed values for the second half of the analysis period.

Sensible heat flux Comparisons of the sensible heat flux from the NCAR LSM and FIFE observations are shown in Figure 3-13. The calculated values of this model are comparable to the observed values—slightly better than the hydrological module in the Climate Model; the range of these calculated values is much larger than the FIFE observations—worse than the Climate Model. This model performs better than the hydrological module in NEM in terms of both range and average values. Just as with λE calculations, the model exaggerates H response to rain events; but unlike with λE the LSM simulations of H for the second and third weeks of August (Julian days 216-235) follow observations best.

Evaporative fraction The evaporative fractions for the NCAR LSM and FIFE observations are shown in Figure 3-14. The calculated daily mean values for days when FIFE measurements are available are comparable to the observations; but the range of calculated values is larger than the range of observations. Due to the sharp peaks in λE and troughs in H soon after rain events, the EF values calculated for immediately after rain events are larger than the values observed—although not quite

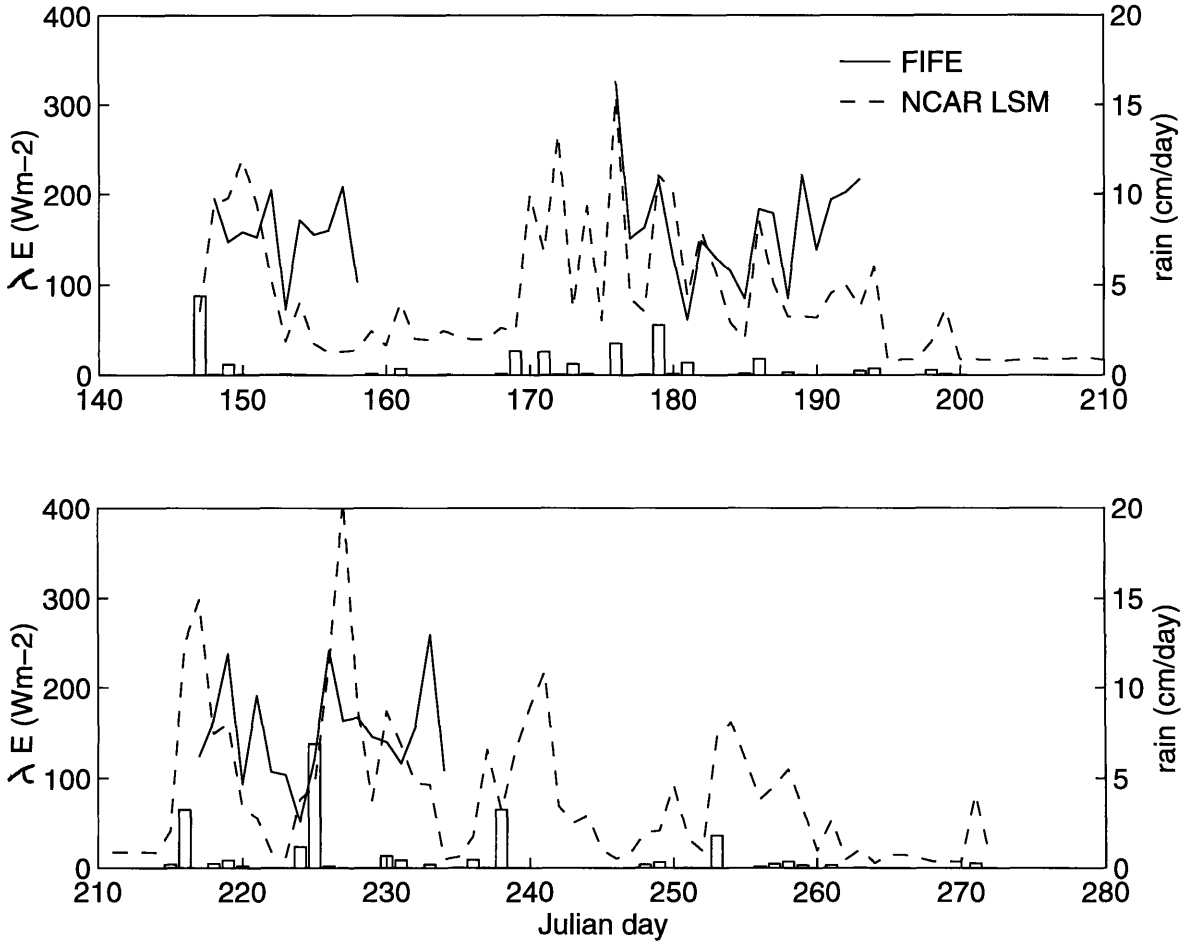

Figure 3-12: The daily mean latent heat fluxes (λE) calculated by the NCAR LSM for the Konza Prairie for May 27 - September 30, 1987, are compared with FIFE observations. The bar-graph shows 24-hour precipitation with the scale on the right axis.

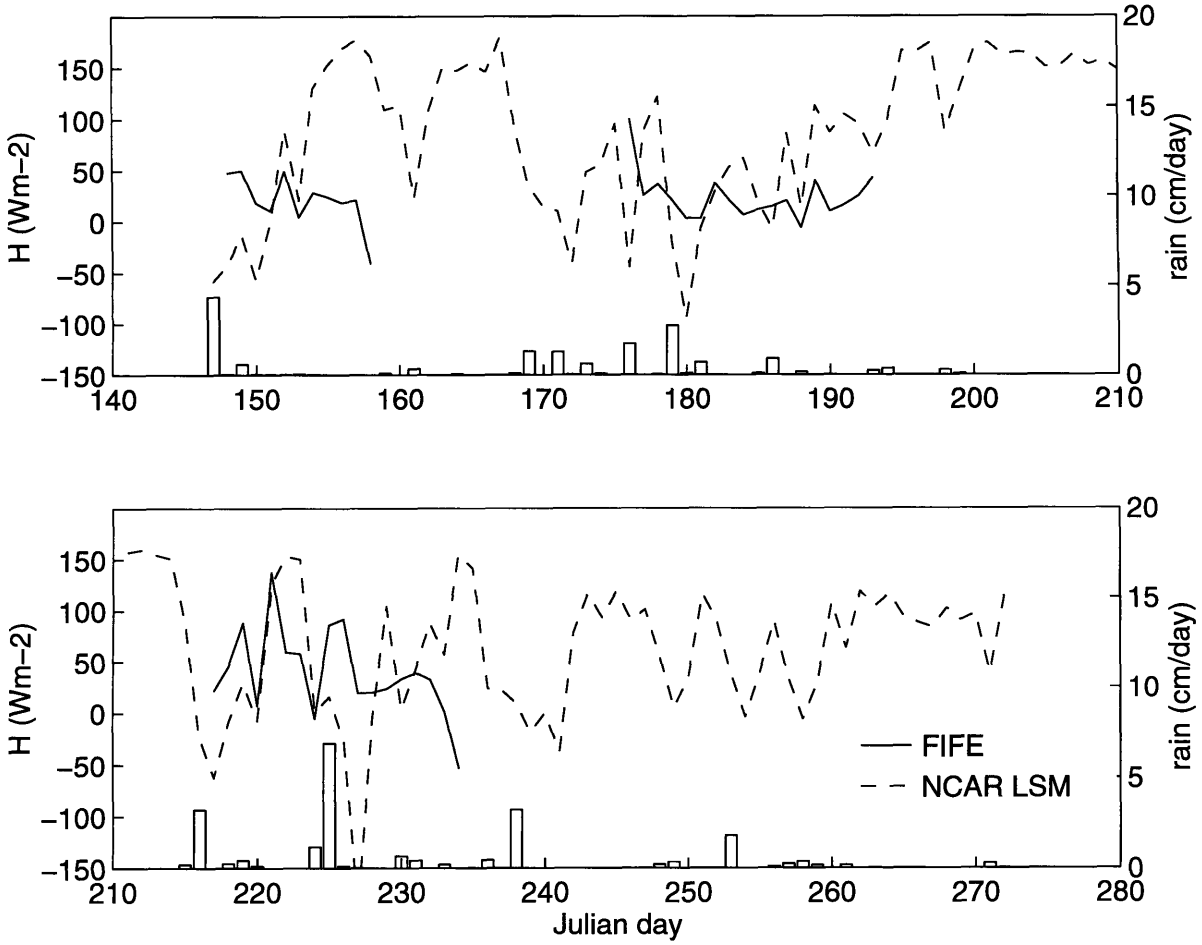

Figure 3-13: The daily mean sensible heat fluxes (H) calculated by the NCAR LSM for the Konza Prairie. The solid lines show the three 2-week periods for which FIFE observations were available. The bar-graph shows 24-hour precipitation with the scale on the right axis.

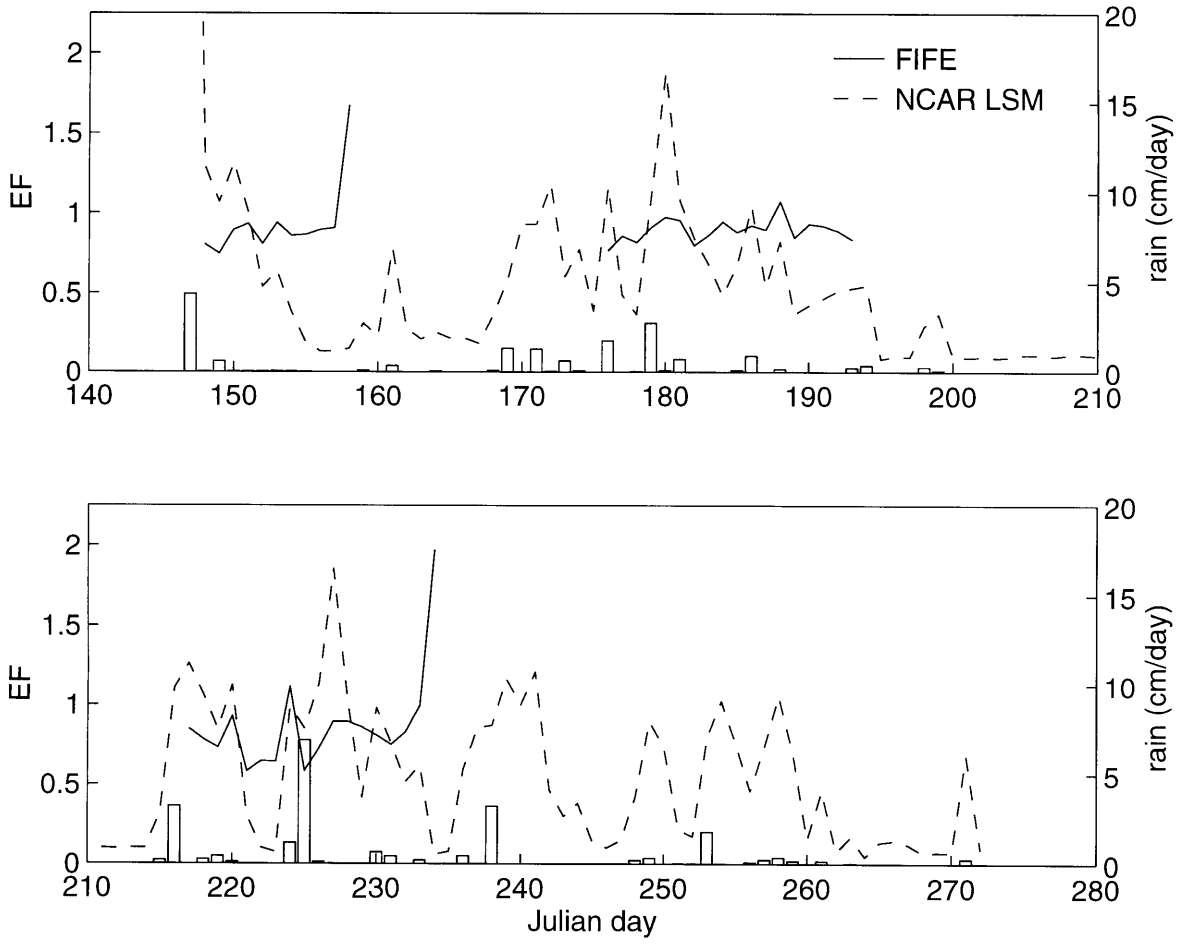

Figure 3-14: The daily mean evaporative fractions (EF) calculated using latent and sensible heat fluxes from the NCAR LSM. The bar-graph shows 24-hour precipitation with the scale on the right axis.

as large as the values from NEM.

Ground heat flux The NCAR LSM daily mean ground heat flux calculations (G) are compared with FIFE daily mean values in Figure 3-15. The magnitudes of calculated daily mean G are slightly larger than FIFE measurements; but the simulated trend follows the observed trend well; and the range of the calculated daily mean values compare well with FIFE observations.

Net radiation Just as in the hydrological module in the Climate Model the calculated NCAR LSM net radiative fluxes follow FIFE observations well. These plots are presented in Figure 3-16. But unlike in the Climate Model, surface albedo is calculated from within the model. Therefore, this model's net radiation calculations will be valid even when the vegetation cover changes in different seasons.

Uppermost soil layer temperature The relationship between the uppermost soil layer temperature of the NCAR LSM and FIFE observations (shown in Figure 3-17) is similar to the relationships found in the two previous modules; but the disparity between the calculated and observed daily mean values is smaller than in the other two modules. The simulated ground temperature is lower than the observed values during and soon after rain events, but higher during dry periods. Here too, the soil temperatures are calculated using heat diffusion and one-dimensional energy conservation equations. Therefore, if the model G, H and λE deviate from the observed values, T_g would also deviate from its observed value during those time steps.

Albedo Figure 3-18 compares the daily mean albedo calculated by the NCAR LSM and the daily mean albedo observed at the Konza prairie. The daily mean albedo is the sum of reflected solar radiation for each day divided by the sum of incident solar radiation for that day. There is a clear difference between the values calculated for June-July and August-September periods. The simulated values improve as the Summer progresses and as the vegetation cover increases. The accuracy of the albedo calculations were limited by data available on Konza soil color, soil distribution and

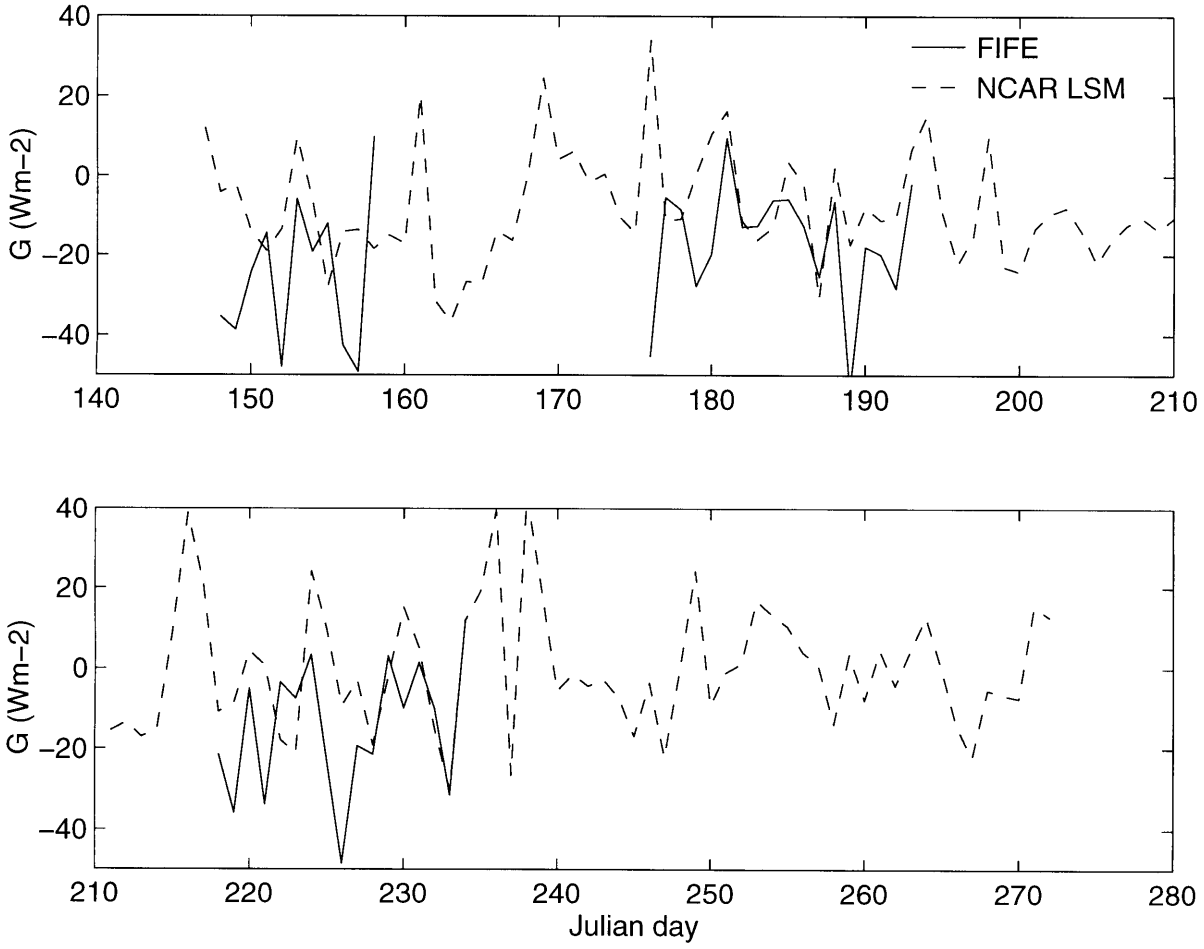

Figure 3-15: The daily mean ground heat fluxes (G) calculated by the NCAR LSM for the Konza Prairie for the May 27 - September 30, 1987, are compared with three 2-week blocks of FIFE observations during the same period.

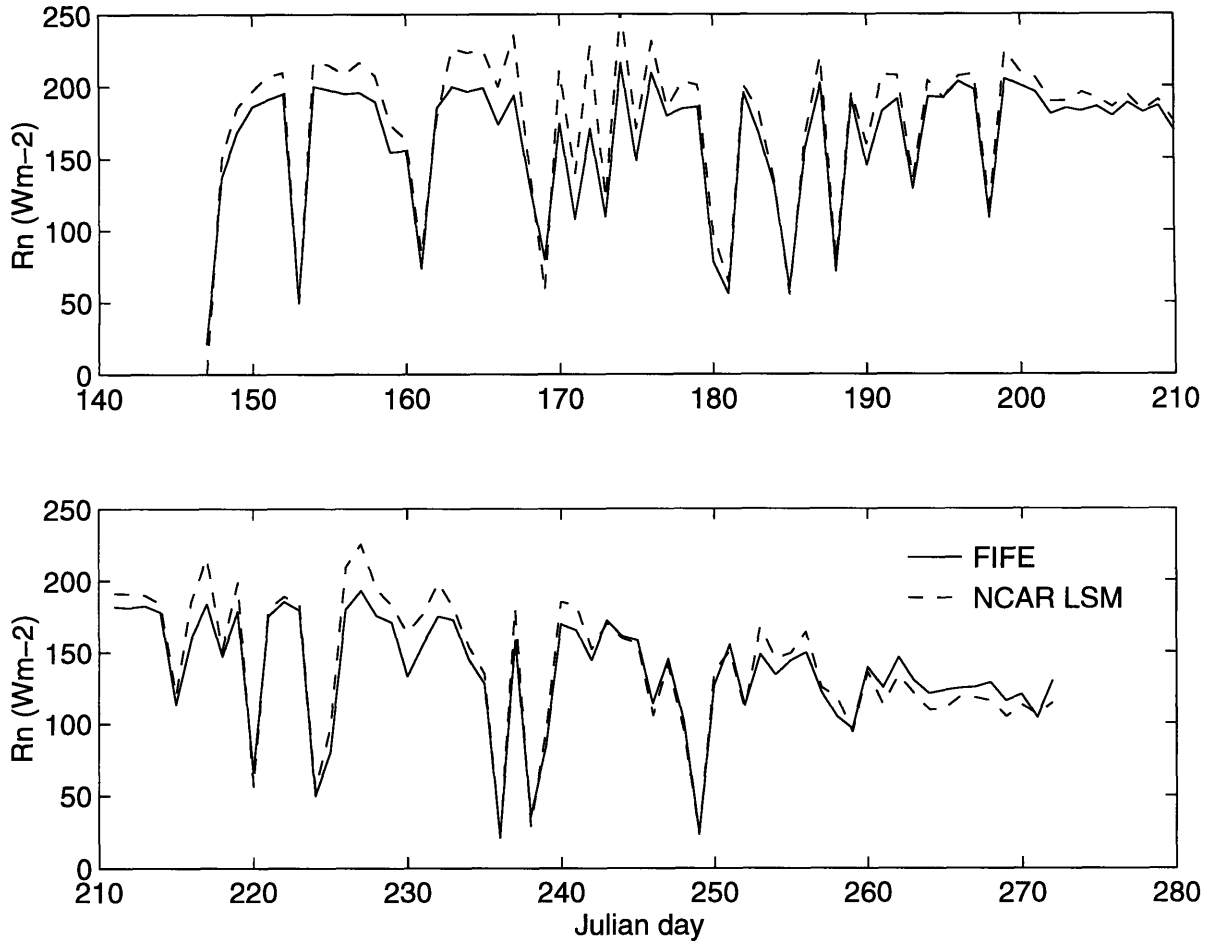

Figure 3-16: The daily mean net radiative fluxes (R_n) calculated by the NCAR LSM for the Konza Prairie for the May 27 - September 30, 1987, are compared with FIFE observations for the same period .

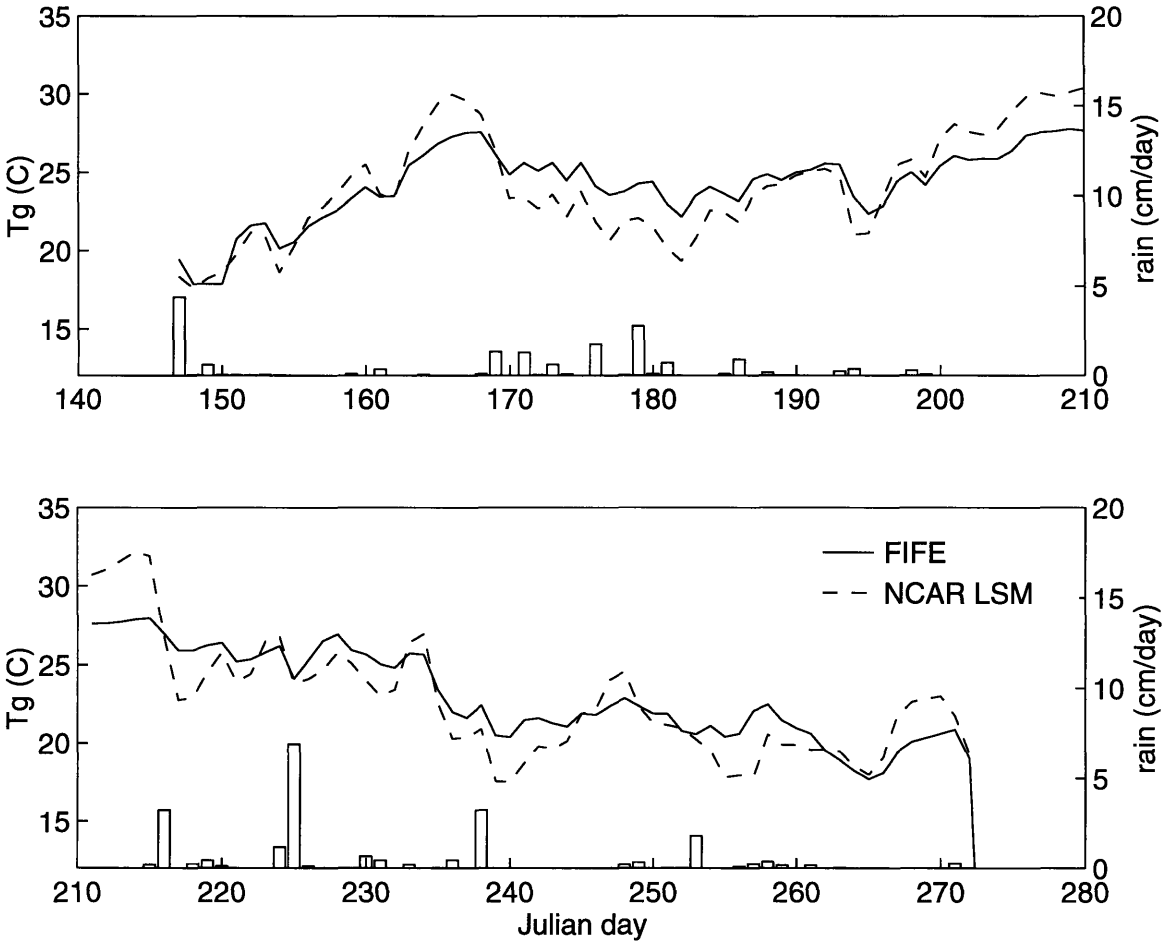

Figure 3-17: The daily mean uppermost soil layer temperatures (T_g) calculated by the NCAR LSM are compared with FIFE observations. The 10 cm thick uppermost soil layer of the NCAR LSM is one of six soil layers in the model; all calculations are done at the center of each layer. The first set of FIFE ground temperature measurements is at a 10 cm depth.

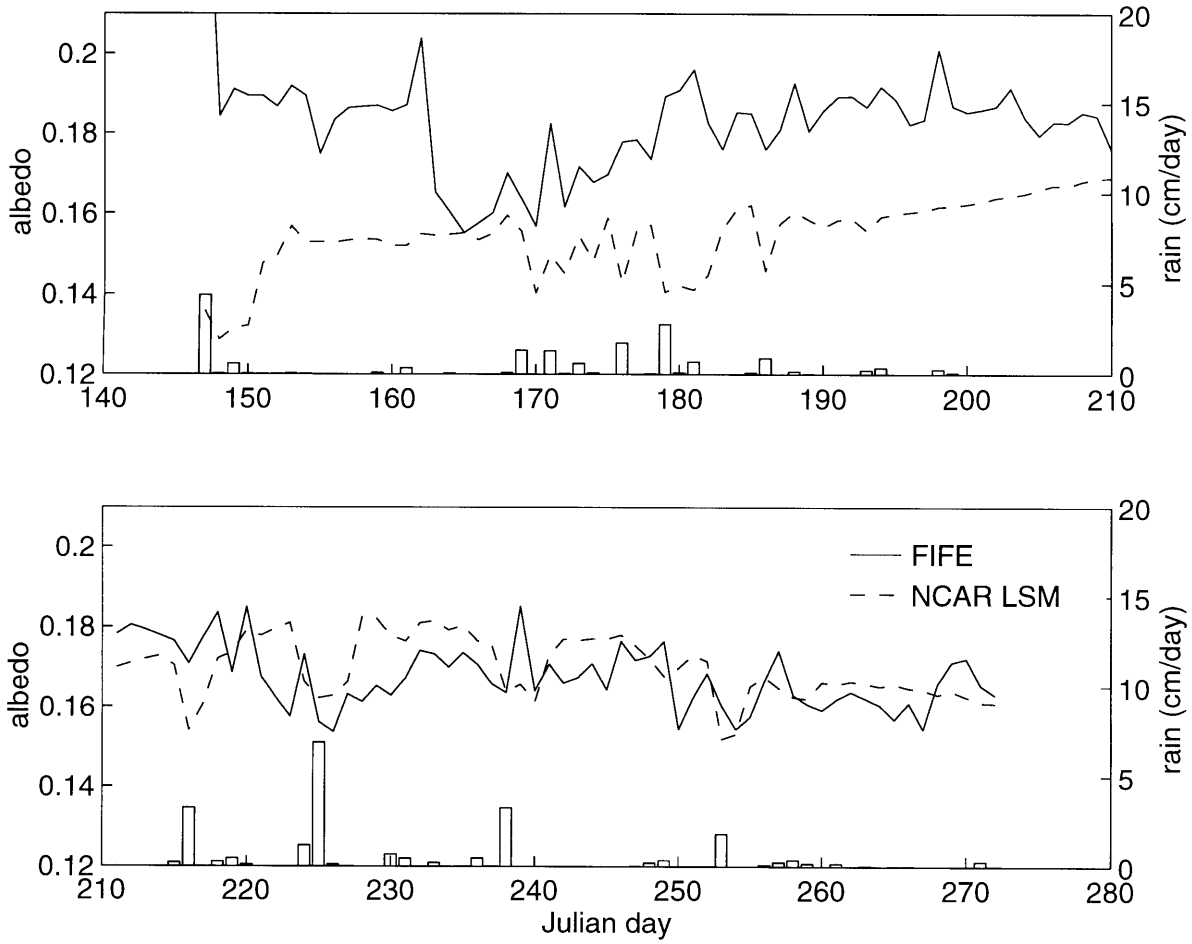

Figure 3-18: Albedos calculated by the NCAR LSM are compared with FIFE observations. Analysis period is from May 27 - September 30, 1987.

composition, and vegetation cover. According to the information available for the Konza Prairie about 40% of the land is covered with warm grass, another 10% with warm broadleaf deciduous trees, and the rest with bare soil; soil is composed of about 10% sand, 65% silt, and about 25% clay. The dark-colored soils that were used for the the entire region may be the reason for the underestimated albedos.

3.4 Intercomparisons of Simulated Daily Mean Values of the Three Models

Latent heat flux Figure 3-19 shows λE flux calculations of all three models. All three models follow similar trends but the amplitudes of the calculations are different; the hydrological module in NEM has the largest amplitude, while that in the Climate Model has the smallest amplitude. The λE flux in the hydrological module in the Climate Model is quick to respond to precipitation excitations, but is equally quick to lose the effect of that excitation; this module simulates its unique peaks that the other two models are ignorant of. While the LSM maintains the persistent nature NEM shows, the LSM does not display the extreme values NEM displays.

Sensible heat flux Figure 3-20 shows intercomparisons of the sensible heat fluxes of the three modules. Similar to λE calculations, the H calculations of the three models follow a common pattern, with the NEM showing the largest amplitude in calculation, and the Climate Model showing the smallest amplitude. The disparities between the models are smallest in July and September (Julian days 195-215 and 244-273) when reduced rainfall suppress soil moisture influences and help avoid the deep troughs in model simulations.

Evaporative fraction The daily mean evaporative fraction for the two hydrological modules and the NCAR LSM are given in Figure 3-21. The amplitude of the values calculated from the Climate Model and LSM simulations are comparable, while the amplitude of NEM simulations are about twice as large as the simulations from the

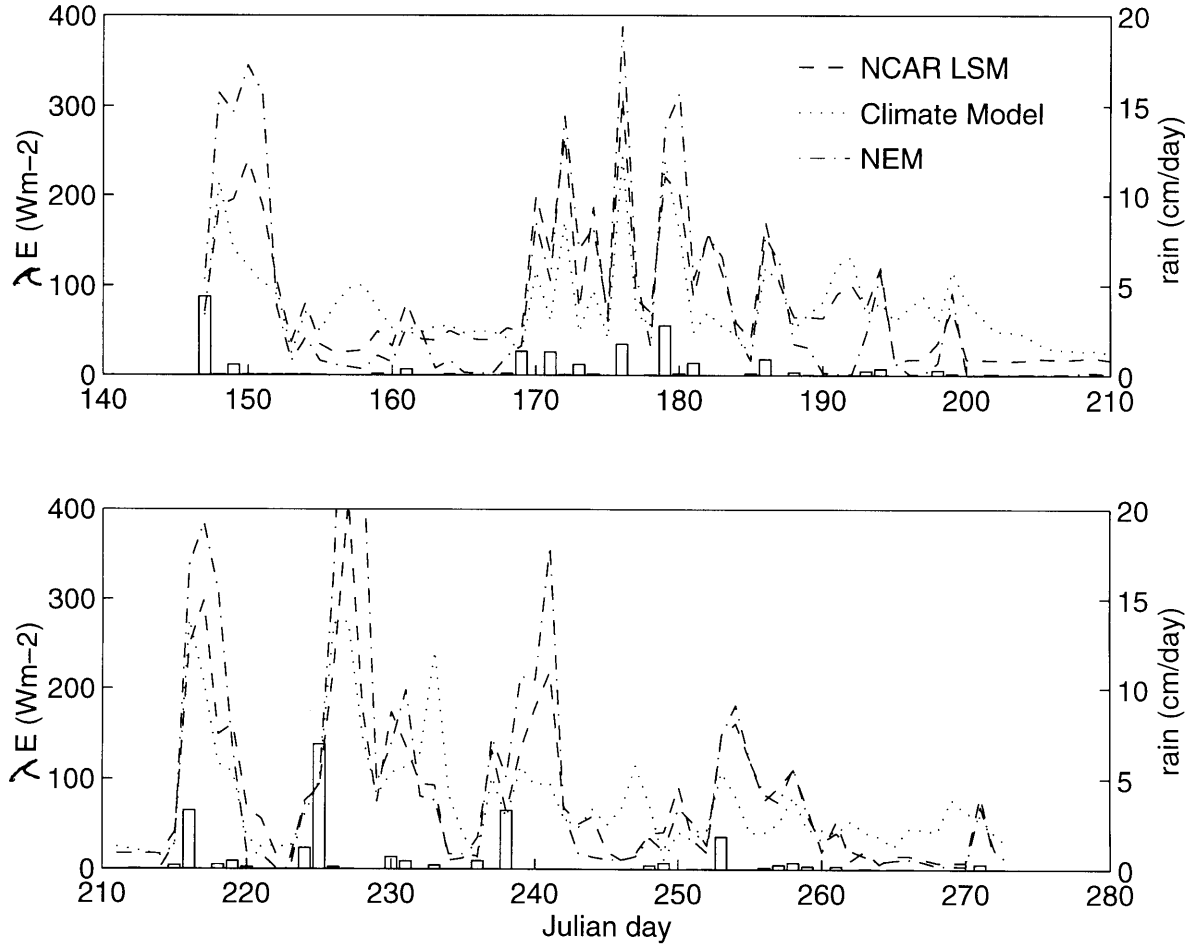

Figure 3-19: Comparison of daily mean latent heat fluxes (λE) between models.

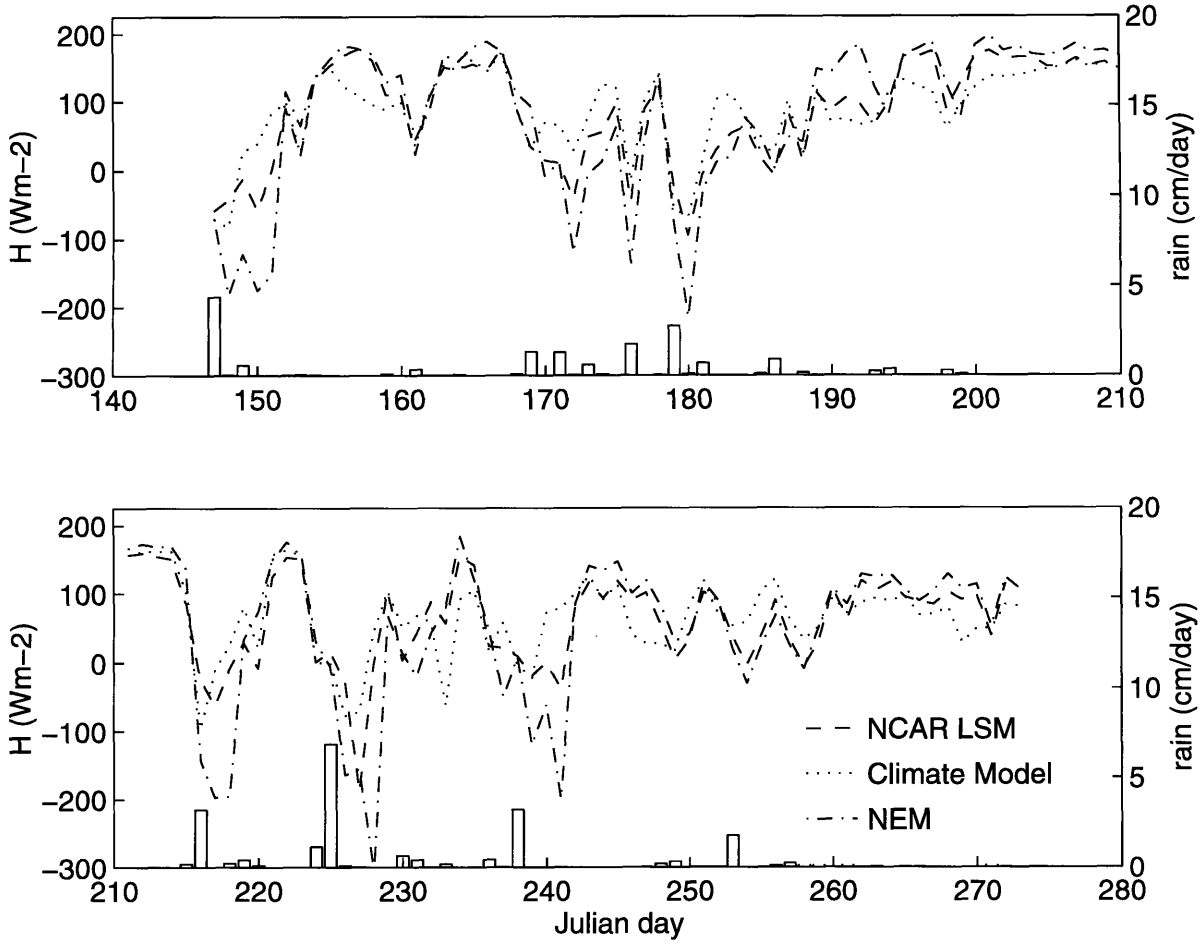

Figure 3-20: Comparison of daily mean sensible heat fluxes (H) between models.

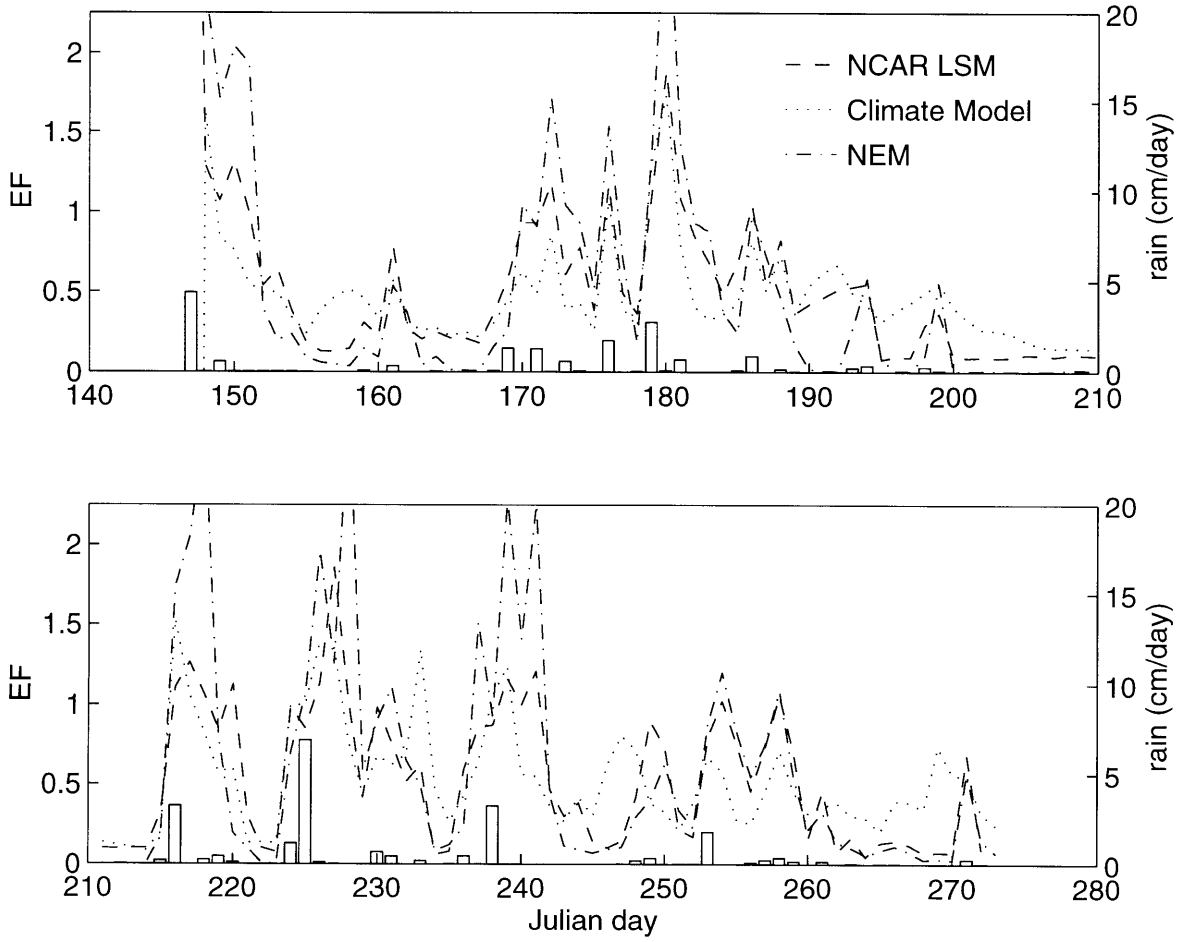

Figure 3-21: Comparison of daily mean evaporative fractions (EF) across models. Daily precipitation is shown by the bar-graph with the scale on the right axis.

other two models. There is better agreement between models when the soil is drier.

Ground heat flux Figure 3-22 compares the daily mean ground heat fluxes of the three models. Here the LSM and NEM calculations are in better agreement for the first three analysis months, and then their amplitudes decrease during September to the amplitude of Climate Model calculations. The Climate Model is less responsive to rain events throughout the analysis period. There is less variation between models in the final month when there are only a few rain events.

Net radiation Intercomparisons of the daily mean net radiative fluxes are shown in Figure 3-23. Simulations of the LSM and the hydrological module in the Climate Model agree almost perfectly. The discrepancies between actual and LSM's calculated albedos emerge in the R_n calculations. The slight variations in the LSM R_n calculations in the first part of the analysis period is due to albedo; but as this figure attests, the effect of the albedo discrepancy is small.

Daily mean uppermost soil layer temperature The uppermost soil layer temperatures of all three models are shown in Figure 3-24. LSM simulations have the smallest amplitude while the Climate Model simulations have the largest amplitude. All three models follow the same trend.

Daily mean soil moisture in the uppermost layer Soil moisture levels affect calculations of many of the other parameters. Soil moisture is among the more important soil characteristics incorporated in ground temperature calculations. While the simpler models calculate λE, H, and G in sequence and then update T_g, more sophisticated models like the NCAR LSM calculate the above fluxes simultaneously, and evaluate ground and soil temperatures that meet the energy balance requirements of the system. The magnitudes of calculated λE and H, which themselves depend on the amount of soil moisture, influence the amount of heat input to the soil column; the soil layer temperature calculations also depend on the relative saturation of each soil layer. Therefore, the accurate representation of soil moisture levels in model

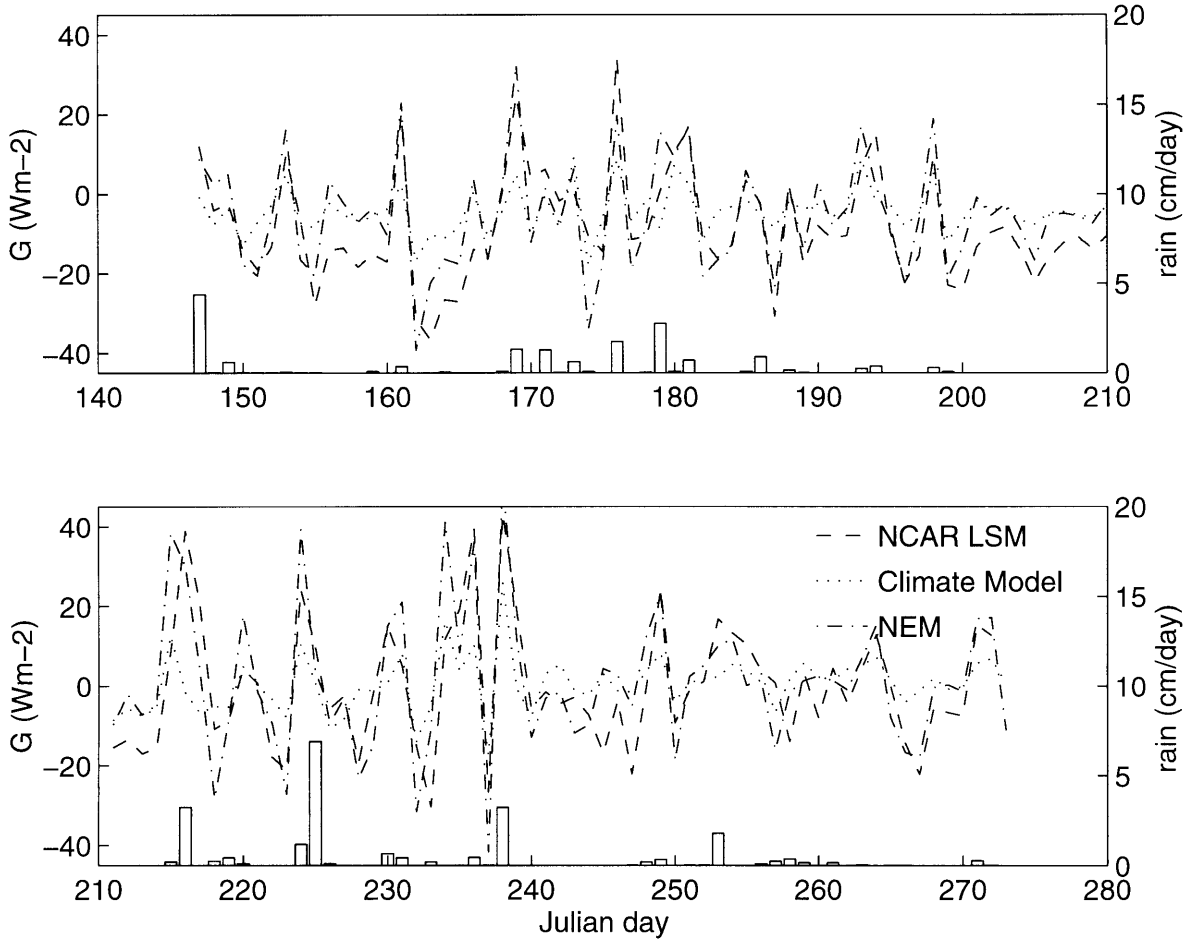

Figure 3-22: Comparison of daily mean ground heat fluxes (G) across models.

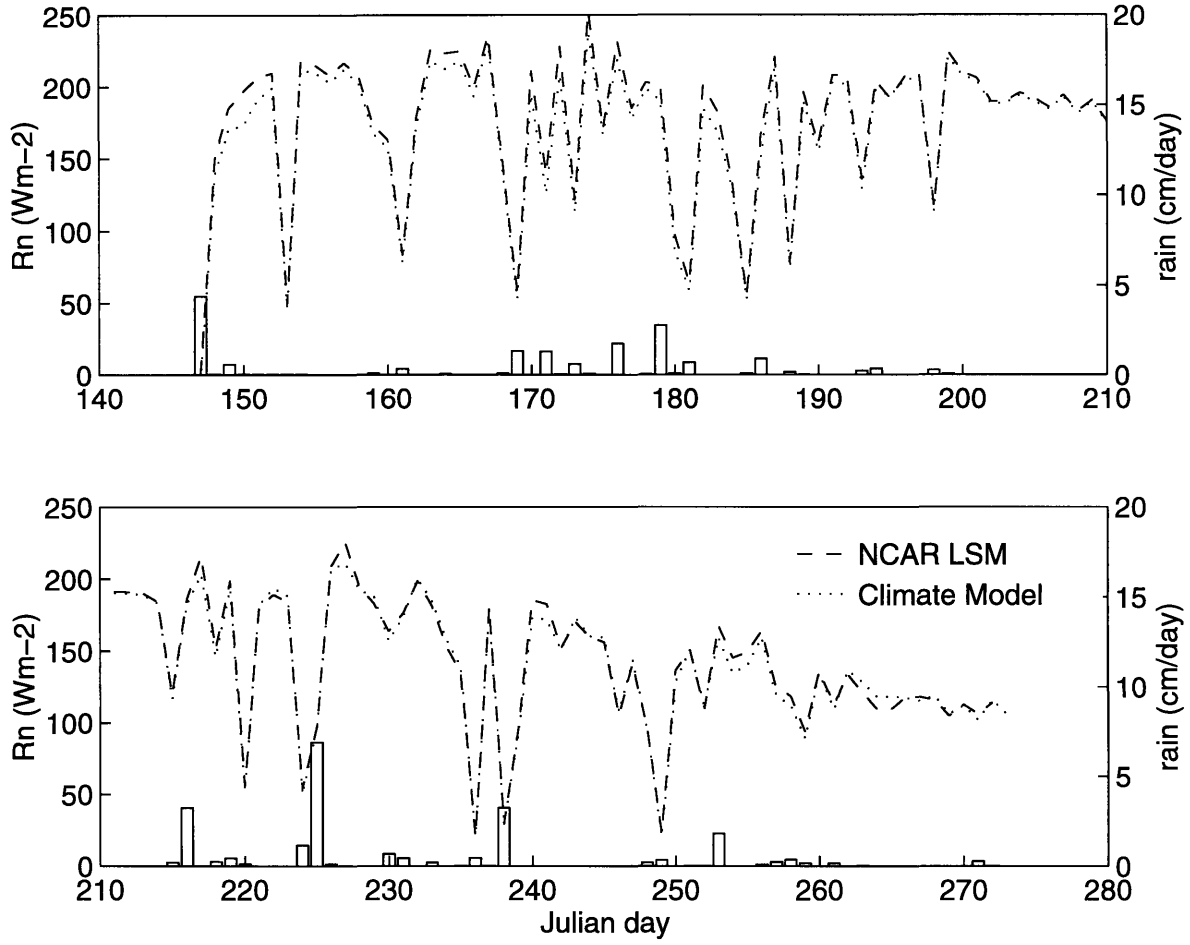

Figure 3-23: Comparison of daily mean net radiative fluxes (R_n) for the NCAR LSM and the Climate Model.

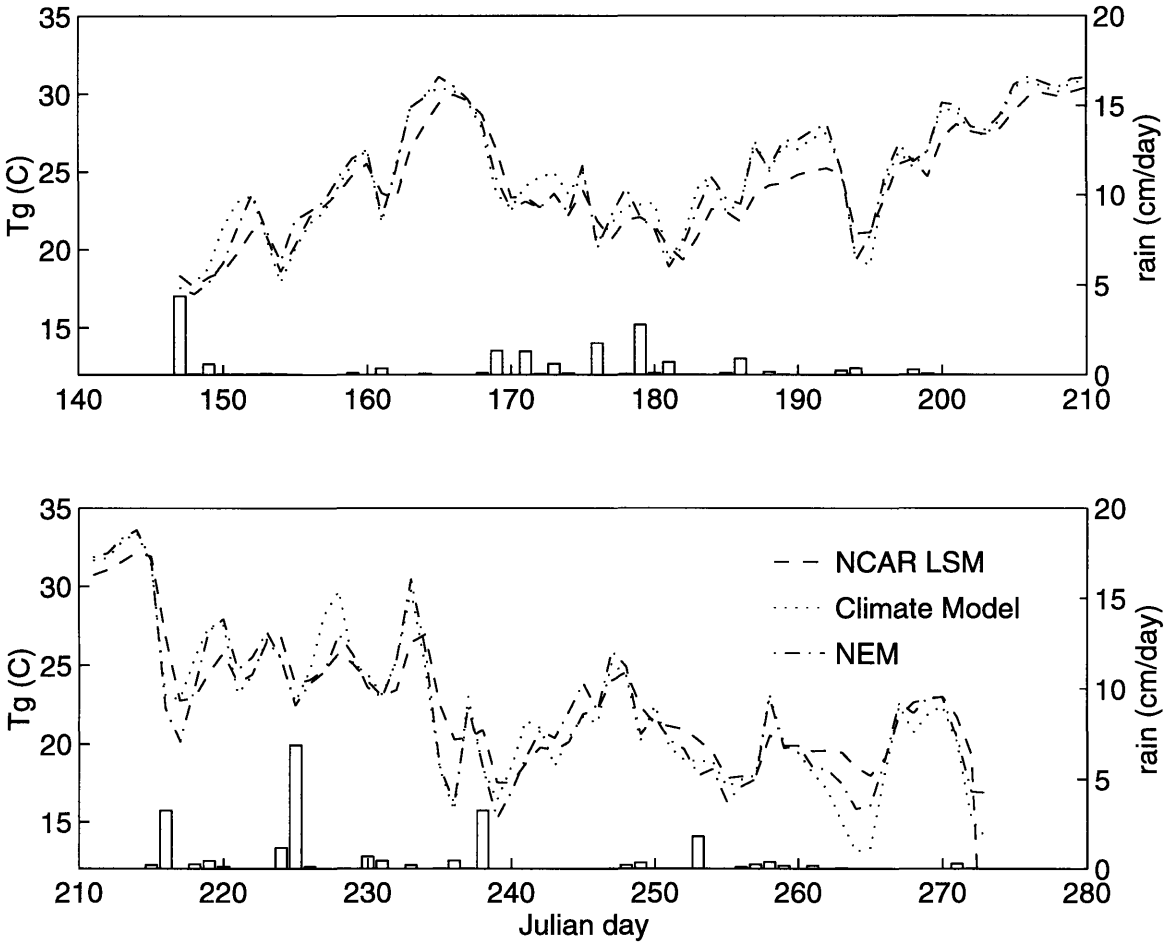

Figure 3-24: Comparison of the daily mean uppermost soil layer temperatures (T_g) for the three modules. The uppermost soil layers of models are 10 cm thick. The NCAR LSM and NEM calculations are done at the center of each layer; the Climate module calculations are at the bottom of the layer.

calculations can strongly influence the ground temperature simulations.

Figure 3-25 shows the daily mean soil moisture content in the uppermost soil layer in each model as a percent of saturated soil moisture. There is considerable variation in the simulations of the three models. Variations between models for many other parameters were larger when the soil was wetter, but here, the variations are larger when the soil is drier. Relative soil saturation is consistently lower in Climate Model simulations; and consistently higher in LSM simulations. Although the FIFE soil moisture data set provides daily volumetric water content values for the entire analysis period, measurements had not been continuous; and the data set does not differentiate between measurements and interpolations. Therefore, these values are used with caution. The solid lines in Figure 3-26 indicate FIFE measurements along with model calculations—the upper line is for the second layer and lower line for the first layer. Due to discontinuities in measurements and rainfall variations over the Konza prairie, the measured moisture values to not respond to rain events as well as the model simulations do. These values are clearly multiple-day means that do not display strong peaks. Therefore, NEM and Climate Model simulations cannot be categorically denounced. Nevertheless, the range of observed values is apparent; and the NCAR LSM values are more appealing—they are sandwiched between values for the top two observational layers, and represent realistic relative saturation values for the Konza region [11]. The FIFE values on rainy days are smaller than those from the NCAR LSM. But as mentioned in Section 2.4 soil moisture values were not measured soon after rain events, so the data set has lower than actual soil moisture values for rainy days [11]. Therefore, the high NCAR LSM peaks in Figure 3-26 might, in fact, indicate appropriate Konza soil moisture conditions.

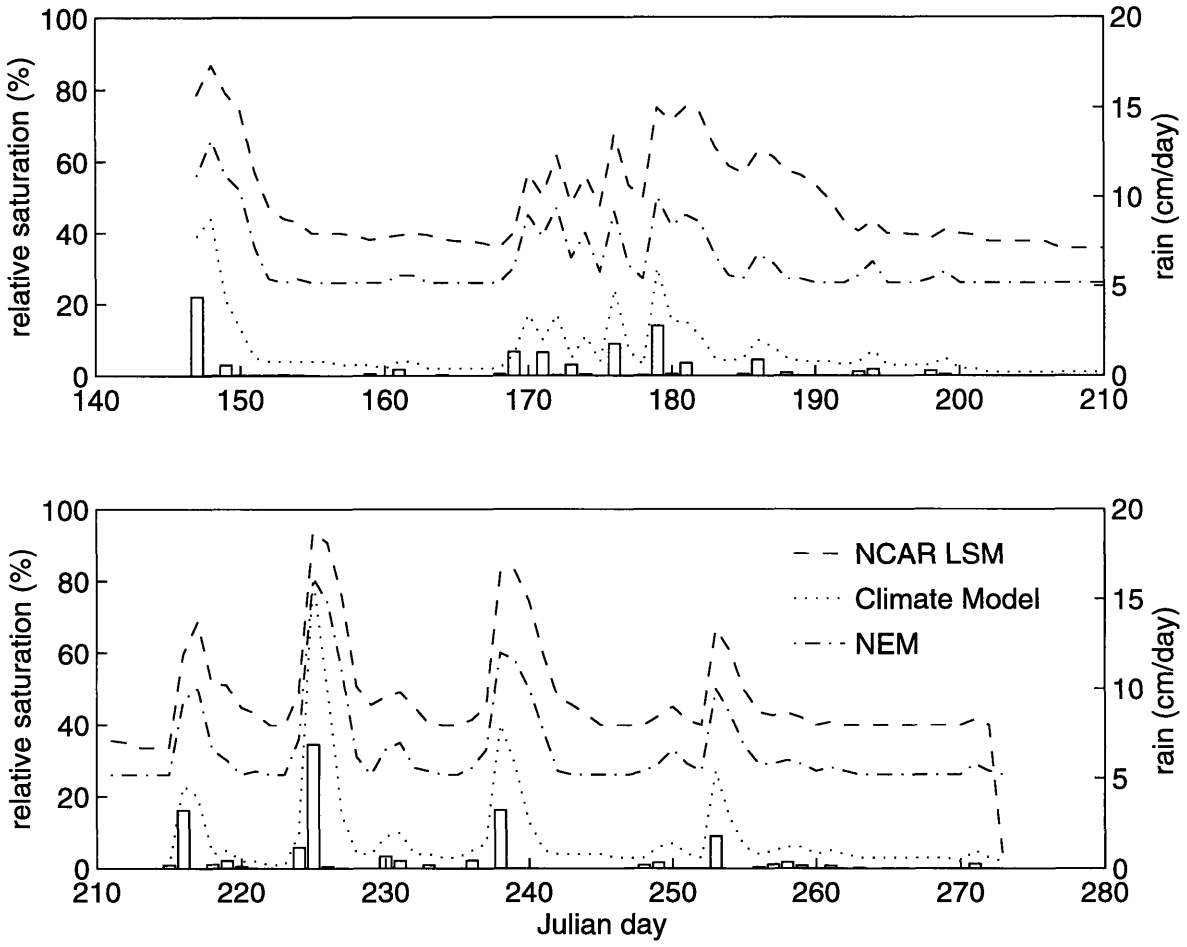

Figure 3-25: Daily mean soil moisture as a percent of saturated soil moisture content for the three modules.

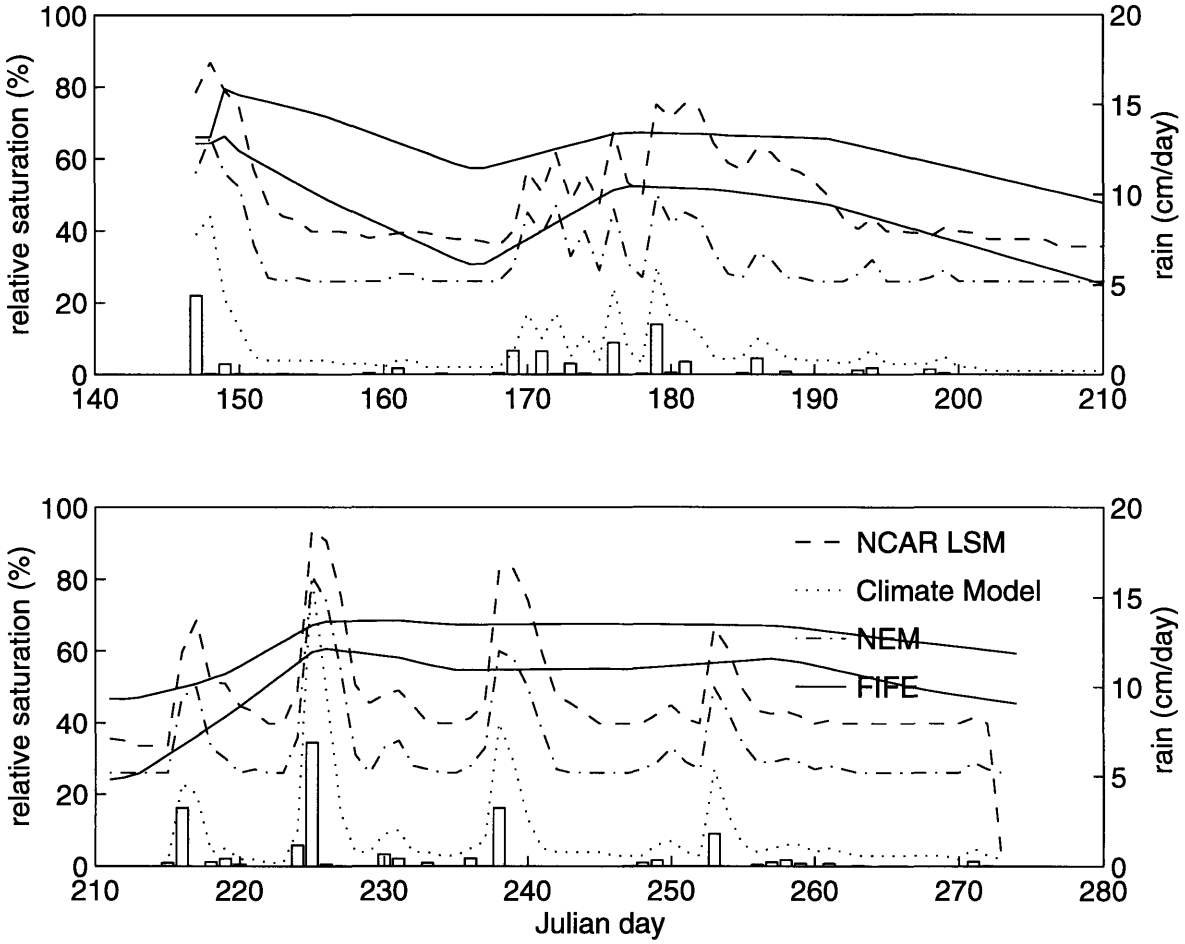

Figure 3-26: Daily mean soil moisture as a percent of saturated soil moisture content for the three modules. The solid lines show FIFE measurements: the upper line shows second layer values, the lower line shows first layer values. These multiple-day averages do not respond to precipitation.

3.5 The Impact of Relative Soil Saturation on Evaporative Fraction

Theoretically, the evaporative fraction must increase as relative saturation in the uppermost soil layer increases. As soil moisture increases, there is more water that could be evaporated from the uppermost layer. Therefore, the energy partition is weighted towards latent heat. But as previously noted, the soil moisture measurements for the uppermost layer had not been gathered continuously; the available values are multiple-day averages. So this expected trend is not evidenced in Figure 3-27.

Ironically, or pleasantly, this expected feature is captured in all three models! Figures 3-28, 3-29, and 3-30 are scatter plots of daily evaporative fraction with daily relative saturation of the uppermost soil layer simulated using the Climate Model, the NEM, and the NCAR LSM. The increasing EF trend with increasing soil moisture are more apparent in the LSM and Climate Model; and is less apparent in NEM.

As these plots indicate, the Climate Model allows the soil to dry excessively; the NEM limits drying at wilting point; the LSM limits drying at a still higher saturation level. The LSM algorithm mimics the observations most closely—at least in its upper and lower saturation boundaries. Due to these appropriate saturation boundaries, and the expected trend between EF and soil saturation, the NCAR LSM will be more reliable at partitioning λE and H at different levels of soil saturation.

These plots elucidate two important points regarding energy partition between λE and H. First, that when the saturation level is less than about 50%, energy partition process in models is biased towards H—and this behavior is realistic. As the soil moisture content increases, more of the incident energy is converted to λE. Second, that the FIFE observations do not show any such trend—multiple-day averages hide important characteristics of the energy partition process. Similarly, if monthly averaged values, instead of high-frequency fluctuations, were used to force the models, the models will be erroneously biased towards calculating H fluxes more often than λE fluxes since mean levels of saturation are drier over longer periods. This highlights the importance of using high-frequency forcings in climate models.

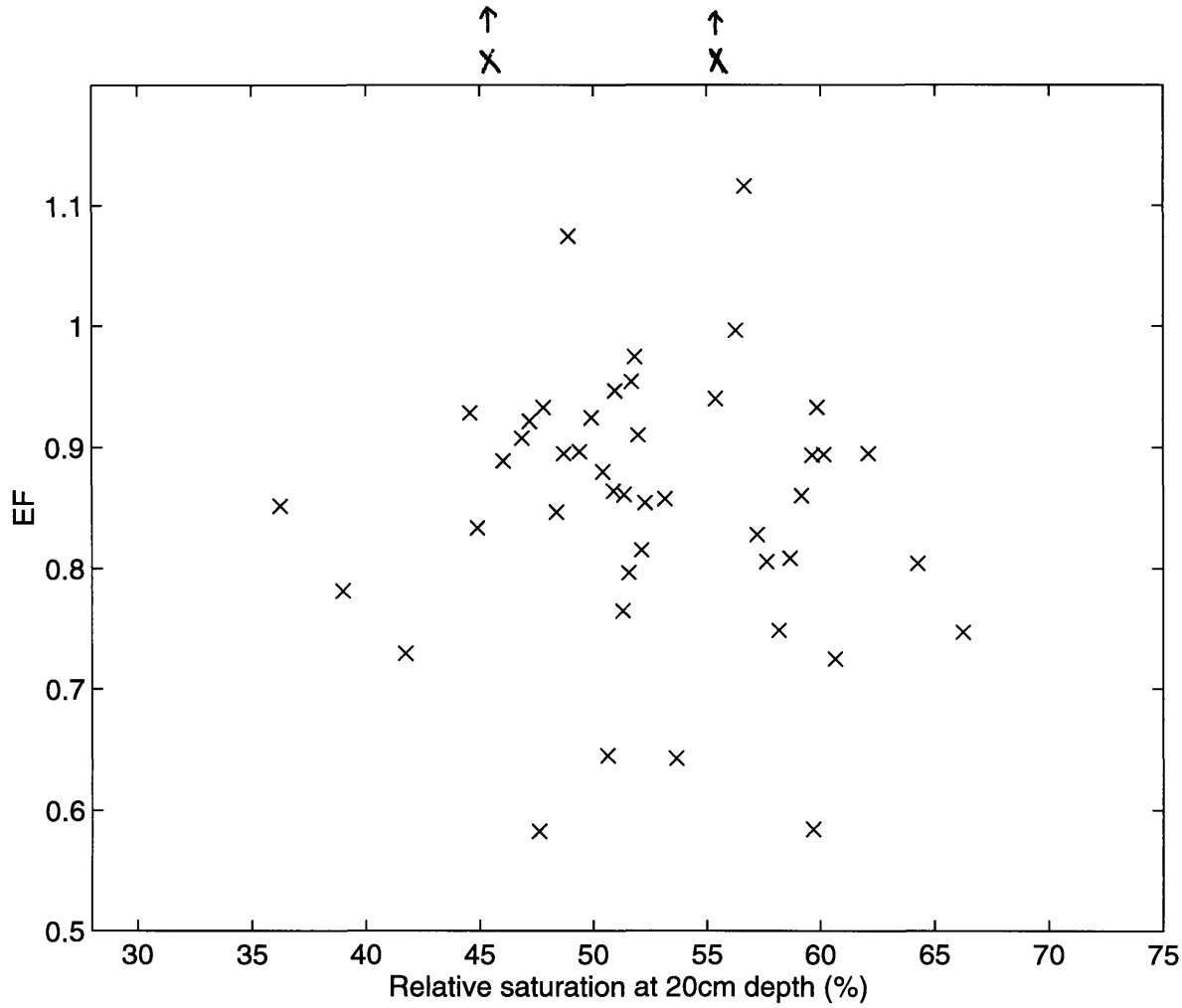

Figure 3-27: A scatter-plot of the daily mean evaporative fractions (EF) with relative soil saturation at 20 cm for FIFE observations.

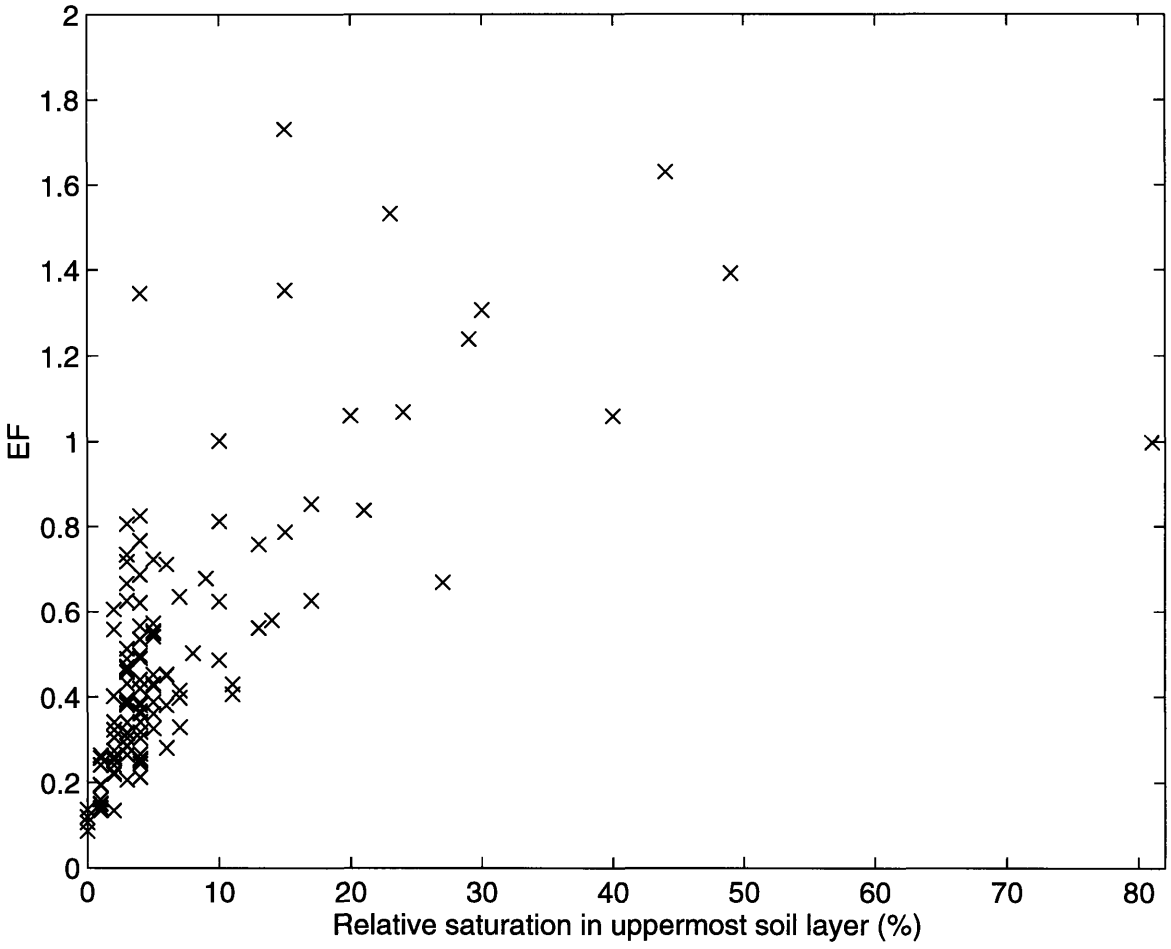

Figure 3-28: A scatter-plot of daily mean evaporative fractions (EF) with the upper soil layer relative saturation for the hydrological module in the Climate Model. The thickness of this module's upper soil layer is 10 cm.

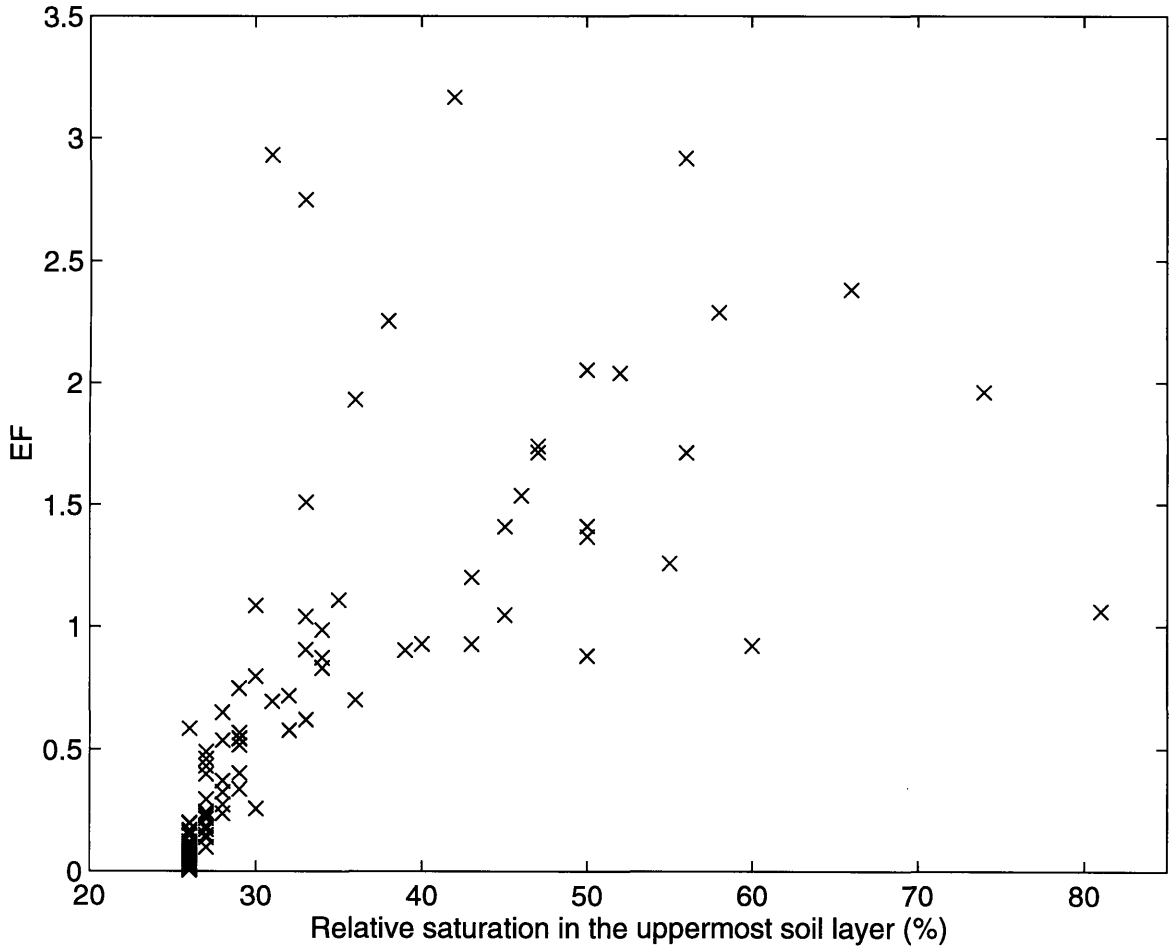

Figure 3-29: A scatter-plot of the daily mean evaporative fractions (EF) with the uppermost soil layer relative saturation for the NEM hydrological module. The uppermost soil layer in this module is 10 cm thick.

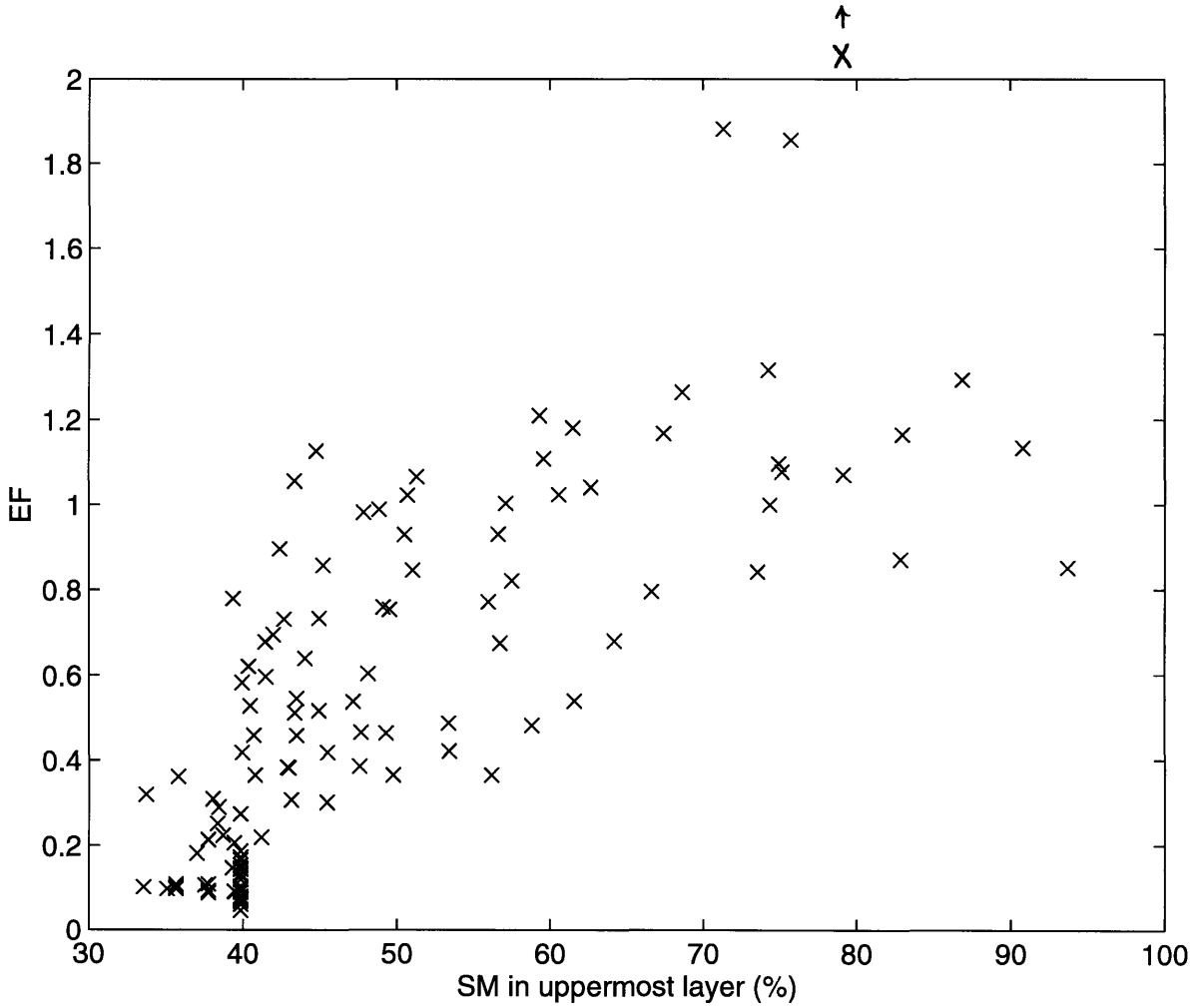

Figure 3-30: A scatter-plot of the NCAR LSM daily mean evaporative fractions (EF) with NCAR LSM 10 cm thick uppermost layer relative soil saturation.

The above comparisons further evidenced that each model has its weaknesses at simulating daily trends. But startlingly apparent was the inconsistency between the hydrological modules in the Climate Model and NEM. The Climate Model's subsurface was often too dry, and this dryness restricted evaporation and exaggerated T_g calculations. The NEM, on the other hand, evaporated excessively during rainy periods. These models were in agreement during dry periods when the soil water content had limited influence over flux calculations. These two inconsistent hydrological modules run simultaneously and support different parts of the MIT Global System Model. These inconsistencies must be eliminated to improve the accuracy of climate predictions and elevate the model's integrity.

The comparisons presented thus far were of fluxes or temperatures at the surface, they ignored the vertical distribution. The next chapter presents both temporal and vertical variations in subsurface temperature and moisture content.

Chapter 4

Soil Moisture and Temperature Profiles and Their Impacts

This Chapter introduces the soil temperature and soil moisture profiles generated by the models, and compares the strengths and robustness of each model's prognostic variable calculations. This also discusses the impacts of prognostic variables when extracting long-term trends from models.

4.1 Soil Moisture Profiles

Figure 4-1 shows the observed daily mean soil moisture profile in the Konza Prairie from May 27 through September 30, 1987. Measurements are available at 20, 30, 40, 50, 60, 80, 100, 120, 140, 160, 180, and 200 cm depths; but the uppermost measurements are less reliable than other measurements [17]. Furthermore, FIFE soil moisture data were not gathered continuously; many of the values are multiple-day averages. Soil moisture values soon after rain events are not available; so soil water contents, especially in the upper layers during and soon after rain events might have been higher than presented here [11]. Darker shades represent drier conditions as demonstrated by the gray scale.

It is apparent that there are large soil moisture fluctuations in the upper layers and almost constant soil moisture levels in deeper layers. There are two dry periods

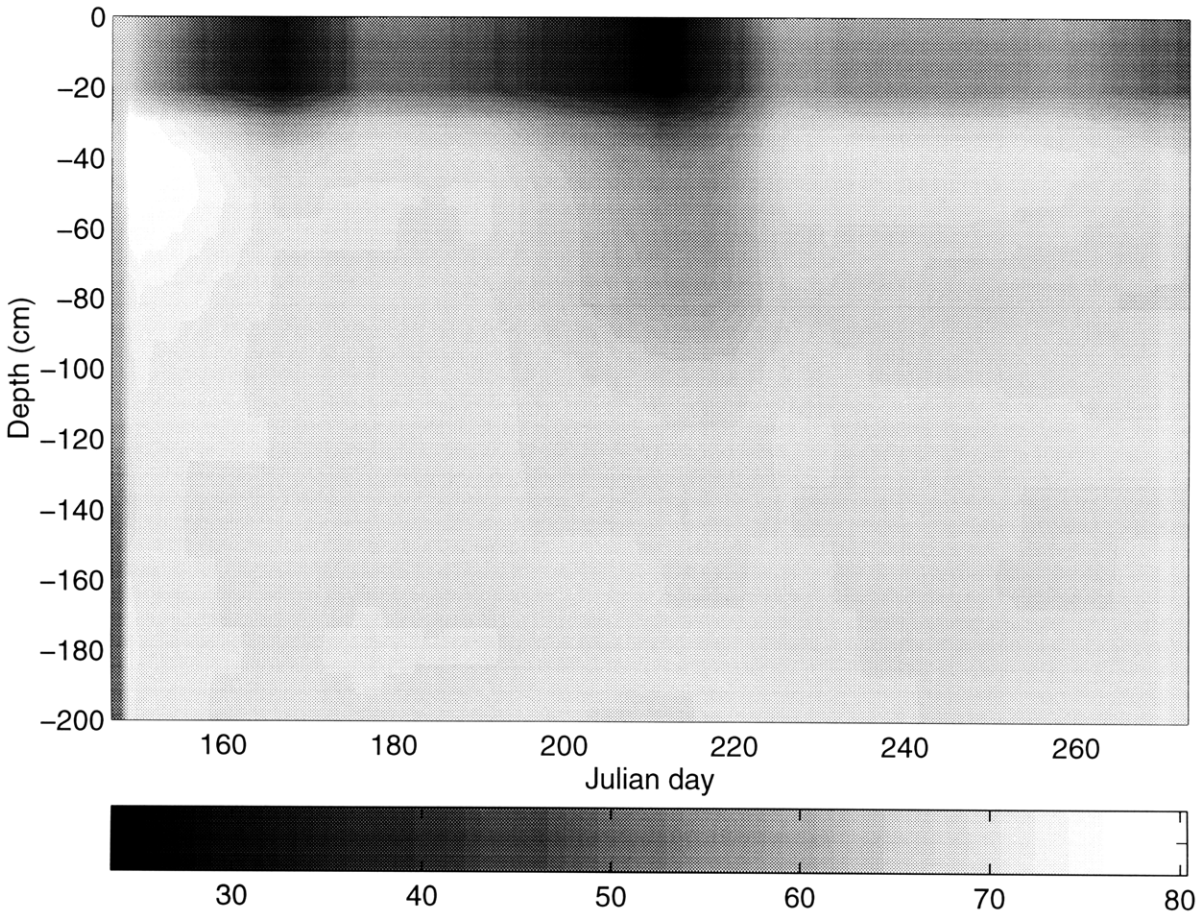

Figure 4-1: The daily observed soil moisture profile in the Konza Prairie from May 27 - September 30, 1987. Soil moisture measurements were available at 20, 30, 40, 50, 60, 80, 100, 120, 140, 160, 180 and 200 cm depths. Measurements for the uppermost layer were noted to be less reliable than for other layers. The gray scale shows relative soil saturation as a percent.

from Julian days 150 to 175 and 196 to 220; this reinforces the observations made with the precipitation bar-graphs that were presented earlier. During the second dry period the drying front penetrates deeper into the soil column—to about 100 cm, as opposed to about 50 cm during the first dry period. There are also two prominent wet periods between Julian days 175 to 180 and 222 to 236. The values corresponding to the figure indicate that the infiltration front of the two precipitation events penetrate to about 50 and 60 cm during these periods. Therefore, to accurately simulate the soil hydrology of the Konza Prairie for Summer 1987, a model that uses gravitational drainage from the lower boundary needs to consider a soil column at least a 100 cm deep; a model that assumes no drainage from the lower boundary needs a still deeper soil column. For annual-scale simulations the soil column might need to be deeper than indicated above.

The above discussion infers that soil moisture measurements were made on level ground over a uniform grid at constant time intervals. But in fact, these soil moisture values are from 32 sites. In addition, rainfall was found to vary over the prairie, even though the measurement area is relatively small—15 X 15 square kilometers [11]. But since 1987 was a dry year and the overall soil moisture levels were lower during that year, therefore the variability is expected to not adversely affect the analyses of this project [11].

Figure 4-2 is the soil moisture profile simulated by the hydrological module in the Climate Model. This module has two soil layers: a 10 cm thick upper layer, and a 190 cm thick lower layer. This module does not sufficiently simulate the Konza conditions because of the deficiency of soil layers. The upper layer thickness is appropriate for this simulation, but even that layer does not mimic actual conditions because it is not appropriately influenced by the lower layer. Although the upper layer experiences constant excitations from the atmosphere, it does not experience the necessary resistance from deeper layers that are felt under actual conditions; therefore, the upper layer dries much faster than the FIFE upper layer. The upper layer indicates the effect of the two wet periods. But the wet and dry representation in the lower layer are too abrupt to be realistic: the 190 cm deep layer is too thick to capture the necessary

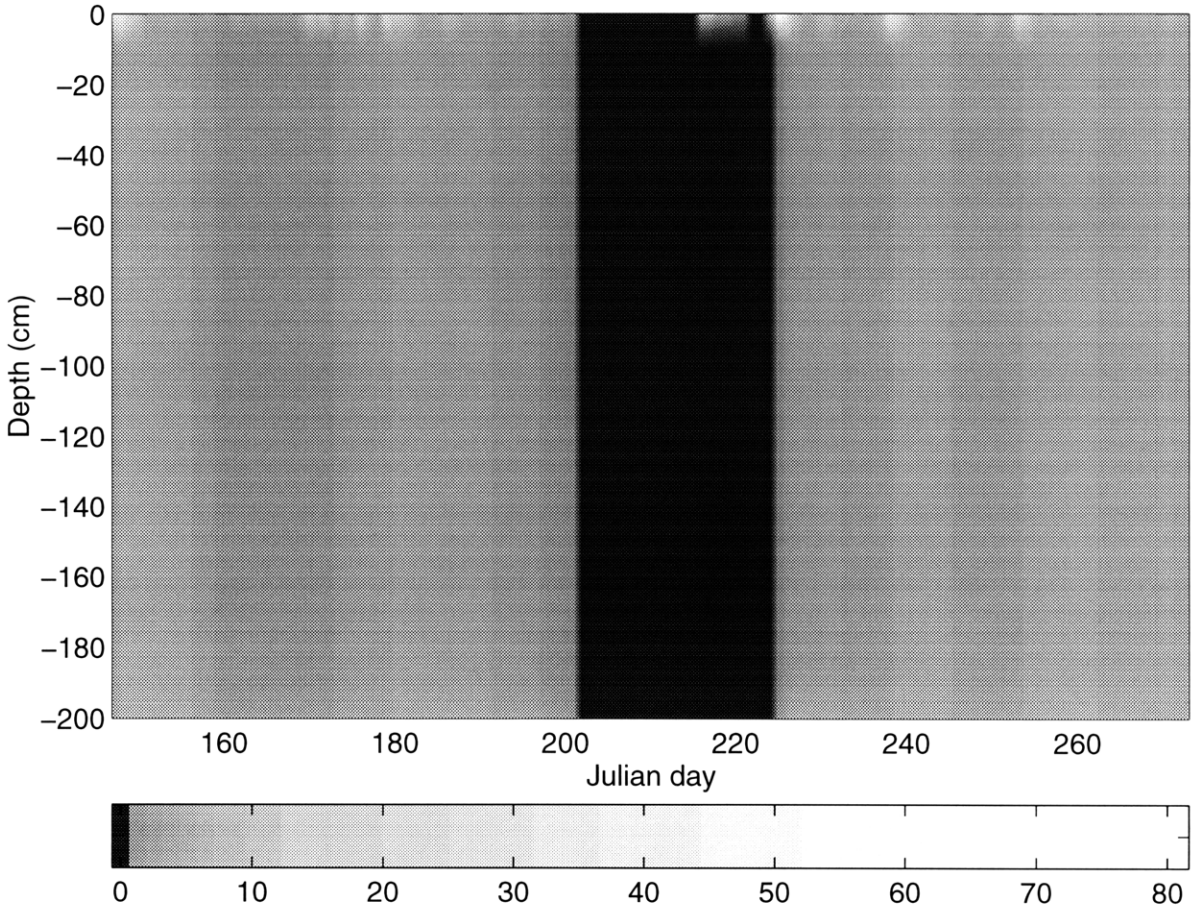

Figure 4-2: Soil moisture profile of the hydrological module in the Climate Model for May 27 - September 30, 1987. The lower boundaries of the soil layers are at 10 and 200 cm depths. The gray scale shows relative soil saturation as a percent.

details, but a shallower soil column will not meet the no-flow boundary conditions at the lower boundary.

This is the reason this module appeared to be biased towards dry in Figure 3-26. According to Figure 4-2 the lower layer is either very dry or wet. In the Climate Model soil moisture simulations there are no wet-dry gradations that were apparent in the FIFE observations. It is clear that the subsurface structure in this model does not meet its requirements: the subsurface does not provide the reservoir and storage for water, nor the "memory" of the hydrological cycle.

Figure 4-3 is the soil moisture profile generated by the hydrological module in the Natural Emissions Model. Note that this model, and therefore the figure, represents only the top 50 cm of the soil column. This module better captures the characteristics seen in the observed profile than does the Climate Model. The upper layers show the wet-dry variations corresponding to the rainy and dry periods. And because this model has five soil layers, the deeper layers exert the necessary resistances against wetting and drying to the upper layers and avoid instantaneous reactions to atmospheric excitations.

There is a clear difference between the two upper layers and the three lower layers; the soil moisture levels in the two upper layers vary more than in the lower layers. This difference is due to the evaporation algorithm: evaporation affects only the top two layers (Section 3.3.2); the absence of vegetation in the module disallows transpiration from deeper layers. If the moisture level in either upper layer is greater than soil field capacity, then that layer evaporates at half the potential evaporation rate; if the moisture level is less than wilting point, then that layer does not evaporate at all; but if the moisture level is between field capacity and wilting point, evaporation is proportional to the water in excess of wilting point. While this formulation may realistically mimic the top layer conditions, the evaporation rate is too high for the second layer. According to Betts *et al.* [5], transpiration dominates evapotranspiration over vegetated land surfaces. The lack of transpiration in the evaporation algorithm might introduce other errors if this module were used over heavily vegetated surfaces.

Next, the total soil column is too shallow. The fifth layer is heavily wetted by

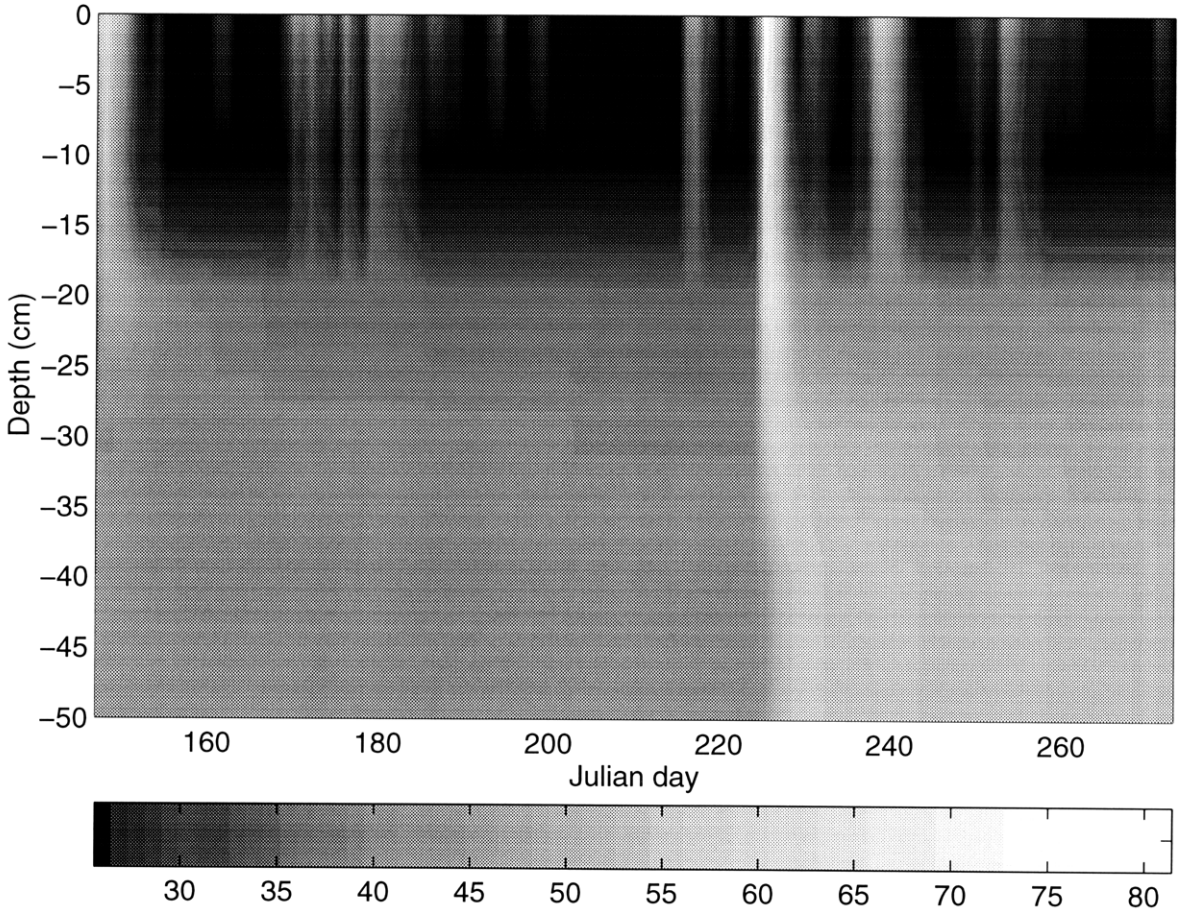

Figure 4-3: Soil moisture profile of the NEM hydrological module. The lower boundaries of the soil layers are at 10, 20, 30, 40 and 50 cm depths. The gray scale shows relative soil saturation as a percent.

the precipitation event on Julian day 225. Gravitational drainage is the only water removal mechanism from the bottom of the soil column. But gravitational drainage alone underestimates water removal when the soil column is nearly saturated because the hydraulic gradient between the fifth layer and deeper soils is much larger than unity under such conditions. The model must use a deeper soil column for gravitational drainage from the lower boundary to be more realistic.

Nevertheless, this module acts as a reservoir and storage of water. But its effect is not sufficient. A deeper soil column with a more realistic evaporation algorithm will further improve the model's subsurface representation.

Figure 4-4 is the soil moisture profile generated by the NCAR LSM. Although this model generates a good moisture profile, owing to the thicker soil layers, it does not show the details as well as in the observed profile. FIFE measurements are available at 10 cm intervals to a depth of 60 cm, and at 20 cm intervals thereafter. The two dominant dry periods are well represented; the effect of the rain event on Julian day 225 is felt by the deeper layers; and this wetness is sustained for a few days. The uppermost soil layer moisture levels fluctuate in response to atmospheric forcings; and the rate and level of the fluctuations in the top layer are dampened by the lower layer resistances.

This model has six soil layers; the thickness of the layers double with increasing depth. The lower boundaries of the soil layers are at 10, 30, 70, 150, 310, and 630 cm depths. The bottom-most soil layer is excluded in Figure 4-4. Here, evaporation affects only the top soil layer, avoiding the over-evaporating problem encountered in the NEM module. Transpiration removes water from each soil layer in proportion to the relative root abundance that corresponds to the vegetation cover assigned to the region. Gravitational drainage, in addition to transpiration, removes water from the lowest layer. These features are absent in the other two modules. Flow out of each layer is the input to the next layer; therefore, the model meets water balance requirements. In addition, the LSM distinguishes between saturated and unsaturated water flow in the soil column.

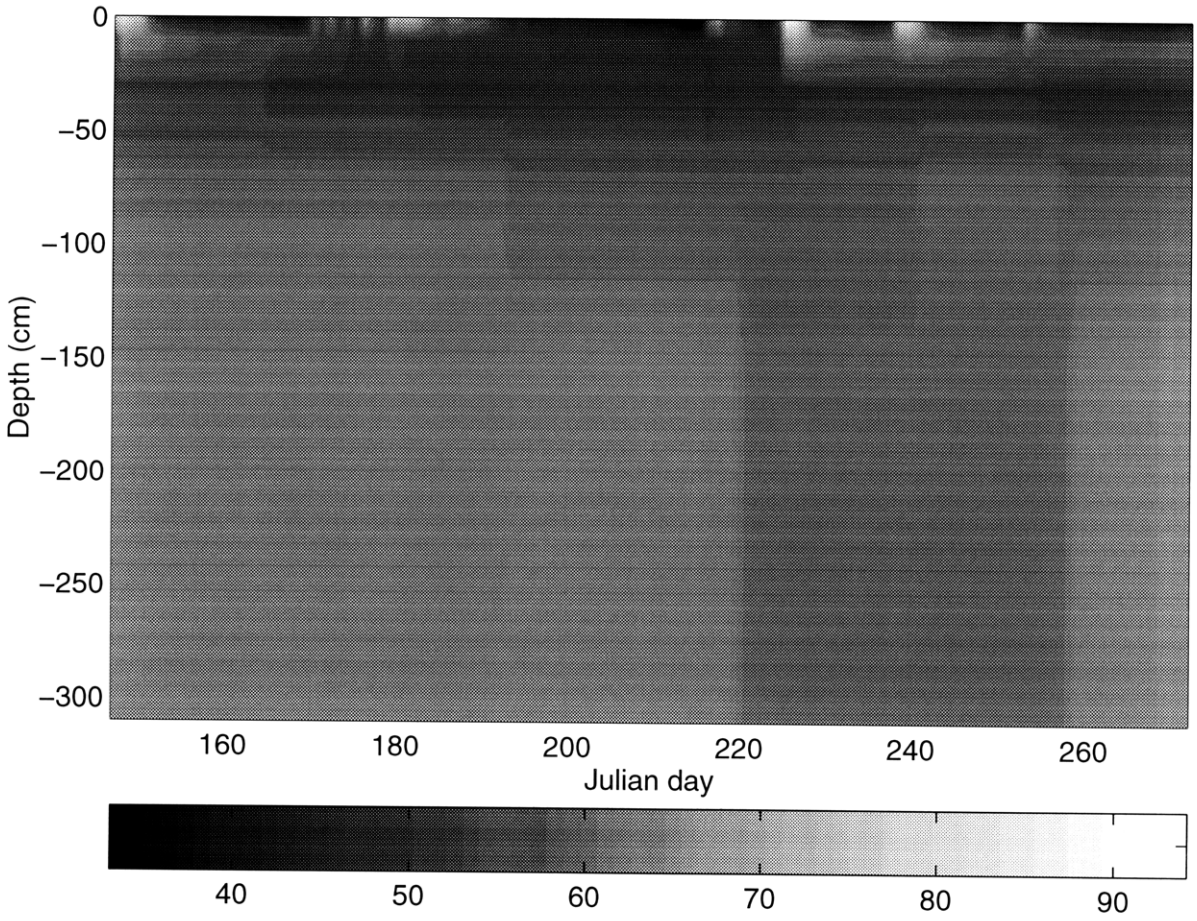

Figure 4-4: Soil moisture profile generated by the NCAR LSM for the Konza Prairie for the May 27 - September 30, 1987 period. Soil layer boundaries are at 10, 30, 70, 150, 310 and 630 cm depths. The bottom-most layer, which showed no discernible variations in its moisture content during this period, is not included in the figure. The gray scale shows relative soil saturation as a percent.

4.2 Soil Temperature Profiles

Figure 4-5 is the observed ground temperature profile for the Konza Prairie. Cooler patches and days are shown by darker shades as demonstrated by the gray scale. FIFE ground temperature measurements are available only at 10 cm and 50 cm depths. So the sparse data do not indicate the smooth temperature transitions in the lower layer.

Figure 4-6 shows the ground temperature profile from the hydrological module in the Climate Model. As with soil moisture calculations, the soil column is discretized into two layers with the lower boundaries at 10 cm and 200 cm depths. The upper layer responds to atmospheric excitations; but the second layer is too thick to capture the detailed processes within it. But if the second layer, and hence the total soil column, were thinner, it will not be able to provide the reservoir and storage characteristics that are required of the deeper layer, nor meet the no-heat and no-water flow conditions this module assumes for its soil column at the lower boundary. Even though measurements are available only at two depths, this two-layer model does not simulate the patterns observed during the FIFE experiment. But the paucity of FIFE data does not allow critical judgments against this model's temperature profile.

Figure 4-7 shows the ground temperature profile of the hydrological module in the NEM. This module displays many temperature gradations, but unfortunately, data do not sufficiently substantiate the simulation. Unlike in this model's moisture profile, the transitions are smoother in the temperature profile; the warm and cold periods are sustained for a few days; the intense forcings are dampened as the effect penetrates to deeper layers. The uppermost 10 cm thick layer is comparable to the upper 10 cm thick FIFE layer. The strong and frequent cold and warm signals found in Figure 4-5 are evident in Figure 4-7 as well: in June and July the top layer temperature fluctuates often; then the soil begins to warm in late July; the weather changes in August and the soil begins to cool again, and the profile turns progressively darker as Fall sets in.

Figure 4-8 shows the ground temperature profile from the LSM; the bottom-most layer is excluded from this figure. The simulated and observed profiles agree well.

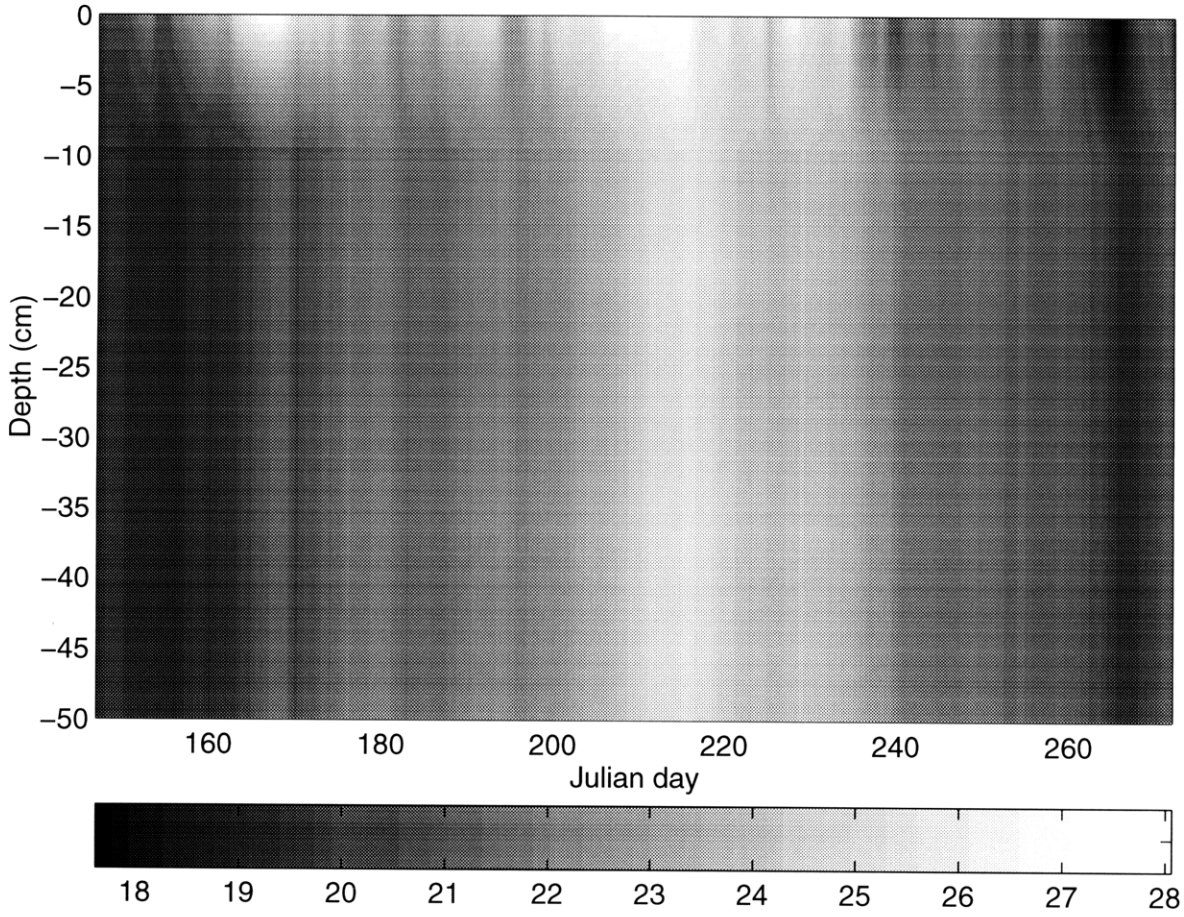

Figure 4-5: The observed ground temperature profile for the Konza Prairie. The gray scale shows temperature range in °C.

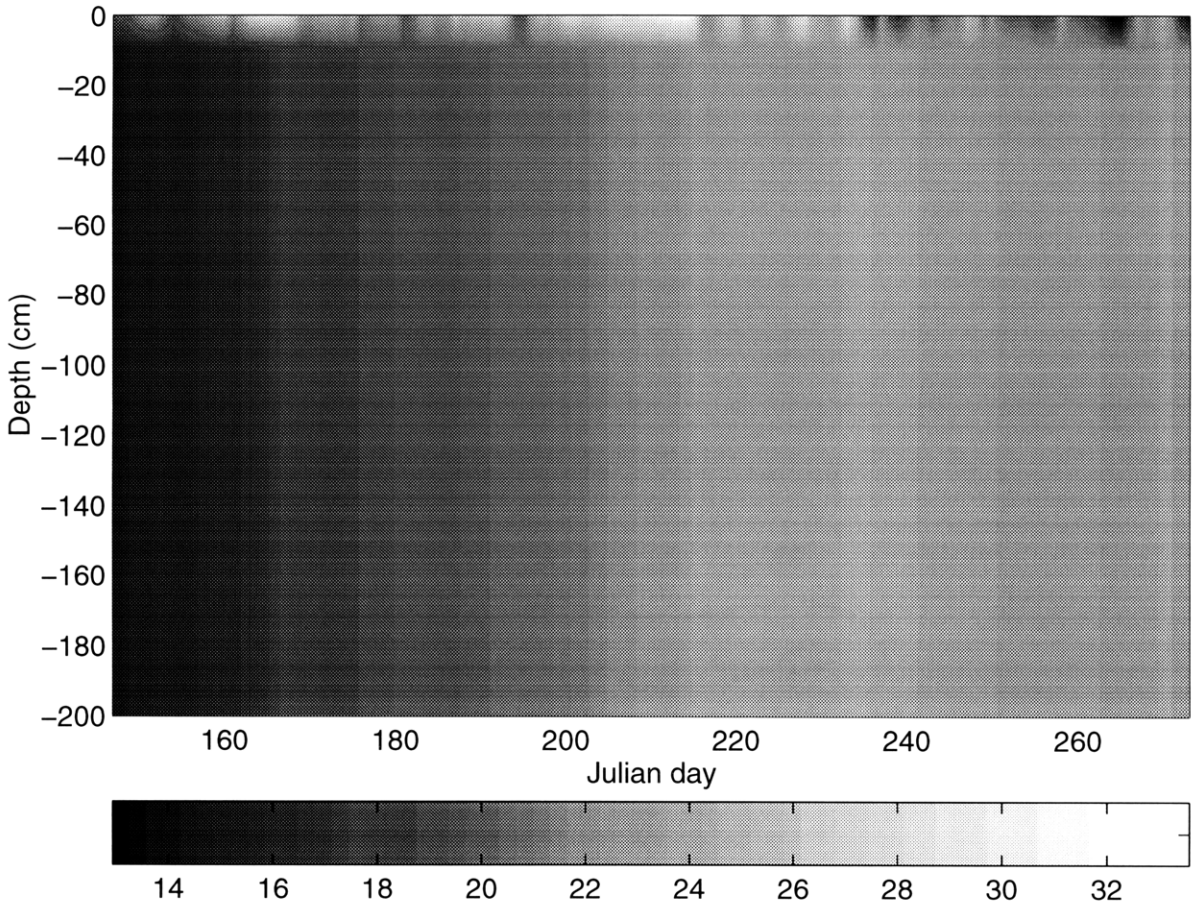

Figure 4-6: The ground temperature profile of the hydrological module in the Climate Model for the Konza Prairie. The lower boundaries of the soil layers are at 10 and 200 cm depths. The gray scale shows temperature range in °C.

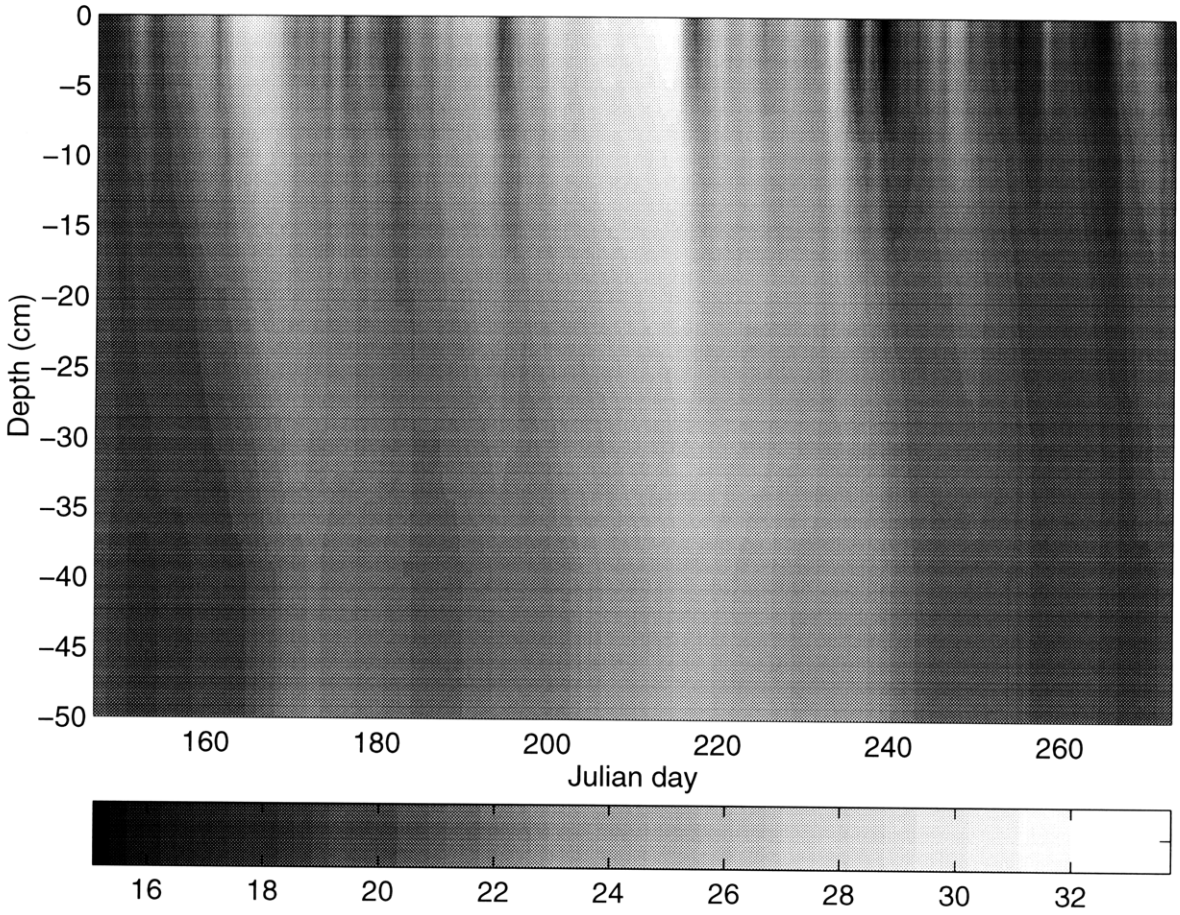

Figure 4-7: Ground temperature profile of the NEM hydrological module. The lower boundaries of the soil layers are at 10, 20, 30, 40 and 50 cm depths. The gray scale shows temperature range in °C.

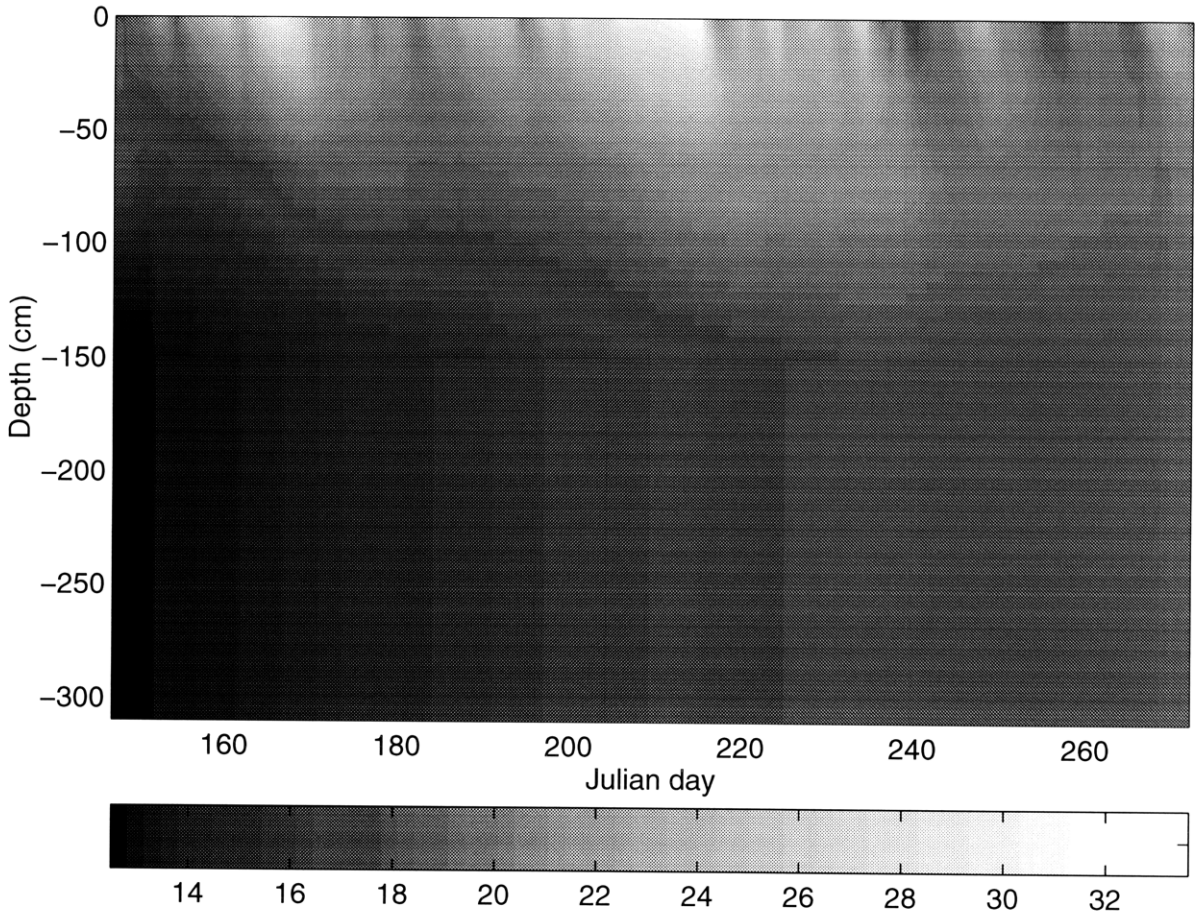

Figure 4-8: Ground temperature profile generated by the NCAR LSM for the Konza Prairie for the May 27 - September 30, 1987 period. Soil layer boundaries are at 10, 30, 70, 150, 310 and 630 cm depths. The bottom-most layer, which showed little variation in its temperature during this period, is not included in the figure. The gray scale shows temperature range in °C.

4.3 Monthly Variations in Ground Heat Flux

The soil-water column has many tasks in the climate prediction process (Section 2.1.1). The shallower soil layers help simulate diurnal fluctuations; the deeper layers provide the "memory" of the model. The previous sections analyzed how each model simulates the temperature and moisture profiles; the following section discusses the impact of the prognostic profiles at capturing the monthly variations in ground heat fluxes. An advanced subsurface representation will induce the model to simulate better long-term ground heat and moisture reservoirs while remaining sensitive to high-frequency diurnal forcings.

Figure 4-9 gives the monthly ground heat flux values for the three models and FIFE observations. In order to allow comparisons, these values were calculated only for days when FIFE ground heat flux measurements were available. The ground heat flux is positive towards the surface. The LSM and NEM simulations are closest in value to FIFE observations. The Climate Model simulations underestimate upward flux; and there is little variation in the this model's monthly flux values from the beginning to the end of Summer. But FIFE values show a clear decrease in the upward ground heat flux, as the Summer gives way to Fall. NEM and the LSM capture this trend from June through August. While values for at least ten days were used to calculate June, July and August monthly mean Gs, mean May G was calculated with only May 27 through May 31 observations and simulations. Therefore, the mean May G given here might not be representative of the entire month.

The deeper soil layers in each model give the model the capacity to act as a store and reservoir of heat: the hydrological module in the Climate Model has a deep soil column, but only two soil layers in it; the NCAR LSM has a deep soil column with six soil layers; and the hydrological module in the NEM has a shallow soil column with five soil layers. Since the NEM and the LSM better simulate the seasonal heat storage, it is clear that a multiple soil layer structure, rather than a mere deep soil column with few soil layers, is more important to capture seasonal trends.

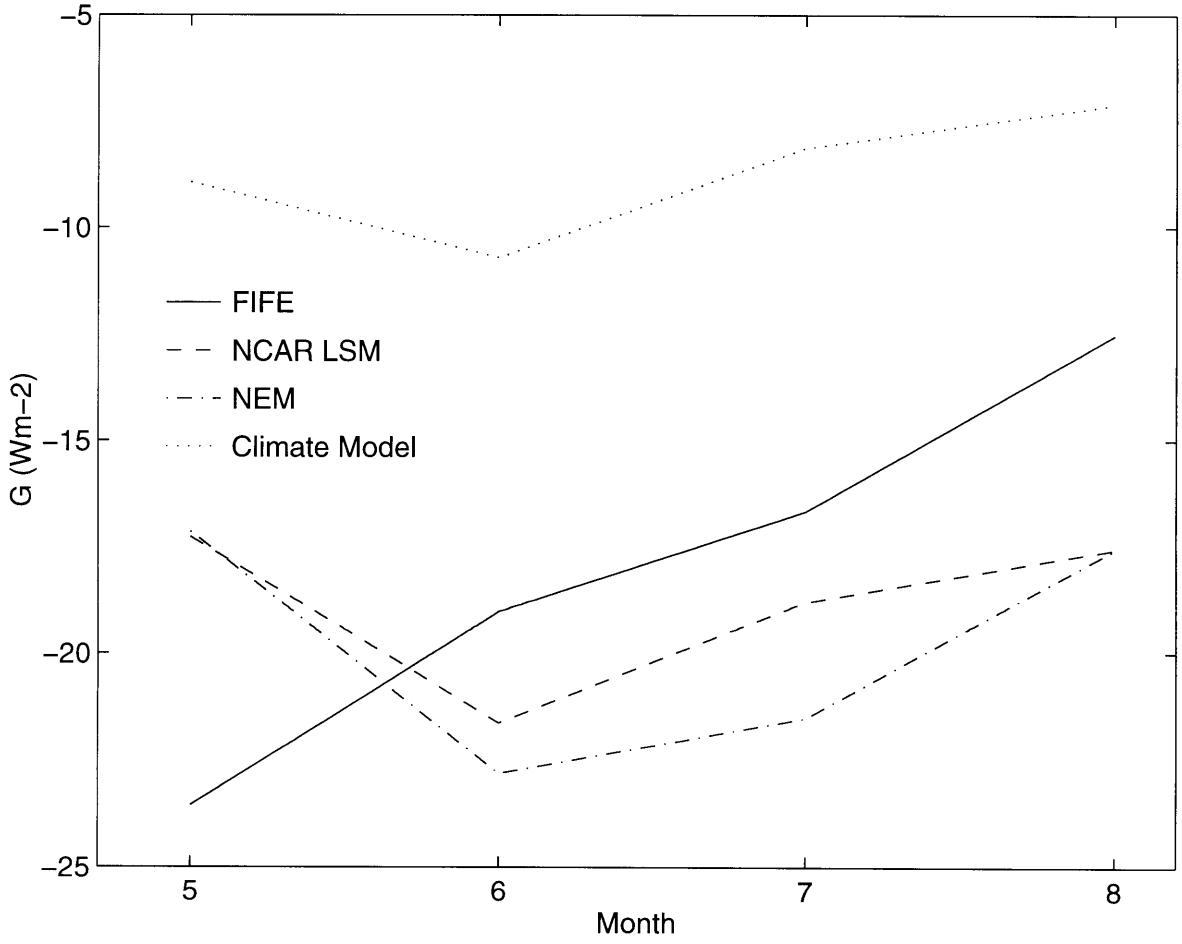

Figure 4-9: Comparison of monthly ground heat fluxes (G) of the three hydrological modules with FIFE observations.

Variable	units	Climate Model	NEM	NCAR LSM
latent heat flux	$[Wm^{-2}]$	76	86	81
sensible heat flux	$[Wm^{-2}]$	77	66	74
ground heat flux	$[Wm^{-2}]$	2	2	4
net radiation	$[Wm^{-2}]$	154	(154)	159

Table 4.1: Comparisons of mean calculated values from May 27 through September 30, 1987. R_n is positive towards the surface; the other fluxes are positive towards the atmosphere. Here, $G = R_n - \lambda E - H$, when rounding off errors are ignored. R_n is an input to NEM.

4.4 Mean Values for the Analysis Period

As noted in Section 1.1, on average, inward fluxes are balanced by outward fluxes at every level—including the outer atmospheric boundary, and the Earth surface boundary. And climate-related modules must mimic this feature. Table 4.1 shows that the three hydrological modules studies in this project do, in fact, conserve energy. This Table gives mean flux values at the surface for the entire analysis period. R_n is positive towards the surface; the other fluxes are positive towards the atmosphere. When rounding off errors are ignored, $R_n - \lambda E - H - G = 0$.

The values in Table 4.2 allow a reality-check. These are means of the diagnostic and prognostic variables considered in the analysis over all days when FIFE IFC data were available. So these values allow comparisons between model simulations and FIFE observations over the Konza Prairie. Not all flux data were available during the same time periods, therefore these values were calculated by averaging fluxes at different times. So while each flux category is comparable across models and FIFE observations, the values are not comparable across fluxes and do not meet energy balance requirements.

The flux values in Table 4.2 agree with the trends observed in the daily mean

Variable	units	Observed	Climate Model	NEM	NCAR LSM
latent heat flux	$[Wm^{-2}]$	153	123	164	138
sensible heat flux	$[Wm^{-2}]$	28	85	31	68
ground heat flux	$[Wm^{-2}]$	16	53	20	19
net radiation	$[Wm^{-2}]$	150	154		159
ground temperature	$[°C]$	24	23	24	24
soil moisture	[%]	49	8	32	50

Table 4.2: Comparisons of mean values over all days when FIFE IFC observations were available. Since the availability of different flux data was not coincident, the calculation periods of the different variables are not the same. So calculations are comparable across models and FIFE observations, but not across fluxes.

figures in Chapter 3. The λE simulations from the Climate Model presented in Figure 3-1 were consistently smaller than the observed daily values, so the mean λE for the analysis period is also smaller than the observed mean. NEM daily mean λEs were often larger than the observed daily values, so the mean value for the analysis period is correspondingly larger than the observed mean. This trend is true for sensible heat, ground heat, and net radiative fluxes.

The simulated multiple-day mean ground temperatures are deceptive. According to Table 4.2 the multiple-day mean from the models agree to within 1°C. But the daily mean values in Figures 3-6, 3-11, and 3-17 did not agree as well; the models calculated larger than observed daily mean T_g on dry days, and smaller than observed daily mean T_g on wet days. Long-term averages hide extreme values. Therefore using these values in climate predictions defeats the purpose of the exercise since the extreme events are often the cause of natural disasters, and are of greatest concern to people.

The next Chapter compares each model's response to high-frequency atmospheric excitations.

Chapter 5

Diurnal Cycles and RMSE

5.1 Significance of Diurnal Cycles

Diurnal values: The diurnal cycle for a particular variable was constructed by averaging model simulations or FIFE measurements at a given time of the day for the periods when observations were available. Since data and model I/O were at half-hourly intervals, the diurnal cycles were also constructed using values at half-hourly intervals.

Comparisons between observed and calculated diurnal mean values test the model's sensitivity to high-frequency atmospheric excitations. The uppermost soil layer, for instance, must be sensitive to incident solar and thermal radiations, and precipitation, since it suffers the immediate impacts of these forcings. The state of the upper soil layer influences the way incident radiation is partitioned, and by that determines the form and magnitude of upward fluxes in the next time step. An isolated fluctuation in incoming radiation or precipitation may have little impact on long-term climate change; but the constant diurnal instabilities are the very drivers of the climate system. In addition, seasonal dependence of precipitation amounts and temperature extremes of many geographical sites are determined by the frequency of occurrences of diurnal features [18], [12].

Total dependence on long-term mean values alone will ignore the more important extreme values. At present, most climate prediction efforts are concentrated

on evaluating globally averaged changes in climate. While a globally averaged 1°C increase in temperature can significantly affect the planet, such a globally averaged value would mean little to policy-makers or the general public—or to most of the scientific community at that! Effects of climate change are felt at short time-scales and at regional-levels. Therefore, the extreme events that occur at smaller spatial and temporal scales, and contribute to that 1°C increase, are more important. So, as computational capabilities increase, model resolution must also increase to account for smaller temporal and spatial variability, and proceed from globally averaged temperature predictions to more specific regional climate predictions.

Diurnal root mean square errors (RMSE): The diurnal root mean square error values were calculated by first squaring the errors in simulations for all time steps for which FIFE observations were available, then summing the errors corresponding to different times of the day and calculating the square roots of the averaged values. The diurnal cycles were also constructed using values at half-hourly intervals.

The diurnal root mean square errors can identify trends that are not captured by the two previous tests—daily means and diurnal cycles. It is nearly impossible to check every model output value with the corresponding observed value for each time step. And even if it were possible to check every value, such a check may not necessarily help identify persistent trends in errors. The diurnal and daily mean values indicate the general trends in prognostics and diagnostics. But if the errors in model simulations were systematically divided above and below the observed values, the simulation means may erroneously indicate perfect diurnal and daily trends. The root mean square errors, on the other hand, will highlight fluctuations of calculated values about the observed values. In addition, root mean square errors help identify the times of the day when errors persistently occur.

5.2 Comparisons of Diurnal Cycles and RMSEs

Latent heat flux The diurnal cycles for λE fluxes simulated by the three modules and the cycle for FIFE observations are shown in Figure 5-1. The horizontal axis gives the local time for Kansas. Simulations from all three models correspond well with FIFE data. Simulated and observed cycles peak just after midday. NEM values are particularly good at midday; the LSM and Climate Model values are particularly good from sunset to sunrise. NEM simulations of λE from sunset to sunrise are larger than the observed values or simulations from other models. But the amplitude of the NEM calculations is closer to FIFE observations than the amplitudes of simulations from the other two models.

Figure 5-2 shows the diurnal RMSEs of the three models. Errors in simulations from the LSM and the Climate Model are about half those in NEM—during both day and night. The RMSEs presented in Figure 5-2 are contrary to what one might expect after a quick glance at Figure 5-1. NEM, which mimicked the FIFE diurnal cycle best, has the largest RMSE; the Climate Model, which most deviated from the FIFE diurnal cycle, has the smallest RMSE. The large errors occur because of the noise in the simulations: the large errors in NEM simulations are due to the many fluctuations in the simulations about the FIFE value. This means that the Climate Model simulations have the lowest noise, but that it consistently simulates smaller λE values—consistent with Figure 3-1; NEM has the most noise—again consistent with Figure 3-7. All model errors also peak just after midday. On average, midday flux values are large, therefore, errors are also large at midday.

Sensible heat flux The diurnal cycles for H fluxes simulated by the three modules and the cycle for FIFE observations are shown in Figure 5-3. None of the models mimic the FIFE cycle well. The LSM and Climate Model have the correct shapes with too large amplitudes; NEM has a comparable amplitude with a wrong shape. All models overestimate during midday.

FIFE observations peak around midday. But the model simulations peak later—the LSM and Climate Model cycles peak about a half hour later, and NEM about

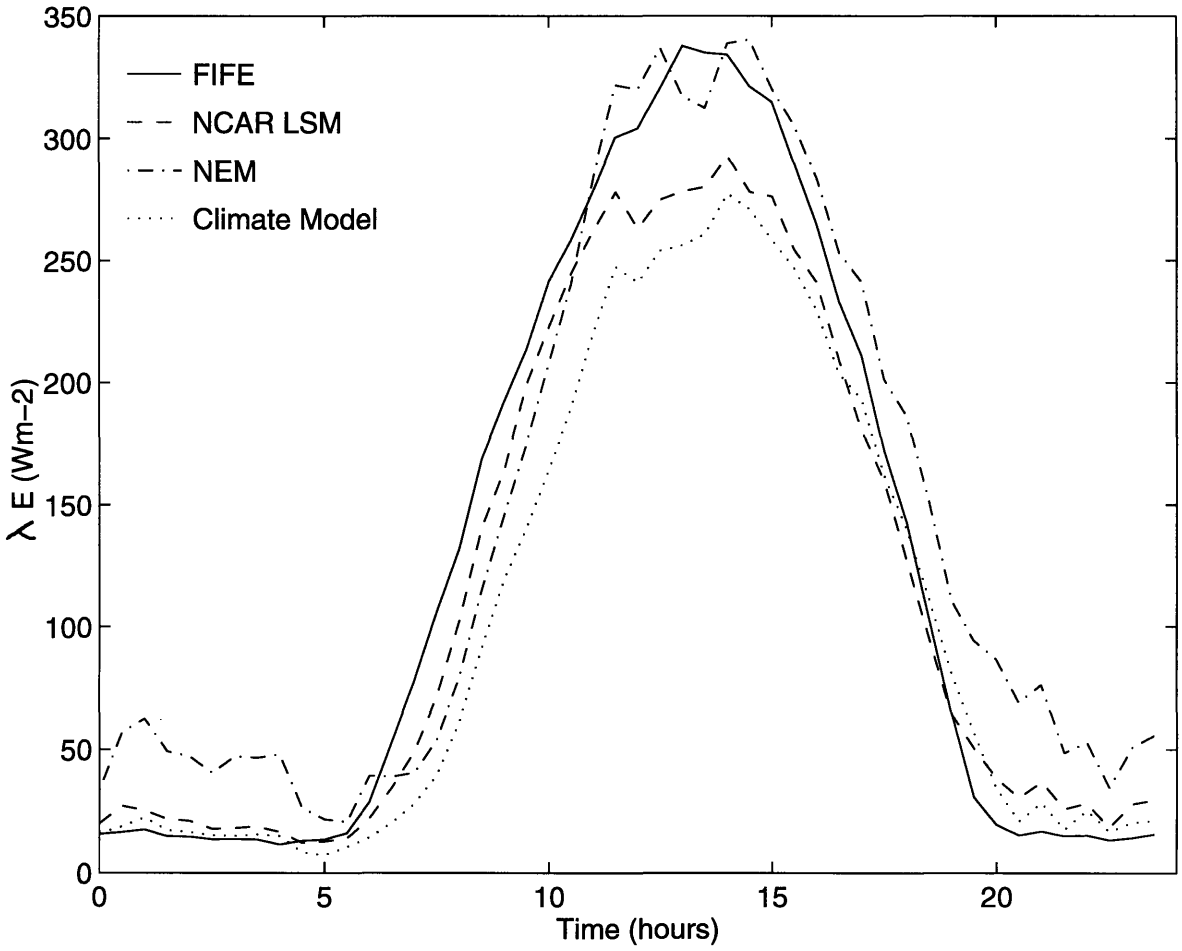

Figure 5-1: Comparison of diurnal cycles of the latent heat fluxes (λE) of the three modules with FIFE observations. The analysis period is limited to days between May 27-September 30, 1987, and when FIFE IFC data are available.

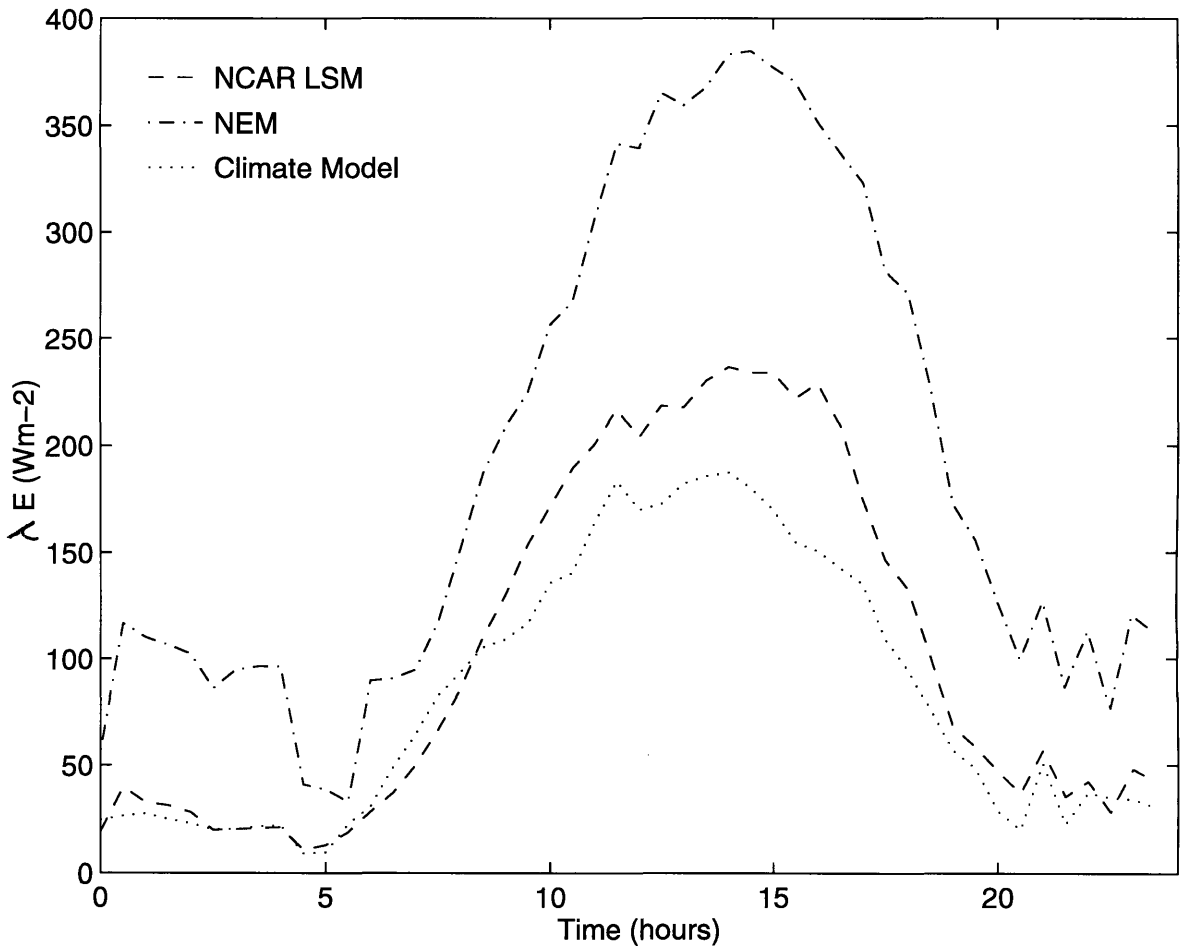

Figure 5-2: Intercomparison of the diurnal root mean square errors in the latent heat flux (λE) calculations of the three modules.

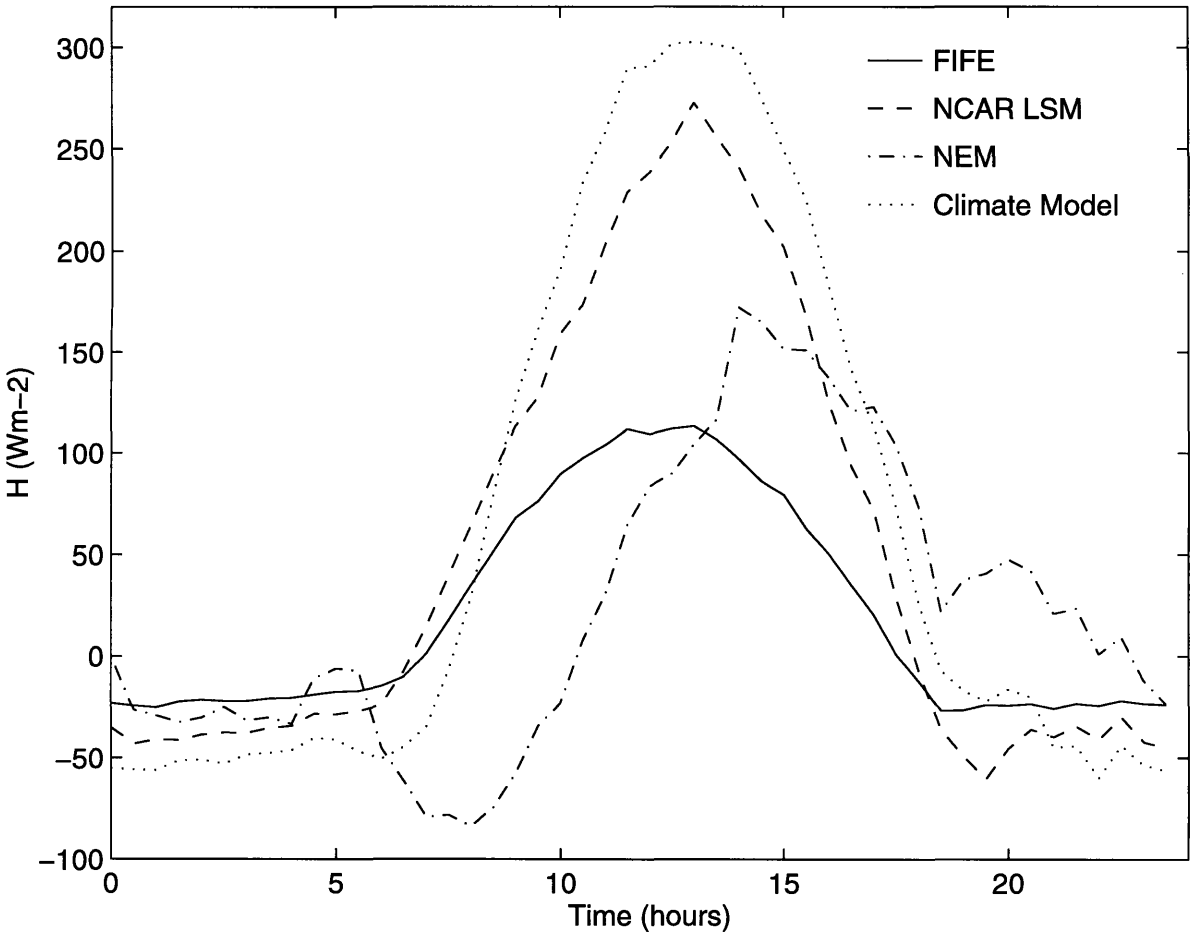

Figure 5-3: Comparison of diurnal cycles of the sensible heat fluxes (H) calculated by the three modules with FIFE observations. The analysis period is limited by FIFE IFC data availability.

two and a half hours later.

Figure 5-4 shows the diurnal RMSEs of the three modules. All three modules have large errors; the errors are often as large as the simulated values. NEM errors are clearly larger than errors in the other two models. The LSM and Climate Model diurnal cycles and diurnal RMSEs are very similar. The largest LSM and Climate Model errors occur during midday, but due to the shift in the NEM diurnal cycle, the largest NEM error occurs at about 15:00 hours. Although the NEM mean morning values compare well with FIFE observations, the large early morning H errors in Figure 5-4 indicate that NEM simulations fluctuate about the observed value in the early morning hours as well.

Ground heat flux The diurnal cycles of G fluxes calculated by the three modules and the cycle for FIFE measurements are shown in Figure 5-5. Flux is positive towards the surface. The LSM simulations follow FIFE observations well, in terms of trend, range and amplitude; but in late morning the LSM G begins to decrease sooner than the measurements and in the evening increases to a value slightly more than the observed level. But both LSM simulations and FIFE values reach a minimum of about -90 Wm^{-2}. NEM and Climate Model diurnal cycles are clearly different from the observed cycle. The minimum NEM value occurs about three hours before FIFE observations, and is about 80 Wm^{-2} smaller than the observed trough; in the evening NEM values increase faster than the FIFE rate to 121 Wm^{-2} at about 20:00 hours and decrease to 50 Wm^{-2}—closer to the observed value. The Climate Model simulations are similar to the NEM simulations, but the peak and trough values are not as extreme as in NEM. When compared to the LSM calculations of G, NEM and Climate Model calculations do not adequately mimic FIFE observations.

Figure 5-6 shows the diurnal RMSEs of the three modules. LSM error is markedly smaller than errors in the other two modules. LSM day-time errors are larger than the night-time errors, but the errors do not follow the cyclical diurnal error pattern found with λE or H. NEM and Climate Model simulations show several error peaks due to the shift in the calculated trough and the unnecessary peaks these two modules

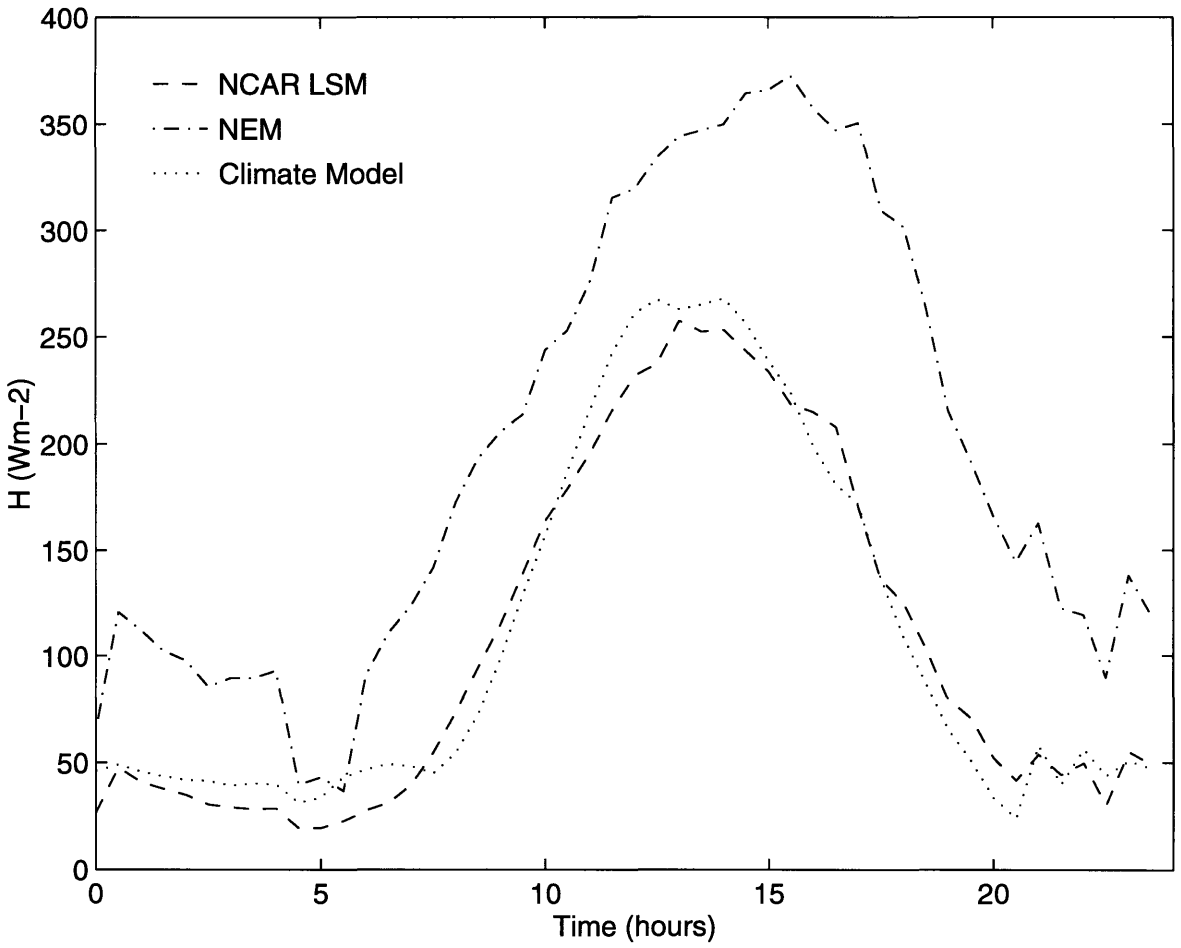

Figure 5-4: Intercomparison of the diurnal root mean square errors in the sensible heat flux (H) calculations of the three modules.

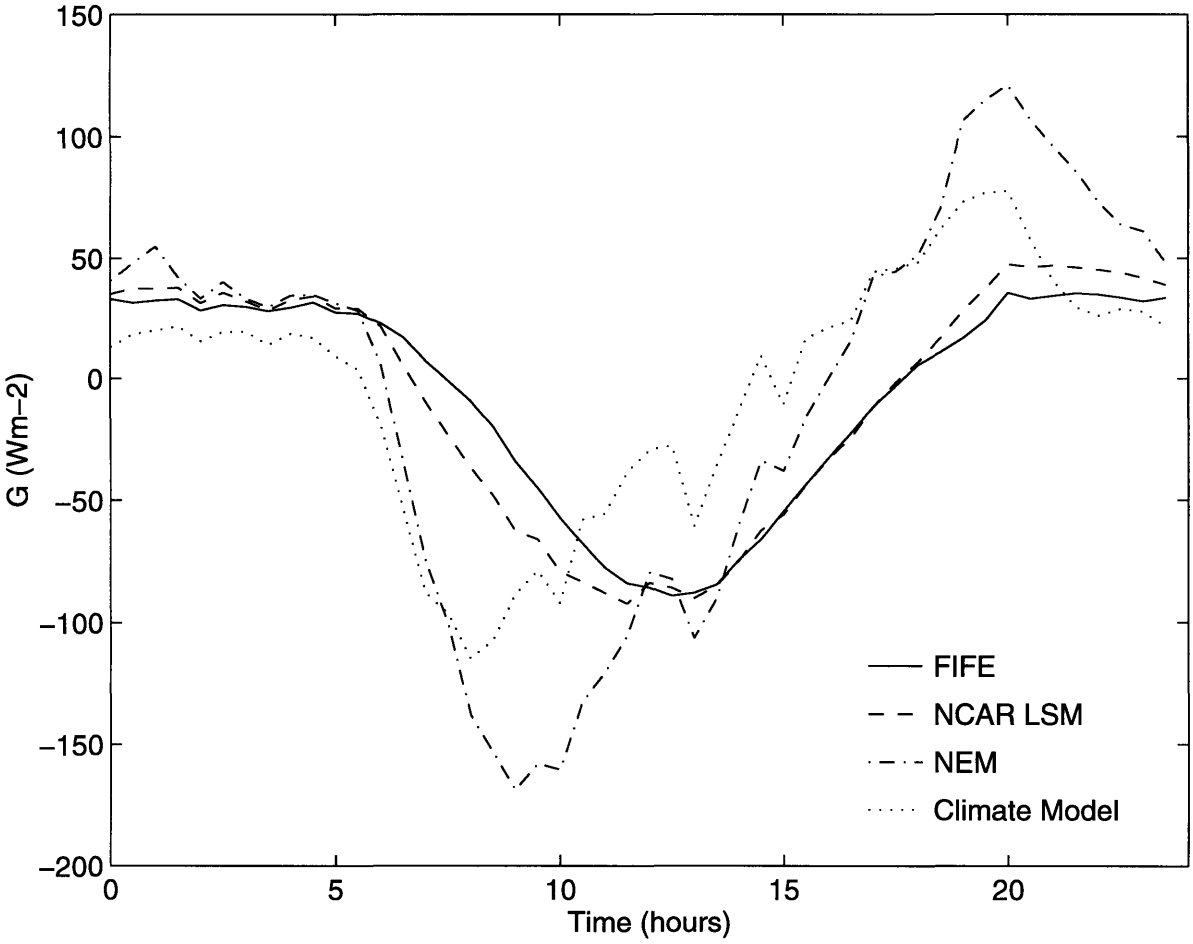

Figure 5-5: Comparison of diurnal ground heat fluxes (G) of the three hydrological modules with FIFE observations.

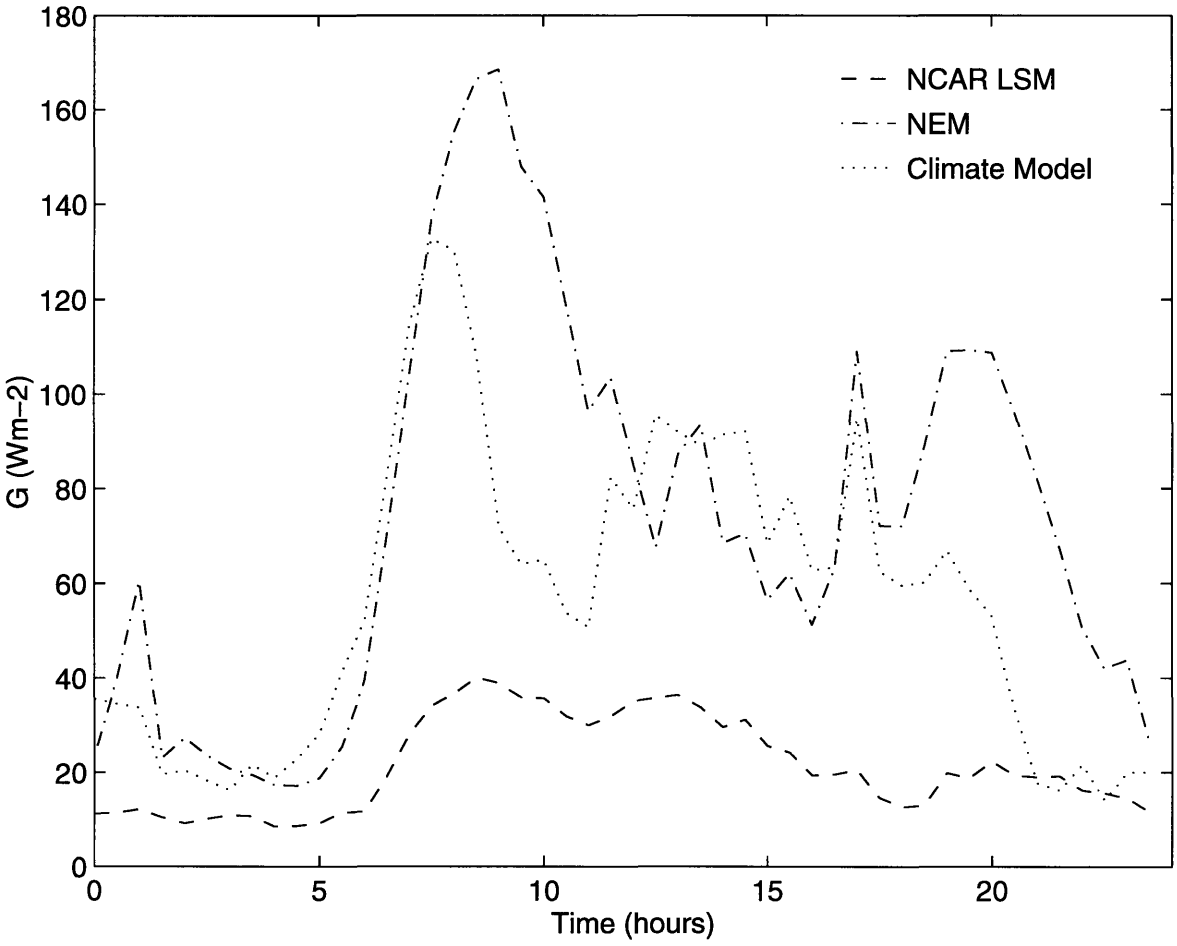

Figure 5-6: Intercomparison of the diurnal root mean square errors in the ground heat flux (G) calculations of the three modules.

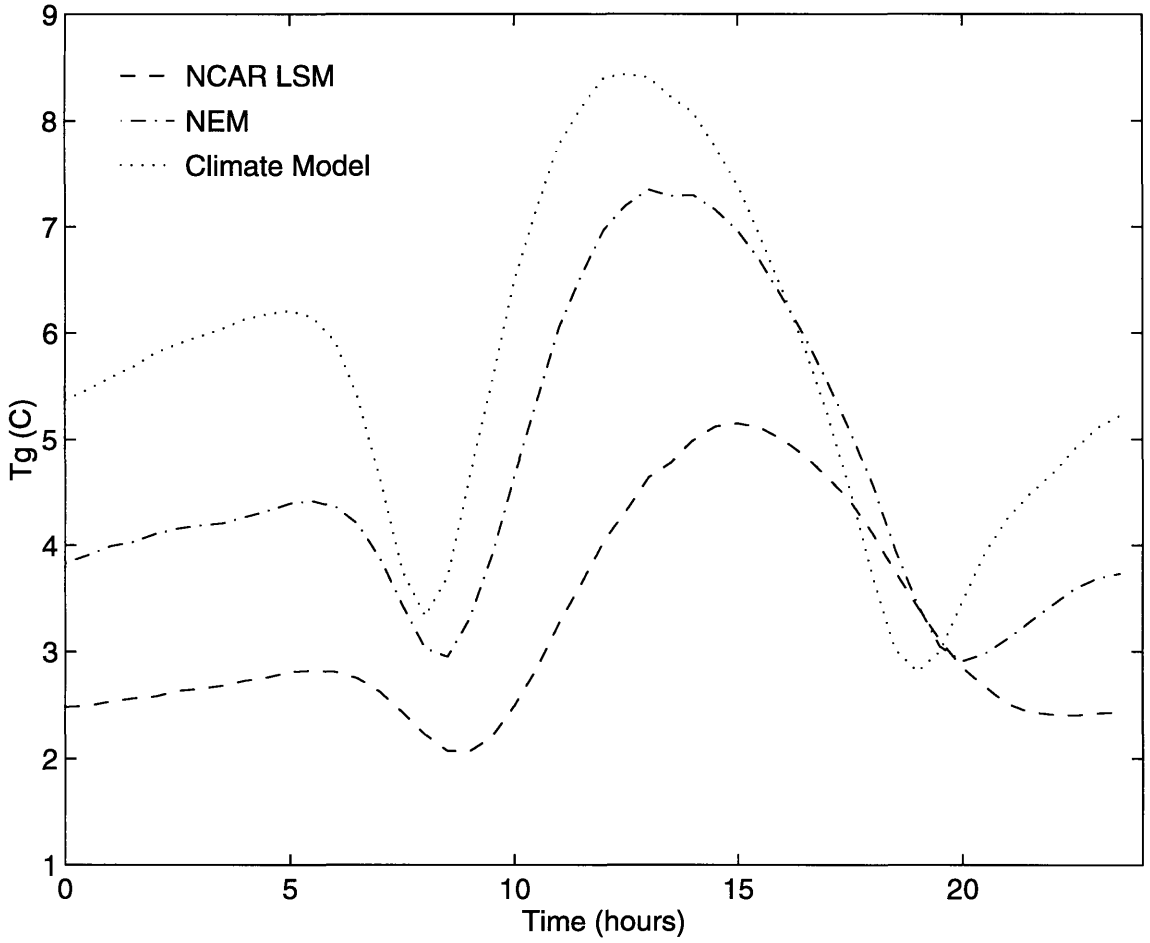

Figure 5-10: Intercomparison of the diurnal root mean square errors in the uppermost soil layer temperature (T_g) calculations of the three modules. The uppermost soil layers in the models are 10 cm thick; NEM and NCAR LSM calculations are at the center of each layer. FIFE upper soil temperature measured at a 10 cm depth.

Variable	units	Observed	Climate Model	NEM	NCAR LSM
latent heat flux	$[Wm^{-2}]$	306	260	359	326
sensible heat flux	$[Wm^{-2}]$	149	431	495	385
ground heat flux	$[Wm^{-2}]$	122	267	345	147
net radiation	$[Wm^{-2}]$	604	712		733
ground temperature	$[°C]$	4	16	13	9
relative saturation	[%]		7	6	7

Table 5.1: Comparison of mean diurnal ranges. Calculations were limited to periods when FIFE IFC measurements were available.

models simulate much larger ranges than observed; the NCAR LSM has the smallest of the calculated mean diurnal ranges. The discrepancy in H flux is a reflection of the ground temperatures calculated by the models. As expected, the means of the diurnal T_g ranges calculated by the models are larger than the observed mean diurnal T_g range.

The mean range of diurnal G flux of the LSM is about 25 Wm^{-2} larger than the observed value; the mean ranges of the Climate Model and NEM are about twice and thrice as large as the observed value. These models do not calculate the surface fluxes simultaneously: the residual of incoming radiation not partitioned to λE or H becomes G. Hence errors in λE and H compound in G. While λE and H ranges in the LSM deviated from the FIFE range, the errors in λE and H do not affect G as much because all the surface fluxes are calculated simultaneously. The calculated R_n mean ranges also overestimate the FIFE R_n mean range.

Since soil moisture measurements were available at daily intervals, diurnal ranges were not calculated for FIFE soil moisture measurements. The mean diurnal soil moisture ranges shown in Table 5.1 are for the uppermost soil layer, and model simulations agree well.

Chapter 6

Computational Demands of the Models

Chapters 3, 4 and 5 indicate that the NCAR LSM is more often better able to reproduce FIFE flux values than the other two modules. The Climate Model had lower RMSEs, but it did not capture the daily and diurnal trends as well as the other models. NEM had large errors—noise—but still captured the diurnal trend well. NEM daily mean trends were less reliable because of excess soil moisture on rainy days; the Climate Model's daily trends were less reliable because its upper soil layer was often too dry. While the NCAR LSM performance was not perfect, it avoided many of the problems encountered with the other models, and successfully simulated diurnal, daily, and monthly trends. But its algorithm is much more complex than those in the Climate Model or NEM.

Hydrological modules of climate prediction models not only need to accurately represent the subsurface, accurately partition energy at the land-atmosphere interface, calculate ground surface temperature, and be sensitive to atmospheric forcings while maintaining seasonal trends, but such modules also have to do all of the above quickly. But models cannot both perform accurate high-resolution calculation, and yet demand little computational time. So modelers often have to trade-off accuracy for computational efficiency. Therefore the modeler must choose the hydrological module that best meets the need.

Field	NCAR LSM	Climate Model	NEM
CPU time devoted to running model (seconds)	21.31	8.51	12.78
CPU time consumed by the kernel to run the model (seconds)	2.43	0.34	0.31
Elapsed wallclock time (seconds)	24.37	9.27	13.7

Table 6.1: Computational demand for a one-month simulation.

Table 6.1 gives the computational demands (including I/O) of the three modules for a one-month analysis period; required computational time and demands of models increase almost linearly with increased analysis periods. It is clear from this table that the NCAR LSM's numerous output variables and robustness comes with a price—it requires about twice as much CPU time as the other two hydrological modules. Nonetheless, it may be possible to further increase computational efficiency by reducing I/O. The LSM is coded in a modular fashion with several nested subroutines that calculate many of the intermediate parameters. So while these calculations add to the computational demand, they also make the model use less restrictive. This model not only allows different plant and soil types within a single grid cell, but it also allows simultaneous calculations over different regions—tropics, deserts, or snow covered regions. Furthermore, the LSM requires twice as many inputs and writes out about five times as many outputs as the other modules at each time step. These additional I/O further add to the LSM's computational demand. But these additional outputs are not in vain. As Table 2.2 indicates, this module calculates many parameters that serve as useful checks for the MIT Global System Model simulations. Besides, if this model were incorporated into the Global System Model, it can replace hydrological modules in the Climate and Natural Emissions Models, and save overall computational time, while providing the above models with more accurate inputs; but more

important, the hydrologic calculations in the different submodels will be internally consistent since all the calculations will be performed by a single module. Further, the NCAR LSM has been formulated and coded to run on stand-alone mode or to be coupled to a climate model. Therefore, this model can be easily and conveniently coupled to the MIT Climate and Chemistry Model.

Chapter 7

Conclusions and Recommendations

This chapter summarizes the key points of each of the previous chapters, and recapitulates the main conclusions of this project. It then lists some of the shortcomings of the project and analyses, and enumerates a few study areas that will improve future modeling efforts. The chapter concludes by relating the implications of this research to policy analyses and decisions.

7.1 Summary of Research

Chapter 1 gave a brief description of global warming and the effects of global warming, emphasizing the impacts on water related issues; climate prediction models were then presented as tools to help understand the nature of these impacts. That chapter also discussed the role of water in climate change, the importance of accurately representing surface hydrology in climate prediction models, and the problems encountered by modelers when including hydrological components owing to the lack of understanding of hydrological relationships, or the lack of data to evaluate the accuracy of known relationships. The uncertainties at the broader political level, and the lack of communication between the scientific and political communities were also discussed in this Chapter. The main purpose of Chapter 1 was to explain the complexity of climate

system modeling, and explicate the importance of water in the climate prediction process—thus, introduce the motivation for this thesis: to examine if better hydrological representation in climate models would improve climate prediction capabilities of those models.

Chapter 2 gave an overview of the formulations of the hydrological modules in the MIT Climate Model and Natural Emissions Model, and the NCAR Land Surface Model, and also outlined the data sets used in this project. The main purpose of Chapter 2 was to give the reader a feel for the levels of complexity of the different models, and convey the key assumptions and characteristics that strengthened or weakened each model.

Chapters 3, 4, and 5 discussed results. Chapter 3 compared daily mean diagnostic values from models with FIFE measurements. Chapter 4 presented subsurface temperature and moisture profiles, and Chapter 5 discussed the accuracy of simulated diurnal cycles. The ground surface temperature, an important player in global warming and climate prediction, was affected by three main factors: (a) the energy input to the ground, (b) the soil column structure, and (c) the soil water content.

- The two hydrological modules calculated the energy into the soil column as the residual of incoming radiation not converted to sensible or latent heat fluxes. Therefore, errors in sensible and latent heat flux calculations affected the ground heat flux as well. Since the NCAR LSM calculated all the fluxes and ground temperature simultaneously, its errors in the ground heat fluxes were smaller than in the other two modules.

- A layered soil column was found to better simulate the ground temperature. Due to poor subsurface representation in the hydrological module in the Climate Model, its ground temperature trend was more like the atmospheric temperature trend, and did not lag behind atmospheric temperature as it does in reality. The simulated diurnal ground temperature trend improved as the number of layers in the soil column increased. The resistance imposed by deeper layers in the layered structure avoided large and frequent changes in shallower layers.

- The layered structure influenced soil moisture calculations as well. The deep lower soil layer in the Climate Model over-drained the upper layer. Owing to this dryness, too much of the incoming radiation was partitioned to sensible heat flux and too little to latent heat flux. The NEM evaporated too much. Even though its uppermost soil layer was drier than the NCAR uppermost layer, evaporation from the NEM soon after rain events was higher than from the NCAR LSM or FIFE observations because this module allowed evaporation from the second soil layer as well. Then after the rain event, the upper layers were too dry, so the evaporative heat loss was lower than observed. Therefore, for improved soil moisture calculations the hydrological module in the Natural Emissions Model required an improved evaporation algorithm; and the hydrological module in the Climate Model required a layered soil column structure. Both these requirements were met in the NCAR LSM.

Analysis of seasonal trends was limited in this project. Even the limited analysis of seasonal changes in ground heat flux indicated that a layered soil column structure, even if shallow, was more important at simulating seasonal trends as well.

Chapter 6 discussed the feasibility of incorporating the NCAR LSM in the MIT Global System Model. While Chapters 3, 4 and 5 evidenced that the LSM is better able to simulate the observed FIFE conditions, Chapter 6 showed that the LSM requires almost twice as much computational resources as the other modules. But since the NCAR LSM is more accurate and will make calculations in the different submodels in the MIT Global System Model consistent, and because the LSM can easily be coupled to the Climate Model, Chapter 6 concluded that it is feasible and advantageous to incorporate the NCAR LSM in the MIT Global System Model.

7.2 Main Conclusions

Two main conclusions can be drawn from the work done during this project.

- This research elucidated that a layered soil column facilitates accurate ground temperature, soil moisture, and surface flux calculations at both diurnal and

seasonal scales. Conventionally, when representing the subsurface, a thin upper soil layer was used to partition energy at the surface and simulate high-frequency diurnal cycles, and a deep lower layer was used to simulate long-term seasonal trends [14]. But this project attested that a layered soil structure is more important at simulating both diurnal and seasonal trends than a merely deep soil column.

- This work also asserted that currently, the hydrological components in the Global System Model are not consistent, and that it is, in fact, beneficial to incorporate the NCAR LSM into the MIT Global System Model. The NCAR LSM will make the Global System Model's hydrology internally consistent and provide the Climate and Natural Emissions Models with more accurate ground temperatures, surface fluxes and soil moisture inputs. Tailoring the LSM's inputs and outputs to suit the Climate Model requirements will minimize the computational burden.

7.3 Possible Improvements

- The main weakness of this project is its limited validation of model outputs. Longer validation periods over different sites will improve the robustness of the analyses. Besides, climate models need to span over the entire globe; models must, therefore, be validated over different regions. But the dearth of data from different parts of the world prohibits such a comprehensive analysis.

- The size and shape of vegetation affect the amount of solar radiation and rain water captured at the surface [28]. The Konza region is a prairie with mostly tall grass. So although the analyses done in this project gave good insight to model performances under prairie conditions, this limited analysis does not help understand model performances over variegated land cover. The NCAR LSM has provision for different plant types within the same grid cell, therefore, it should be able to model over regions with different vegetation. However the

FIFE data cannot exploit this capacity.

- FIFE 1987 was a particularly dry year [11]. Therefore, model performances during a typical year may have been left out in this analysis.
- The analysis duration is short. A longer validation period might have helped identify other deficiencies of models, and better understand reasons for those deficiencies.
- FIFE IFC data are for 1987 summer. No data are available during winter months. It is imperative to test hydrological modules with winter data because these modules may not perform well with snow and ice cover. Therefore, the hydrological modules may introduce further inconsistencies under frozen conditions. This hypothesis needs to be first validated with observations.

7.4 Future Research

The list of recommendations for future research can be a long one including suggestions for better parameterization of vegetation effects; determining if physical relationships at larger temporal and spatial scales exist which, while simulating at the larger scales maintain the accuracy of small scale relationships; or better understanding soil-atmosphere-water interactions. However such studies can be undertaken only in the long-term. But there are many areas that can be improved in the interim and short-term.

This project very heavily relied on the availability and reliability of FIFE data. The FIFE data sets are among the best atmospheric, flux and soil moisture data sets currently available. But even these data sets had several shortcomings as detailed in previous chapters: the durations of the data sets were short; not all data were available and reliable; not all data were consistent—different monitoring stations gathered different data, therefore, intercomparisons, and regional heterogeneities introduced errors. These deficiencies can be remedied in the medium-term by using more sophisticated and accurate measuring instruments, and planning the data gathering process

better.

In the short-term, better documentation can greatly facilitate modeling efforts. The FIFE data sets, for instance, were accompanied by descriptive documentation, and further supported by a regularly updated webpage. Yet, many other publications were referenced to obtain information regarding the FIFE experiment and Konza region. It is impossible for one source to provide all the necessary information regarding a data set, but a comprehensive bibliography of publications based on a particular data set will better direct modelers towards necessary information.

7.5 Implications for Policy Decisions

This project required the detailed study of hydrological modules in the MIT Integrated Global System Model, and the NCAR LSM. The study evinced that these different modules are not consistent—regardless of their accuracies. The uncertainties inferred to in Sections 1.6, 1.7, and 1.10 were confirmed in the analyses in subsequent chapters. There were many differences in their formulations and therefore, their simulations. Climate prediction models are composed of several smaller modules such as the hydrological modules compared in this project. These modules feed in uncertainties along with relevant information and trends into the integrated model. This plenitude of errors that compound in the integrated models caution the use of their predictions in policy decisions and actions without consideration of uncertainty bounds.

In addition to the many model uncertainties, policy-makers and the general public must be aware that natural climatic variations can dwarf any human-induced climatic change, and that no existing model can reproduce past climates [24]. Therefore model predictions and temperature projections must be perceived in context of natural variations.

The above caution does not imply that policy-makers should ignore global warming possibilities, or that current trade and development policies and plans should not incorporate steps to prevent possible unusual anthropogenic warming. But when for-

mulating policies, model predictions should be used as a guide, and not as the basis for the decision. Future atmospheric temperature projections, for instance, should be used to understand the relative magnitudes of possible future temperatures, and not as the exact future scenario.

As explained in Section 1.6, the uncertainties and deficiencies do not trivialize models' predictions. Climate prediction models serve an important role in helping to understand the nature of our climate, our impact on the climate, and about possible future climatic scenarios. But the integrity of these models' predictions are limited by model formulations, which depend on our understanding of the climate and our knowledge of the future, and the reliability of the input data. Therefore, model outputs should be interpreted accordingly, and used in the proper context.

Bibliography

[1] R.B. Bacastow, C.D. Keeling, and T.P. Whorf. Seasonal amplitude increase in atmospheric CO_2 concentration at Mauna Loa, Hawaii, 1959-1982. *Journal of Geophysical Research*, 10(D6):10529–10540, 1985.

[2] M. Beran. The role of water in global environmental change processes. In H. R. Oliver and S. A. Oliver, editors, *The Role of Water and the Hydrological Cycle in Global Change*, number 31 in NATO ASI Series—Series I: Global Environmental Change, chapter 1, pages 1–22. Springer–Verlag Berlin Heidelberg in cooperation with NATO Scientific Affairs Division, New York, 1995.

[3] H. W. Jr. Bernard. *Global Warming Unchecked: Signs to Watch For.* Indiana University Press, 1993.

[4] A. K. Betts, P. Viterbo, and A. C.M. Beljaars. Comparison of the Land-Surface Interaction in the ECMWF Reanalysis Model with the 1987 FIFE Data. *Monthly Weather Review*, 126:186–198, January 1998.

[5] A.K. Betts and J.H. Ball. FIFE Surface Climate and Site-Average Dataset 1987-89. *Journal of Atmospheric Sciences*, 55(7):1091–1108, April 1998.

[6] G. B. Bonan. *A Land Surface Model (LSM version 1.0) for Ecological, Hydrological, and Atmospheric Studies: Technical Description and User's Guide.* Climate and Global Dynamics Division, National Center for Atmospheric Research, Boulder, Colorado, January 1996. NCAR Technical Note NCAR/TN-417+STR.

[7] G. B. Bonan. NCAR Land Surface Model Summary. [http://www.cgd.ucar.edu:80/cms/lsm], 1996.

[8] R. Bras. Lecture on *Environment, Water and Climate Change.* MIT, January 1998.

[9] R.B. Clapp and G.M. Hornberger. Empirical equations for some soil hydraulic properties. *Water Resources Research*, 14:601–604, 1978.

[10] D.A. DeVries. Heat transfer in soils. In D.A. DeVries and N.H. Afgan, editors, *Heat and Mass Transfer in the Biosphere*, 1. John Wiley, New York, 1975.

[11] Q.Y. Duan, J.C. Schaake, and V.I. Koren. FIFE 1987 water budget analysis. *Journal of Geophysical Research*, 101(D3):7197–7207, March 1996.

[12] D. Entekhabi. MIT, 1998. Personal communication.

[13] The Center for Global Change Science, the Center for Energy, and Environmental Policy Research. MIT Joint Program on the Science and Policy of Global Change. One Amherst Street, Bldg. E40-271, Cambridge, MA 02139, May 1996.

[14] J. Hansen, G. Russell, D. Rind, P. Stone, S. Lacis, A. Lebedeff, R. Ruedy, and L. Travis. Efficient three-dimensional global models for climate studies: Models I and II. *Monthly Weather Review*, 111(4):609–629, 1983.

[15] J. Houghton. *Global Warming: the Complete Briefing.* Lion Publishing Inc., Sandy Lane West, Oxford, England, 1994.

[16] C. G. Johnson and L.R. Smith, editors. *The biological significance of climatic changes in Britain.* Academic Press, 1965.

[17] D. R. Landis. The FIFE experiment overview. [http://www-eosdis.ornl.gov/daacpages/fife.html], 1995.

[18] N. C. Lau. *Climate System Modeling*, chapter 19. Cambridge University Press, 1992.

[19] Y. Liu. Modeling the emissions of nitrous oxide and methane from the terrestrial biosphere to the atmosphere. Report 10, MIT Joint Program on the Science and Policy of Global Change, One Amherst Street, Bldg. E40-271, Cambridge, MA 02139, August 1996.

[20] FIFE data sets. [http://www-eosdis.ornl.gov/daacpages/fife.html].

[21] M. Oppenheimer. Talk on *Climate Change*. MIT.

[22] C. Perry. International Water Management Institute. Personal communication.

[23] R. Peters and J.D. Darling. The greenhouse effect and natural reserves. *Bio Science*, 35(11):707–717, 1985.

[24] R. Prinn. Lecture on *The Science* and *Policy* of *Climate Change: Where are we after Kyoto?* MIT, 1998.

[25] R. Prinn, H. Jacoby, A. Sokolov, C. Wang, X. Xiao, Z. Yang, R. Eckaus, P. Stone, D. Ellerman, J. Melillo, J. Fitzmaurice, D. Kicklighter, Y. Liu, and G. Holian. Integrated Global System Model for Climate Policy Analysis: 1. Model Framework and Sensitivity Studies. Report 7, MIT Joint Program on the Science and Policy of Global Change, One Amherst Street, Bldg. E40-271, Cambridge, MA 02139, June 1996.

[26] L. Roberts. How fast can trees migrate? *Science*, 243:735–737, 1989.

[27] P. R. Rowntree and L. Dümenil. Hydrology in climate models and effects on climate. In H. R. Oliver and S. A. Oliver, editors, *The Role of Water and the Hydrological Cycle in Global Change*, number 31 in NATO ASI Series—Series I: Global Environmental Change, chapter 3, pages 59–104. Springer–Verlag Berlin Heidelberg in cooperation with NATO Scientific Affairs Division, New York, 1995.

[28] W. J. Shuttleworth. Soil-vegetation-atmosphere relations: Process and prospect. In H. R. Oliver and S. A. Oliver, editors, *The Role of Water and the Hydrological*

Cycle in Global Change, number 31 in NATO ASI Series—Series I: Global Environmental Change, chapter 5, pages 135–164. Springer–Verlag Berlin Heidelberg in cooperation with NATO Scientific Affairs Division, New York, 1995.

[29] C. W. Thornthwaite. An approach towards a rational classification of climate. *Geographical Review*, 38:55–89, 1948.

[30] Z. Yang, R.S. Eckhaus, A.D. Ellerman, and H.D. Jacoby. The MIT Emissions Prediction and Policy Analysis (EPPA) Model. Report 6, MIT Joint Program on the Science and Policy of Global Change, One Amherst Street, Bldg. E40-271, Cambridge, MA 02139, 1996.

Appendix A

NCAR Copyright Notice

The copyright notice for the NCAR Land Surface Model follows.

NCAR Land Surface Model, version 1.0

Copyright ©1996

University Corporation for Atmospheric Research

All rights reserved.

DISTRIBUTION TERMS AND CONDITIONS NOTICE

Copyright © 1996 University Corporation for Atmospheric Research National Center for Atmospheric Research Climate and Global Dynamics Division.

This software, the Land Surface Model (LSM), version 1, was developed by the Climate and Global Dynamics Division (CGD) Climate Modeling Section (CMS) of the National Center for Atmospheric Research (NCAR), which is operated by the University Corporation for Atmospheric Research (UCAR) and sponsored by the National Science Foundation (NSF).

Access and use of this software shall impose the following obligations and understandings on the user. The user is granted the right, without any fee or cost, to use, copy, modify, alter, enhance and distribute this software, and any derivative works

thereof, and its supporting documentation for any purpose whatsoever, except commercial sales, provided that this entire notice appears in all copies of the software, derivative works and supporting documentation. Further, the user agrees to credit UCAR/NCAR/CGD in any publications that result from the use of this software or in any software package that includes this software. The names UCAR/NCAR/CGD, however, may not be used in any advertising or publicity to endorse or promote any products or commercial entity unless specific written permission is obtained from UCAR/NCAR/CGD.

The LSM materials are made available with the understanding that UCAR/NCAR/CGD is not obligated to provide (and will not provide) the user with any support, consulting, training, or assistance of any kind with regard to the use, operation and performance of this software, nor to provide the user with any updates, revisions, new versions, or "bug fixes."

This software is provided by UCAR/NCAR/CGD "as is" and any express or implied warranties, including but not limited to, the implied warranties of merchantability and fitness for a particular purpose are disclaimed. In no event shall UCAR/NCAR/CGD be liable for any special, indirect or consequential damages or any damages whatsoever, including but not limited to claims associated with the loss of data or profits, which may result from an action in contract, negligence or other tortious claim that arises out of or in connection with the access, use or performance of this software.

Appendix B

Notation

The notation used to present relationships in the different hydrological modules is consistent with the notation in the NCAR LSM. Therefore, the GISS and NEM notation presented here may be different from the original papers. The following table lists the parameters and variables that are presented differently from the original papers.

Variable	**Climate Model**	**NEM**	**NCAR LSM**
thermal conductivity	λ	k	k
volumetric heat capacity	c_g	C	ρc
thermal diffusivity	K_g		
absorbed solar radiation	F_{sw}		$\overline{S_g}$
net longwave radiation	F_{lw}		$\overline{L}$
sensible heat flux	F_h		H
latent heat flux	F_q		λE
heat flux between soil layers	$F(-z)$	q	G_z
evaporation	E		
precipitation	P_r		
run-off	R		
relative saturation	W	W	
time constant for moisture diffusion	τ		
field capacity	f		
ground heat flux at upper boundary	$F(0)$		G
hydraulic conductivity		K	
hydraulic head		h	
hydraulic depth		z	
soil porosity		n	
heat capacity			c_p
flux of water into and out of soil	Q		q_i, q_o

BIOGRAPHY

RADHIKA DE SILVA was born on November 23, 1971 in Moratuwa, Sri Lanka. She completed her primary and secondary education at Holy Family Convent in Colombo. She attended Harvard College in Massachusetts, U.S.A., and received her Bachelor of Science degree in Engineering Sciences in 1995.

After graduation, she returned to Sri Lanka, and was employed as a research assistant by the International Irrigation Management Institute (IIMI). The research report *World Water Demand and Supply, 1990 to 2025: Scenarios and Issues* she co-authored with Dr. David Seckler was among her contributions to IIMI.

Radhika de Silva joined the graduate programs in Civil and Environmental Engineering (CEE), and Technology and Policy Program (TPP) at the Massachusetts Institute of Technology in September, 1996. She studied the importance of hydrological representation in integrated climate prediction models under the supervision of Professor Dara Entekhabi, and received Masters of Science degrees in CEE and TPP in June, 1998.